REVIEW ARTICLE VOLCANICA

Volcanological applications of unoccupied aircraft systems (UAS): Developments, strategies, and future challenges

Mike R. James[*α,β], Brett B. Carr[γ], Fiona D'Arcy[δ], Angela K. Diefenbach[ε], Hannah R. Dietterich[ζ], Alessandro Fornaciai[η], Einat Lev[γ], Emma J. Liu[ϑ], David C. Pieri[ι], Mel Rodgers[ϰ], Benoît Smets[λ], Akihiko Terada[μ], Felix W. von Aulock[ν], Thomas R. Walter[ξ], Kieran T. Wood[ο], Edgar U. Zorn[ξ]

[α] *Lancaster Environment Centre, Lancaster University, Lancaster, LA1 4YQ UK.*
[⋆] *Full list of affiliations given in Affiliations section.*

Abstract

Unoccupied aircraft systems (UAS) are developing into fundamental tools for tackling the grand challenges in volcanology; here, we review the systems used and their diverse applications. UAS can typically provide image and topographic data at two orders of magnitude better spatial resolution than space-based remote sensing, and close-range observations at temporal resolutions down to those of video frame rates. Responsive deployments facilitate dense time-series measurements, unique opportunities for geophysical surveys, sample collection from hostile environments such as volcanic plumes and crater lakes, and emergency deployment of ground-based sensors (and robots) into hazardous regions. UAS have already been used to support hazard management and decision-makers during eruptive crises. As technologies advance, increased system capabilities, autonomy, and availability—supported by more diverse and lighter-weight sensors—will offer unparalleled potential for hazard monitoring. UAS are expected to provide opportunities for pivotal advances in our understanding of complex physical and chemical volcanic processes.

Non-technical Summary

Unoccupied aircraft systems (UAS) are developing into essential tools for understanding and monitoring volcanoes. UAS can typically provide much more detailed imagery and 3-D maps of the Earth's surface, and more frequently, than satellites are able to. They can also make measurements and collect samples for geochemical analysis from hazardous regions such as volcanic plumes and near active vents. Through being quick to deploy, they offer key advantages during initial stages of volcano unrest as well as throughout eruptions. Data from UAS have already been used to support hazard management and decision-makers during crises. In the future, UAS will become increasingly capable of flying longer and more complex missions, more autonomously and with more sophisticated sensors, and are likely to become key components of broader sensor networks for monitoring and research.

Keywords: UAS; UAV; RPAS; Drone; Aerial Imaging; SfM; Gas Sampling; Geophysics; Volcano; Geothermal Area; Volcanic Plume; Lava Flow; Lava Dome

1 Introduction

The last few decades have seen major advances in our understanding of volcanic processes. Nevertheless, accurate eruption and hazard forecasting, and quantification of the volcanic life cycle globally, remain grand challenges [National Academies of Sciences, Engineering, and Medicine 2017]. To help tackle these challenges, remotely piloted and autonomous airborne systems offer paradigm-shifting potential for sampling and measurement from the inaccessible and hostile environments involved. In this review, we summarise such systems being applied in volcanology and the procedures used, before highlighting the advances made and discussing future opportunities.

Despite the current wealth of volcanological measurement and monitoring systems, critical gaps in data acquisition capabilities remain due to the rapid, unpredictable and hazardous nature of many key processes. Consequently, remotely piloted and autonomous systems represent game-changing technologies through offering rapid, responsive (or regular) data acquisition from remote locations, imaging at down to sub-centimetre-scale resolutions, and options for direct sampling. Over recent decades, exciting opportunities have been provided by specialised surface- or submarine-based platforms, e.g. observing submarine

*Corresponding author: m.james@lancaster.ac.uk

activity [Ikegami et al. 2018; Oshima et al. 1991], exploring crater lakes [Watanabe et al. 2016], gas sampling [Bares and Wettergreen 1999; Caltabiano and Muscato 2005; Caltabiano et al. 2005; Krotkov et al. 1994; Muscato et al. 2003], and mapping fissures [Parcheta et al. 2016]. Here, we focus on airborne systems that are now widely available and seeing rapidly accelerating use. The sweeping diversity of disciplines in which airborne systems are deployed has led to the use of a range of representative terms (e.g. remotely piloted aerial system (RPAS), unmanned aerial vehicle (UAV), unmanned/unoccupied aircraft system (UAS), or 'drone'). Throughout this review we adopt UAS as our preferred terminology based on its increasingly widespread use within scientific work [Granshaw 2018], and we follow NASA's lead in using 'unoccupied' for an ungendered variant [NASA 2012]. With 'UAS' representing the system as a whole, we refer to the vehicle specifically when only the airborne platform is implied (readers interested in UAS nomenclature should see Granshaw [2018] for a detailed review).

1.1 Measurement requirements in volcanology

Our understanding of volcanic processes has developed from a synergy of theoretical and numerical models, laboratory approaches, and field observations. However, the wide range of spatial and temporal scales over which processes operate, often in remote and hazardous environments, present difficulties for comprehensive measurement. For example, volcanic plumes can extend thousands of kilometres, yet comprise particulate distributions with important components down to the micron-scale. Plumes evolve through a complex combination of interacting macro- and microphysicochemical processes within environments ranging from near-surface magmatic-temperature jets to the stratospheric atmosphere at tens of kilometres in altitude. On the ground, near-vent hazards such as pyroclastic flows can limit access for observations to distances greater than multiple kilometres, and yet arguably, reliable measurements should be obtained in these key phases of elevated activity. The timing of high-hazard events can be difficult to predict, with triggering processes effective over sub-minute timescales to years (e.g. column collapse due to eruption rate changes, or lava dome collapse from hydrothermal alteration [Ball et al. 2013; Darmawan et al. 2018b; Heap et al. 2018]). Magma effusion rate, and its temporal variability, also affect lava flow runout lengths, along with topography over length scales down to decimetres [Dietterich et al. 2015; Rumpf et al. 2018]. Timely observations of lava channel velocities (e.g. minute to hourly intervals), and of flow front advance and inflation rates, are essential components for forecasting lava runout lengths, detecting breakouts and monitoring diversions [Dietterich and Cashman 2014; Favalli et al. 2010]. Further insight into past lava eruption rates, flow rheology, cooling and stress-strain history can be gained from mapping surface roughness of existing deposits over extents of up to tens of kilometres, and scales down to centimetres [Cashman et al. 2006; Favalli et al. 2018; Gregg and Fink 1995]. For geothermal systems with surface expressions of mud volcanoes, geysers, or fumaroles, frequent changes in thermal output, degassing, and topography reflect changes in shallow hydrothermal systems. However, site access can be difficult due to high temperatures, strong degassing, and hazardous mud pools.

Such characteristics often make ground-based field measurements challenging and limit direct sampling opportunities. For example, although proximal sampling of volcanic gases by either direct sampling [e.g. Giggenbach 1996] or multiple gas analyser systems sampling (e.g. multi-GAS; Aiuppa et al. [2005] and Shinohara [2005]) crucially enables detection of the full range of gas species, concentrated, high-temperature emissions are often not safely accessible. Ground-based topographic measurements can be spatially accurate (e.g. millimetre- to centimetre-accuracy point measurements using a total station or real-time kinematic global navigation satellite system (RTK-GNSS) receivers) but provide either sparse coverage or are limited in extent. Airborne surveys using conventional crewed aircraft have provided high-resolution measurements of volcanic gas composition and flux at several remote and explosive volcanoes [Doukas and McGee 2007; Fischer and Lopez 2016; Gerlach et al. 1997; Gerlach et al. 1998; Ilyinskaya et al. 2018; Kelly et al. 2013; Shinohara et al. 2003; Werner et al. 2011; Werner et al. 2013; Werner et al. 2017]. However, the limited availability of crewed aircraft, and their associated high costs, complex planning and logistics requirements, and restrictions in hazardous areas, mean that regular surveys [e.g. Doukas and McGee 2007; Favalli et al. 2010; Gerlach et al. 2008; Schilling et al. 2008; Werner et al. 2011; Werner et al. 2013] remain relatively rare.

In contrast, satellite imagery has improved steadily in spatial resolution and temporal availability. Kilometre-scale resolution data (such as MODIS thermal imagery) acquired at a rate of a few images per day, are now augmented by sub-hourly data (e.g. SEVIRI, providing ~5-km-resolution data at 15-minute intervals, and NOAA GOES-R, providing 0.5–2-km-resolution data at 5–15-minute intervals, or every 30 s on request). Relatively high spatial resolution and extended duration optical datasets (e.g. 30-m Landsat imagery, available since the early 1980s) are now joined by sub-metre resolution commercial data sources (e.g. from GeoEye and WorldView satellites) and near-daily data at ~3 m resolution (Planet Labs). High-resolution multi-view optical systems (e.g. Pleiades) can now deliver of order metre-resolution digital elevation models (DEMs), and radar satellites (e.g. ERS, Envisat, TerraSAR-X, Sentinel 1) provide all-weather topo-

graphic data at multi-metre resolutions and surface deformation detection with millimetric sensitivity. Kilometre- to multi-kilometre-resolution multispectral data (e.g. ultraviolet, infrared and thermal) can be used to derive heat flux from vents and lava flows (using sub-pixel techniques) and to estimate gas and ash concentrations in dispersing volcanic plumes (IASI, OMI/TROPOMI and ASTER [Campion 2014; Campion et al. 2010; Carn et al. 2017; McCormick et al. 2012]). In the near future, picosatellite capabilities are anticipated to offer 3-D video and synchronous multi-satellite imaging to capture the dynamics of rapidly evolving systems such as ascending eruption columns [e.g. Zakšek et al. 2018].

The wide-ranging capabilities of satellite systems can be complemented by near-surface measurements that provide advantages not available from space, such as observing from below cloud layers, centimetre-resolution imaging, responsive timing over a range of scales, and direct sampling. Of the multitude of volcanic gas species, only SO_2 is currently detectable at sufficient resolution for volcanological applications by space-based remote sensing methods, and with the considerable uncertainties associated with observing through the overlying atmosphere, although CO_2 could be added soon [e.g. Eldering et al. 2019; Schwandner et al. 2017].

1.2 UAS-based advantages and advances

The use of UAS can strongly augment existing data streams by providing new opportunities in terms of access, resolution, and timing of data collection. They can support the generation of dense time-series data through facilitating more frequent, lower-cost (compared to conventional aircraft), higher-resolution (compared to satellite data, although not yet compared to specialist sensing systems on conventional aircraft), and extensive (compared to ground-based observations) measurement of gas, thermal signature, and surface change across volcanic systems. Such advantages are already exploited in other areas of the geosciences, for example, for centimetre-scale topographic change detection in geomorphic studies [e.g. Eltner et al. 2015], atmospheric characterisation and pollution sampling [e.g. Aurell et al. 2017; Brady et al. 2016; Chang et al. 2016], glaciology [e.g. Immerzeel et al. 2014; Wigmore and Mark 2017], crop or coastal zone monitoring [e.g. Berni et al. 2009; Lelong et al. 2008; Mancini et al. 2017] and landslide analysis [e.g. Lucieer et al. 2014; Niethammer et al. 2010; Peppa et al. 2017]. In some scientific disciplines, UAS use might be considered more developed than in volcanology, and several general and subject-specific reviews contain relevant insight for volcanological applications [e.g. Bhardwaj et al. 2016; Colomina and Molina 2014; Dering et al. 2019; Giordan et al. 2018; Nex and Remondino 2014; Turner et al. 2016; Villa et al. 2016; Zhang and Kovacs 2012]. Here, we build on a recent review of the use of small UAS in volcanic landscapes [Jordan 2019], to explore the wider application of UAS in volcanology, and detail the procedures involved.

Within volcanology, the spatial extents and challenging field environments that characterise volcanic systems constrained initial UAS applications. Consequently, early UAS adopters used relatively large-scale systems that required substantial expertise and, often, considerable investment. Pioneering work is exemplified by the proof-of-concept deployment of a 5 kg combustion-powered helicopter at Vulcano, Italy in 2007 [McGonigle et al. 2008]. Through combining horizontal traverses beneath the plume for spectroscopic measurements of SO_2 flux, with in-plume Multi-GAS measurements of CO_2/SO_2 molar ratios, McGonigle et al. [2008] derived CO_2 fluxes that were in good agreement with ground-based estimates [Aiuppa et al. 2005]. The authors also highlighted the enhanced access and improved spatial resolution offered by UAS-based measurements compared to those from more expensive conventional aircraft surveys.

UAS conclusively demonstrated long-range remote monitoring capabilities during the eruption of Nishinoshima Volcano, which emerged from the Pacific, offshore of Chichijima Island, Japan, in 2013. Repeat orthomosaics and DEMs (0.2 m resolution) were acquired of the ~1 km^2 growing island using a 15 kg combustion-powered fixed-wing UAS, flying ~3-hr missions over the sea for distances of up to 130 km from take-off and landing on Chichijima [Nakano et al. 2014]. The results enabled the identification of pyroclastic cones, lava channels and quantification of the growth rate of the subaerial portion of the island (~0.10×10^6 m^3 per day, ~1.2 $m^3 s^{-1}$ [Nakano et al. 2014]). This remains an outstanding example of extreme-range operations and, as UAS technologies have matured, the spatio-temporal capabilities of easy-to-use, prosumer- and consumer-grade systems, aided by the progressive miniaturisation of sensors, have increasingly overlapped the requirements for addressing volcanological problems, and applications are becoming widespread (Table 1).

This review aims to provide an overview of volcanologically appropriate UAS hardware and sensors, and to outline the procedures and protocols for successful mission planning, survey execution, and data acquisition. We illustrate the insights already gained through UAS technology within multiple areas of volcanology, and highlight likely near-future developments and wider possibilities.

2 UAS vehicles, payloads and ground stations

The 'system' term within 'UAS' implicitly recognises the often complex network of resources required to be

Table 1 – Example UAS applications in volcanology.

Location	UAS-based work	References
Lava flows, fissures and domes		
Nishinoshima, Japan	Generating DEMs and orthomosaics for: Lava area and volume estimates of an emerging island	Nakano et al. [2014]
Mt. Etna, Italy	Lava volume estimates and structural and morphological measurements	De Beni et al. [2019]; Favalli et al. [2018];
Holuhraun, Iceland	Determining structural complexity in fissure development and spatter cone construction (through supporting interpretation of video, satellite and TLS data)	Müller et al. [2017]; Witt et al. [2018]
Merapi, Indonesia	Detecting dome weakening through fracture mapping (including using UAS-thermal imaging)	Darmawan et al. [2018a]; Darmawan et al. [2018b]
Agung, Indonesia	Assessment of emplaced lava	Andaru and Rau [2019]; Syahbana et al. [2019]
Kīlauea, Hawai'i, USA	Lava hazard forecasting and emergency response	Turner et al. [2017b]; Diefenbach et al. [2018]; Diefenbach et al. [2018]
Cones, craters and calderas		
Izu-Oshima, Shinmoe-dake and Tarumae, Japan	Aeromagnetic observations of shallow-level structures such as dykes within a caldera, and post-eruption surveys	Kaneko et al. [2011]; Koyama et al. [2013]; Hashimoto et al. [2014]
Deception Island, Antarctica	Aeromagnetic survey in support of ship-borne surveys	Catalán et al. [2014]
Merapi and Kelud, Indonesia	Supporting vulnerability and post-disaster mapping	Rokhmana and Andaru [2017]; Hisbaron et al. [2018]
Aso, Japan	Landslide detection	Saito et al. [2018]
Volcán de Colima, Mexico	Identifying hurricane-triggered erosion	Walter et al. [2018b]
Etna, Sicily	High-resolution DEMs for reducing gravity measurements	Zahorec et al. [2018]
Kīlauea, Hawai'i, USA	Monitoring caldera collapse	Diefenbach et al. [2018]; Diefenbach et al. [2018]
Geothermal systems: Mud volcanoes		
Salinelle, Sicily, Italy	High-resolution DEM for reducing gravity measurements, orthomosaic for mapping evolution of the system	Greco et al. [2016]; Amici et al. [2013b]; Federico et al. [2019]
Lumpur Sidoarjo (LUSI), Indonesia	Infrared orthomosaics	Di Felice et al. [2018]; Iarocci et al. [2014]
Nirano, Italy	DEM and integration with TLS data	Santagata [2017]
Geothermal systems: Geothermal areas		
Wairakei–Tauhara and Waikite, N. Zealand Hsiaoyukeng and Tatun, Taiwan	Visible and thermal IR imaging for monitoring and mapping	Harvey et al. [2016]; Nishar et al. [2016]; Chio and Lin [2017]; Lai et al. [2018]
Volcanic plumes		
Vulcano, Italy	*In situ* measurements of: CO_2 and SO_2 concentrations	McGonigle et al. [2008]
Kirishima, Japan	CO_2, SO_2, H_2S, H_2O and H_2 during Vulcanian eruptions	Shinohara [2013]
Turrialba, Costa Rica	CO_2, H_2S, SO_2,	Pieri et al. [2013a]; Diaz et al. [2015]; Pieri and Diaz [2015] Xi et al. [2016]
Turrialba, Costa Rica, Masaya, Nicaragua	CO_2, SO_2, H_2S, H_2O and aerosol concentrations	Stix et al. [2018b]
Poás, Costa Rica	CO_2, SO_2 and H_2S	de Moor et al. [2019]
Mt. Ontake, Japan	CO_2, SO_2, H_2S, H_2O, H_2 and particle sampling	Mori et al. [2016]
Masaya, Turrialba and Stromboli	CO_2, SO_2 and halogen species	Rüdiger et al. [2018]
Kuchinoerabujima, Japan	H_2O, CO_2, SO_2, H_2S, H_2, HCl, and HF	Kazahaya et al. [2019]

Continued on next page.

Table 1: [cont.] – Example UAS applications in volcanology.

Location	UAS-based work	References
Agung, Indonesia	H_2O, CO_2, SO_2, and H_2S	Syahbana et al. [2019]
White Island, N. Zealand	Filter pack sampling for measuring metal transport	Mandon et al. [2019]
Yasur, Vanuatu and Pacaya, Guatemala	Image-based 3-D modelling of plume extent	Gomez and Kennedy [2018]; Wood et al. [2019]
Villarrica, Chile	Vent DEM and video to support interpretation of ground-based plume composition measurements; CO_2, SO_2, H_2S, H_2O concentrations and fluxes, as part of a simultaneous ground and airborne data inter-comparison	Moussallam et al. [2016]; Liu et al. [2019]
Sampling and deployment		
Kusatsu-Shirane, Japan	Water sampling from a crater lake	Terada et al. [2018]
Lumpur Sidoarjo (LUSI), Indonesia	Mud and water sampling	Di Stefano et al. [2018]
Asama, Japan	Development and testing of UAS-deployed ground rovers for sampling and imaging activity	Nagatani et al. [2013]; Nagatani et al. [2014]
Asama, Fuj, Izu Oshima, and Sakurajima, Japan	Testing of a 'soil sampling' device for retrieving volcanic sediments for debris flow assessments	Nagatani et al. [2018]
Sakurajima and Kuchinoerabujima, Japan	Deployment of near-vent seismometers	Ohminato et al. [2011]; Ohminato et al. [2017]
Volcán de Fuego, Guatemala	In-plume ash sampling using adhesive stubs and development of a plume detection algorithm	Schellenberg et al. [2019]

able to conduct aerial research. In addition to the aerial vehicle itself, a UAS includes all the supporting equipment and personnel, such as ground stations, pilots, refuelling facilities, sensor payloads, and can extend to the use of external resources such as GNSS. The starting point for any UAS use is to determine which system would be most appropriate, and what equipment would be involved.

2.1 Vehicle types

Different aircraft designs (e.g. Figure 1, Table 2) offer different strengths and limitations, and are best-suited for different tasks and environments. Vehicles can be classified by how they generate lift to fly: 'fixed-wing' covers all aircraft which have wings for lift (such as conventional aircraft), 'rotary' includes all vehicles using one or more vertical propeller, and 'non-powered' covers vehicles such as balloons and kites. Fixed-wing vehicles typically have the longest ranges and endurance, but have a minimum airspeed so cannot necessarily measure or sample slowly (and cannot execute a stationary hover), and they require suitable areas for horizontal take-off and landing. Rotary vehicles typically survey at lower speeds and have less restrictive take-off and landing requirements, because this is done vertically. However, vertical rotor lift generation is less efficient than with a wing, so flight durations are usually less than similarly sized fixed-wing vehicles. Some advanced vehicles have vertical take-off and landing (VTOL) capabilities, for example as tilt-wing or quad-planes (a cross between fixed and rotary classifications to combine their advantages, Figure 1C). In volcanology, the use of kites, balloons and tethered helikites is less common [e.g. Belousov and Belousova 2004; Diaz et al. 2015; Müller et al. 2017; Nicoll et al. 2019; Pieri et al. 2013a], but can offer advantages in places where regulations restrict the deployment of free-flying UAS.

The relatively large UAS initially used in volcanology, mainly comprised commercial fixed-wing and single-rotor helicopter-type vehicles, often based on products aimed at industrial use or the remote control model aircraft community (for example, the Yamaha RMAX (Figure 1H) which was developed in the 1990s and had seen regular use in agriculture [Sato 2003]). Such systems could carry multi-kilogram payloads, but usually required considerable expertise to pilot and were generally combustion-powered, which can cause problems for applications such as gas sensing, and can limit maximum operational altitudes.

The now ubiquitous multi-rotor type vehicles were first developed in the 1990s and used for recreation or robotics research [e.g. Pounds et al. 2002]. Early vehicles were almost exclusively flown indoors, had very restricted payloads, so were of limited relevance to volcanology. By 2010, developments in the avionics systems allowed a generalised autopilot system [Meier et al. 2011] to fully stabilise the 3-D position of custom-built vehicles using GNSS data. This considerably reduced the requirements for technical development and, in combination with increasing payload capabilities, allowed these vehicles to become aerial 'platforms' to carry other sensors. The adoption and further development of these systems by commercial companies (e.g. DJI, Parrot), and advances in autopilot systems, have transformed multi-rotor technology into easy-to-operate and affordable products. Simultaneously, market opportunities in the film industry, agriculture, and

Table 2 – Example vehicle characteristics.

System	Payload weight (total weight)	Flight endurance (min.)	Approx. range (km)	Reference
Single rotor				
Thunder Tiger Raptor 90	3 kg (8.2 kg)	12	16	McGonigle et al. [2008]
RMAX-G1	10 kg (94 kg)	~90	~5	Kaneko et al. [2011]; Koyama et al. [2013]; Ohminato et al. [2017]; Kazahaya et al. [2019]
Multi-rotor				
LAB645	4 kg (12 kg)	~40	~4	Terada et al. [2018]
Vulcan UAV X8	800 g (~10.5 kg)	12–18	2–4	Liu et al. [2019]; Pering et al. [2019]
αUAV	2.5 kg	~35	~4	Mori et al. [2016]
Phantom 4 Pro	(1.4 kg)	<25		Manufacturer specifications: www.dji.com/phantom-4-pro
Fixed-wing				
VectorWing 100	1 kg (3.6 kg)	30–45	10–15	Pieri et al. [2013a]
Skywalker Titan	1.0 kg (8.5 kg)	30–45	5–10	
Skywalker X8	0.2 kg (4.2 kg)	30–45	5–10	Schellenberg et al. [2019]

consumer interest in action and aerial photography has led to substantial improvements in the integration of cameras into such off-the-shelf systems.

Diverse requirements and challenging volcanological environments, however, have also led to the use of customised systems, an approach that offers both advantages and disadvantages over using off-the-shelf products directly (Table 3). In practice, the current wide availability of easy-to-operate autopilot and intuitive control systems has bridged the gap between commissioning custom-built systems and using a fully commercial product. Such control systems facilitate the modification of off-the-shelf UAS by helping sensor payloads to be added to vehicles not necessarily designed for the task. This is becoming an increasingly common approach since it removes the technological hurdle and time investment of designing an entirely custom-built UAS.

The complexity of the on-board GNSS that measures the vehicle position provides yet another classification to distinguish UAS. Increasingly, UAS are capable of using differential corrections to improve vehicle positional data, in either real-time (through applying RTK corrections from a mobile network or from a fixed ground station) or in post-processing (post-processed kinematic, PPK). Applying such corrections can improve the accuracy of vehicle positional data from <10 m to <0.1 m, with post-processing-based approaches having the additional advantage of not requiring continuous transmission of correction information to the vehicle. Such 'RTK/PPK-capable' UAS have advantages for making accurately georeferenced 3-D models in areas where ground access to the survey area for control or reference measurements, is restricted (e.g. by hazards; see Subsection 3.5).

2.2 Payloads

Many modern UAS used in volcanology enable multi-parameter analyses, from imaging to geophysical measurements and the deployment of gas, mud, and water samplers and contact thermometers [e.g. Di Stefano et al. 2018]. Larger or custom-built UAS platforms generally offer versatility for transporting payloads ranging from (or combining) simple mechanical devices to advanced electronics and associated software. Sensor developers are increasingly working with UAS applications in mind, driving miniaturisation, lower sensor masses, and increased communication options to integrate with platform avionics (e.g. FLIR thermal cameras). Real-time transmission of data from the instrument payload to the ground-station can be invaluable for monitoring mission performance and for updating flight plans on-the-fly, for example, to adapt gas sensing locations for a moving plume position. For measurement position and timing data, sensors may have

Figure 1: Examples of UAS platforms. [A] A 2.2-m-wingspan fixed-wing Skywalker Titan airframe with custom avionics, used for long-range aerial gas measurements at Manam, Papua New Guinea. [B] A 2.8-m-wingspan aircraft from Air Photo Service Inc., Japan used for imaging lava flow activity on Nishinoshima island [Nakano et al. 2014]. [C] A Foxtech Baby Shark quad vertical takeoff and landing (VTOL) aircraft, used for gas measurements at Tavurvur, Papua New Guinea. [D] A fixed-wing Skywalker X8 with custom avionics, used for ash sampling at Volcán de Fuego, Guatemala [Schellenberg et al. 2019]. [E] VectorWing 100 at Turrialba, which has undertaken autonomous SO_2 concentration measurements in the plume at maximum altitudes of >3.5 km [Pieri et al. 2013a] [F]. DJI F550 hexacopter, with a consumer-grade Sony NEX-5T camera used for photogrammetric campaigns over La Fossa cone, Vulcano (Aeolian Islands, Italy). [G] A DJI Matrice 100 with a Sensys MagDrone R3 aero-magnetic sensor, surveying buried lava flows and cinder cones at Crater Flats, Yucca Mountain, Nevada, USA. [H] The RMAX-G1 used for aero-magnetic measurements and seismometer deployments at Kuchinoerabujima, Japan [Ohminato et al. 2017] [I] Custom-built hexacopter carrying sensor pod (CO_2, P, T, Rh) for remote deployment and retrieval at Rabaul, Papua New Guinea (credit: Jones, J., and Fricke, G.M). [J] αUAV-series octocopter, used at Mt. Ontake for multi-GAS measurements (black box), note also the white adhesive sheet for particle sampling (reproduced from Mori et al. [2016] under the Creative Commons Attribution 4.0 International License). [K] A DJI Phantom 4 RTK used for photogrammetry in the Lost River Range, Idaho, USA.

Table 3 – Comparison of characteristics of commercial and custom-built UAS.

	Commercial off-the-shelf	Custom-built designs
Specifications	Fixed but published payload and endurance specifications. Real world performance is often lower than stated by the manufacturer.	Decided as an integral part of the design, to meet project requirements.
Build and test	Many turn-key solutions with zero build and test time. Wide user-bases enable issues to be corrected rapidly by the manufacturer (e.g. by firmware updates).	Requires time and wide-ranging expertise. Practical limits to testing unlikely to uncover all potential issues. Open source autopilot software allows sharing of custom modifications within the research community.
Standards and quality assurance	Radio-frequency communication and other quality assurance regulations are met; e.g. plastic-armoured DJI batteries meet the UN Manual of Tests and Criteria Part III Subsection 38.3, covering the damage tolerance of lithium batteries.	Need to be considered at design time. Hobbyist radio controlled devices are often outside of national regulations. Note that commonly used raw pouch-cell lithium batteries do not meet UN Manual of Tests and Criteria Part III Subsection 38.3.
Ease-of-use	Generally straightforward to use due to modern autopilots.	Variable, but generally more complex than off-the-shelf systems.
Transport	Often supplied as one piece with limited ability to deconstruct, although packing solutions usually available.	Potentially more import/export issues due to not being as familiar to officials as well-known commercial products.
Flight restrictions	Some restrictions may be in-built into flight control software through geo-fencing, which prevents flights within no-fly zones: many US volcanoes are in National Park administered land and are thus no-fly zones. Some systems may also implement vertical ascent limits.	Local restrictions must be considered by the operator and followed manually. Altitude limits based only on system performance (and hence, considered at design time).
Sensors	Usually limited sensor mounting points; small commercial drones are often aimed at camera payload, visual, thermal, and multispectral imaging only, and do not have spaces for specialised payloads.	Can be flexible, and should be considered at design time.
Cost	Variable (e.g. hundreds of USD to tens of thousands of USD), depending on requirements. Consumer demand for small systems reduces prices.	Hardware costs relatively low, but cost of build-time should not be neglected.

their own GNSS receiver or be linked to the UAS's GNSS data stream.

2.2.1 *Cameras*

UAS equipped with visible-wavelength, thermal, and multispectral cameras have been used for many years, and are a standard in surveying and fire detection [Ambrosia et al. 2005]. The primary use of resulting imagery is often to produce orthomosaics and DEMs from photogrammetric processing, but real-time camera data can also be used for monitoring the UAS status and activities. Such real-time telemetered video feeds are essential for any operations in which the aircraft is beyond visible line of sight of the pilot. Note that these style of operations usually require special authorisation (Subsection 3.1).

The range of camera options is greatest for visible-

wavelengths, varying from small and light-weight webcam- or action-style devices (e.g. to live-stream operations) to larger digital single lens reflex (dSLRs) capable of high-quality imaging for accurate 3-D topographic modelling. For platforms with smaller payload capability, compact cameras can offer a useful compromise between image quality and camera weight, but they are becoming less commonly used due to many affordable (~US$1000) consumer-grade UAS now already having integrated camera systems. Such integrated cameras have improved rapidly and can now generate imagery of sufficient quality for valuable 2-D and 3-D results. Image sizes are typically ~10–20 megapixels and, when acquired from typical altitudes of ~100 m or less, result in ground resolutions of order centimetres [e.g. Favalli et al. 2018]. Although camera features such as rolling shutter and in-camera image stabilisation can visually enhance video feeds, they will degrade the quality of photogrammetric results and should be avoided or disabled if imagery are being acquired for accurate 3-D topographic modelling or multispectral data analyses [e.g. Mosbrucker et al. 2017; O'Connor et al. 2017].

Thermal (e.g. FLIR Tau 2) and multispectral (e.g. Parrot Sequoia) cameras are generally substantially more expensive and offer much reduced spatial resolution. UAS-mounted thermal cameras are often the microbolometer type and have considerably lower-resolution (e.g. 640 × 512 pixels) sensors than most visible-wavelength cameras. Multispectral cameras often have an associated visible-wavelength camera which allows the apparent spatial resolution of spectral bands to be increased by pan-sharpening during data processing. Some multispectral sensors also have a sun illumination sensor, for direct and accurate measurements of surface reflectance without image post-processing for atmospheric correction. Current multispectral cameras <US$10,000 cover UV-visible-NIR wavelengths (the spectral range used in most commercial applications), with SWIR and hyperspectral instruments being as much as, or greater than, an order of magnitude more expensive.

2.2.2 *Geophysics*

The exploration industry has deployed UAS-born magnetic and electromagnetic surveys for many years [Malehmir et al. 2017; Samson et al. 2010; Williams and Harris 2003] but in volcanology, of the many geophysical techniques in general use, only magnetic surveys have been carried out from UAS [Glen et al. 2012; Koyama et al. 2013; Ohminato et al. 2017; Rodgers et al. 2020; Rodgers et al. 2019]. Many UAS magnetic surveys use sensors developed for use with crewed aircraft, e.g. optically pumped alkali vapour, proton precession, and fluxgate magnetometers. However, lightweight UAS-specific sensors have been developed and typically contain data logging, a GNSS receiver, and internal batteries. As examples, the Sensys MagDrone R3 is a <1 kg, dual fluxgate magnetic gradiometer, designed to be attached to the landing gear of a rotary wing system (e.g. Figure 1G), and the Geometrics MagArrow is a single caesium vapour sensor designed to be slung below a rotary wing or towed. These sensors specifically filter out the electromagnetic signals from propulsion motors so that they can be used in close proximity to the vehicle. Most vehicles are constructed from plastic or carbon fibre, so have minimal magnetic signature but, for larger designs with metallic components, users may need to consider a slung or towed sensor. The weight of the sensors involved tends to restrict their use to fixed-wing or heavy-lift rotary platforms but, as sensors are becoming smaller and more affordable, and suitable heavy-lift UAS are becoming more available, the use of such sensors will increase.

UAS have also been used to make atmospheric electrical measurements through electric charge sensors on meteorological radiosondes. Such sensors are supporting a recent resurgence of interest in the electrification of volcanic plumes by enabling vertical transects of average space charge density measurements [Nicoll et al. 2019]. These measurements represent a strong advance over previous estimates made from sparse ground-based atmospheric electric gradient measurements [e.g. Anderson et al. 1965; Hatakeyama 1943; James et al. 1998; Lane and Gilbert 1992; Miura et al. 1995].

2.2.3 *Gas sensors*

In situ gas composition measurements can be carried out by miniaturised, pumped analyser systems for multiple gas species, which include electrochemical sensors for sulphur species (SO_2 and H_2S) and non-dispersive infrared (NDIR) sensors for CO_2 and CH_4 [e.g. Di Stefano et al. 2018; Kazahaya et al. 2019; McGonigle et al. 2008; Mori et al. 2016; Rüdiger et al. 2018; Shinohara 2013; Syahbana et al. 2019]. Miniaturised mass spectrometer systems are also under development [Diaz et al. 2015] but their power requirements, and need for associated electronics and vacuum systems, results in instruments aimed at payload capabilities of either 3–5 kg or up to 20–50 kg for the full configuration [Diaz et al. 2015].

Alternatively, horizontal traverses beneath volcanic plumes use remote sensing approaches based on upward pointing UV spectrometers. Such methods determine SO_2 integrated column concentrations by differential optical absorption spectroscopy (DOAS) and thus, in combination with wind speed data, enable estimates of SO_2 flux [McGonigle et al. 2008; Mori et al. 2016; Rüdiger et al. 2018; Stix et al. 2018b].

2.2.4 *Samplers*

Sampling systems enable the acquisition of physical samples from the atmosphere (e.g. gas or ash from dis-

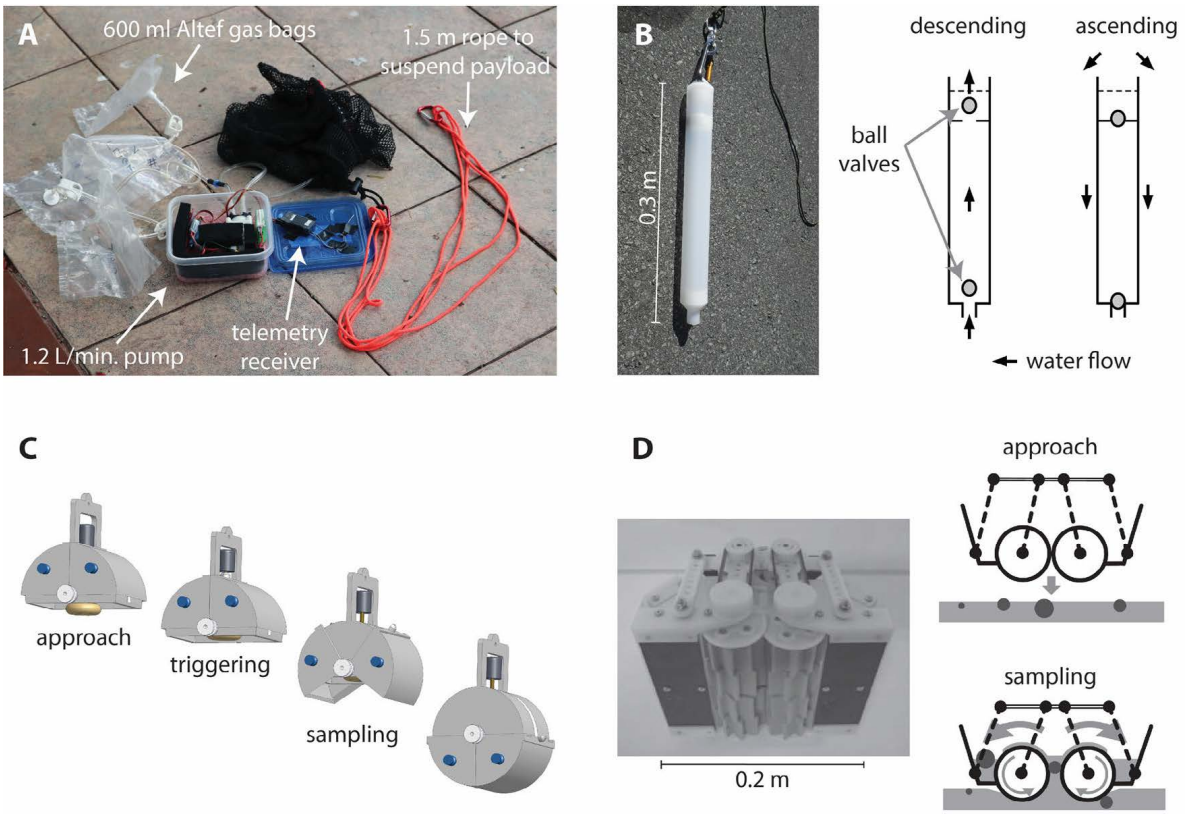

Figure 2: UAS-borne sample collection systems. [A] Gas sampling equipment. [B] Water sampler (left: photograph, right: cross-sectional schematic of sampling method; adapted from Terada et al. [2018] under the Creative Commons Attribution 4.0 International License). [C] 'LUSI drone' mud sampler conceptual diagram of operation [Di Stefano et al. 2018]. [D] Sediment sampler (left: photo; right: cross-sectional schematic of sampling method; adapted from Nagatani et al. [2018]).

persing volcanic plumes), or from the ground (e.g. water, sediment or rock), for laboratory analysis (Figure 2). For sampling in plumes, micron-scale particulate material including fine ash (e.g. respirable PM_{10}; <10 µm in diameter) and condensed aerosol (e.g. sulphates, chlorides, mostly <2 µm in diameter) can be collected using filter packs with a coarse membrane made from inert material such as polytetrafluoroethylene (PTFE), or cascade impactors [Mandon et al. 2019; Mason et al. 2019], or measured *in situ* using optical particle counters (e.g. at Turrialba; Stix et al. [2018b]). For larger particle sizes, such as coarser ash, adhesive-based collectors such as tape, sheets or carbon stubs (conductive tabs used to mount samples for scanning electron microscopy), have also been used (e.g. at Volcán de Fuego [Schellenberg et al. 2019] and Mount Ontake [Mori et al. 2016]). Adhesive collectors are extremely lightweight, allowing synchronous measurement with a larger payload (e.g. a Multi-GAS analyser or optical particle counter), but cannot guarantee the collection of a representative particle size distribution, unlike cascade impactors with specifically designed 'isokinetic' inlets. Inlets and adhesive collectors require protection within a remotely operated enclosure to prevent contamination during take-off and landing [Schellenberg et al. 2019].

When collecting gas samples for laboratory isotopic analysis, volumes of several hundred millilitres are often required, which limits the number of samples that can be acquired in any one flight. Thus, ideally, sampling should be triggered when the vehicle is in the plume, and this can be determined by using an electrochemical SO_2 sensor (or an optical particle counter for particle-rich plumes) to telemeter real-time data to the operator. Once sampling is triggered, a remote-controlled pump and one-way valves fill the gas bags (e.g. Figure 2A), or needles can be used to pierce the sealing membranes of pre-evacuated sample tubes [Di Stefano et al. 2018].

Sampling of either liquids or solids from the surface has been enabled by a variety of specialised systems designed for use from hovering rotor-based platforms (e.g. Figure 2B–D; Di Stefano et al. [2018]; Nagatani et al. [2018]; Terada et al. [2018]). For safety, samplers are generally suspended below the aerial vehicle on a rope with an emergency release system in case the sampler becomes trapped on the surface. The use of a winch can increase the flexibility of deployment and sample retrieval, but increases payload weight and hence impacts mission durations. Due to payload limitations,

sample masses tend to be restricted to less than ~1 kg.

2.3 Ground stations

The ground station represents an essential component of any UAS, as the pilot's user interface to the flying vehicle. Communication is via wireless radio-frequency links, which typically convey pilot commands, vehicle telemetry, and a live video feed. For vehicles using RTK GNSS, the ground station also provides the position corrections back to the vehicle.

Commercial products often include a ground station directly integrated with the controller unit, or require the user to connect to a tablet or smartphone running proprietary software. The radio link between the flying vehicle and the ground station controller will use unrestricted frequency bands and comply with maximum emitted power regulations; for example, the 2.4 GHz and 5.8 GHz bands are almost globally unlicensed. Custom systems can be designed but care must be taken to comply with local regulations regarding frequency, emitted power, duty cycle, and frequency-hopping (e.g. UK regulations from Ofcom). For example, in Europe, equipment can make use of the license-free 868 MHz band; however, in the USA this band is restricted and the 915 MHz band is preferred for UAS data telemetry.

The advantage of a custom system (or software) is the ability to modify the data stream to contain measurement data from payloads [Liu et al. 2019], or to send commands to the vehicle to activate/deactivate mechanisms or sensors [Schellenberg et al. 2019]. In these cases, update data rates can be slow (e.g. ~1–10 Hz) but sufficient for slow sampling sensors, with faster sampling systems requiring data aggregation before transmission, or communication of only status messages.

3 UAS deployment: theory and practice

Safe and successful data acquisition is underpinned by robust flight planning, which considers the underlying mission requirements (e.g. scientific or monitoring objectives), but also reflects the local flying regulations, the UAS specifications and limitations, the flight environment (e.g. topography, nearby infrastructure), and expected weather conditions. Data acquisition requirements usually dictate key components within the flight planning (particularly for the survey component of the flight), but many other considerations such as regulations and safety are independent of the specific mission objectives. When implementing a mission, human expertise represents a key component of any UAS and the importance of an experienced pilot—supported by competent personnel—should not be underestimated. In most UAS missions, it is recommended to have at least one visual observer to identify potential hazards (i.e. birds, aircraft, weather patterns) and assist in recording flight times, battery, GPS, and received signal strength indicator levels throughout each flight. As with any complex task, the likelihood of success is enhanced by checklists, and their use is a recommended procedure for UAS missions (see Supplementary Material for an example flight checklist and log template). Employers and organisations frequently have additional documentation procedures too; for example, just as for conventional aviation work, US Federal agencies require a Project Aviation Safety Plan (PASP) be written, reviewed, and signed off before any UAS mission. UAS-PASPs include the scientific objectives, pre-syn-post flight checklists, a risk matrix, and emergency procedures (see Supplementary Material for an example). To alert other air users of UAS operations, it is good practice (and required in some cases) to submit planned flight information to the Federal Aviation Administration (FAA), which allows them to issue a notice to airmen advisory (NOTAM) or 'DROTAM' (drone NOTAM). UAS pilots should also check for NOTAMs relevant to their operations, for example, to identify any temporary changes in local airspace restrictions.

3.1 Regulations and safety

The rapid increase of UAS activities exposed gaps in the existing airspace regulations aimed at safeguarding people, property and other airspace users. Aircraft are classified by their maximum take-off weight (MTOW) as well as other characteristics and, with most UAS used for scientific and recreational purposes weighing <150 kg, they are not covered by international aviation rules (e.g. European Union Aviation Safety Agency (EASA) Regulation CE no. 216/2008). As a result, to reduce risk, countries have adopted their own rules to cover UAS operations through national aviation authorities and are subsequently updating them independently; by 2016, nearly a third of countries had UAS regulations in place [Stöcker et al. 2017]. As examples, in Italian airspace, UAS operations are covered by Ente Nazionale per l'Aviazione Civile (ENAC, https://www.enac.gov.it/) rules which, at the time of writing, had been last updated in May 2018. In the USA, regulations and requirements were updated by the Federal Aviation Administration (FAA) reauthorization bill in October 2018.

Despite independent national bodies defining UAS regulations, their consistent aim of risk reduction has led to similarities in key areas (such as MTOW limits), and they generally consider the same broad areas [Rosa et al. 2018; Stöcker et al. 2017]:

- *UAS classification*. Authorities have established detailed rules based on take-off weight of aircraft. In Italy, for example, ENAC distinguish between rotary and fixed-wing systems, and between UAS with operating take-off weight <25 kg, and those ≥25 kg and <150 kg. In the USA, UAS aircraft <25 kg are considered 'small' and can be flown ei-

ther recreationally or with a standard certificate. MTOW is one of the most important aspects to consider in UAS risk evaluation.

- *Limits to operations*. Most countries impose a maximum flying altitude and use retaining visual line of sight (VLOS) between the pilot and the aircraft as a range limit criterion. Operations may occur at distances that exceed VLOS either by following regulations for 'beyond visual line of sight' (BVLOS) or by complying with VLOS conditions through using alternative means, as defined by 'extended visual line of sight' (EVLOS) regulations. In general, requirements and authorisations vary depending on whether operations are over critical areas (e.g. crowds, urban areas, infrastructure, etc.) or non-critical areas.
- *Certification and licence requirements for the operator and UAS*. Some countries require that UAS are registered with their national competent authority and have an airworthiness certificate. The operator is the person holding the licence to fly and must be registered at the national competent authority.
- *Airspace requirements*. In some cases, operators must request authorization or provide local authorities with an intent-to-fly declaration prior to surveys being carried out. However, some countries waive this requirement for UAS operations within internationally recognised Class G airspace [International Civil Aviation Organization 2015].
- *Pilot requirements*. Pilot training is essential to ensure that operators hold all necessary skills and have a minimum required level understanding of aviation safety rules. In many countries, prospective pilots will be required to pass a written exam and a flight test to demonstrate aeronautical knowledge and piloting capability. In Italy, the pilot must be certified (for flight operations and for medical fitness), over 18 years of age and insured, with different permissions and certificates for operating over 'non-critical' and 'critical' zones. In the USA, a remote pilot certificate must be obtained for commercial or research UAS operations. However, with varying certification requirements between countries, qualifications are not necessarily transferrable and a valid qualification in one country may not be recognised in another.

In general, countries allow UAS operations for foreign operators as for residents, providing that the appropriate regulations are followed. Stöcker et al. [2017] provide a valuable global overview but, given that regulations can be extensive and are frequently updated, it is essential to check the local details before planning a UAS campaign; non-compliance with the appropriate current regulations may lead to financial and/or legal consequences. Useful web resources for background information are:

- Joint Authorities for Regulation of Unmanned Systems (JARUS, an expert group of global regulatory expertise whose stated purpose is "to recommend a single set of technical, safety and operational requirements for all aspects linked to the safe operation of the Remotely Piloted Aircraft Systems (RPAS)"; http://jarus-rpas.org/regulations),
- Global UAV Regulations Database (a collaborative Wiki; https://droneregulations.info/index.html), and
- DroneRules for Europe (http://dronerules.eu/).

3.2 System characteristics and limitations

The variety of available UAS provides options for a wide range of mission requirements. Multi-rotor and VTOL aircraft offer the most flexibility for operational deployment since landing and take-off need only a level area slightly larger than the vehicle itself (e.g. Figure 1F–K). In contrast, fixed-wing aircraft (e.g. Figure 1A, B, D, E), and especially those with an undercarriage (e.g. Figure 1B), require much larger areas for launch and recovery, and require the surrounding airspace to be relatively clear of obstructions due to shallow approach flight angles. Furthermore, launch and recovery should be carried out into wind, and identifying suitable locations in rough terrain can be challenging. In some cases, parachutes or nets can be used to reduce the need for a large landing area by catching the vehicle in flight; however, these methods increase the risk of damage to the airframe and payload.

The efficiency of fixed-wing designs usually make them the platform of choice for missions that require long durations or distances to a survey area, although some combustion-powered helicopters have multi-kilometre ranges with multi-kilogram payloads (Table 2). Generally, battery-powered systems have less endurance than those using combustion engines but, for *in situ* gas sampling, battery-powered UAS are considered preferable to eliminate potential contamination of samples from exhaust products [Kazahaya et al. 2019]. For geophysical surveys (e.g. magnetic), the magnitude of the interference generated by the motor, electronics and the vehicle body also needs to be considered when selecting the system [e.g. Cao and Zhang 2014].

3.3 Flight planning and survey design

Considering flight missions in segments—for instance representing take off, aircraft transit to the survey area, the survey itself, then return and landing—facilitates planning and operations. Most commercial UAS have associated software to assist mission planning (e.g. eMotion for eBee, DJI GS Pro for DJI Phantom series) or third party software can be used (e.g. Pix4D Capture,

Drone Deploy, Litchi, Mission Planner), and all mission segments may require tailored approaches. Working in areas of steep topography can restrict areas for take-off and landing, and be subject to complex and unpredictable wind fields that can require in-flight changes to maintain into-wind landing of fixed-wing platforms. At high altitudes, strong winds, the low-density atmosphere, and low temperatures (which can significantly affect battery performance) can reduce the duration of possible missions. Mission plans should account for reduced endurance and include contingencies for rapid changes in weather or volcanic activity and for unexpected aircraft or bird encounters. Here, we summarise only the main design considerations that contribute to the survey (data collection) component of missions.

3.3.1 *Imaging and photogrammetric surveys*

For topographic imaging (either to generate 2-D products such as orthomosaics, or to derive 3-D and 2.5-D products such as digital elevation models), the survey component of the flight can be designed based on established photogrammetric principles developed for conventional nadir-viewing aerial surveys [e.g. Abdullah et al. 2013]. Due to imaging surveys being a common use of UAS, mission planning software usually includes specific design support for photogrammetric data collection. Survey design starts from a definition of the measurement requirements, for example, identifying the survey area, the ground sampling distance (GSD) required, and the planimetric (or 3-D) measurement precision and accuracy to be achieved. The GSD depends on the imaging sensor characteristics (e.g. camera focal length and pixel pitch) and the flight height (e.g. see O'Connor et al. [2017] for a readable summary). Based on these relations, flight planning software can estimate the image capture positions once the required survey area is defined and other parameters such as image overlap are provided. For areas of steep topography, flying at a fixed altitude can result in significant changes in GSD between high- and low-elevation areas and, in some instances, may result in a failure to obtain sufficient overlap. For these areas, a terrain-following flight plan may be best, where the UAS follows a 'draped' survey at a constant height above the ground.

Surveys designed for 2-D products (e.g. orthomosaics), usually collect images in conventional parallel strips (in a 'lawnmower' pattern), with overlaps between adjacent images of 60–90 % (Figure 3A). Where 3-D data are required, the photogrammetric network is strengthened by adding cross-strips and by having image overlaps at the upper end of the range. Carrying out such surveys from tens to hundreds of metres above ground usually enables efficient automatic execution (image acquisition and navigating the flight path) under full autopilot control. In systems where the camera control is not integrated with the autopilot system, image acquisition can be set at a specific time interval, with any excess images not forwarded for processing.

High quality results generally require crisp, well-focused images of highly textured stationary scenes, making colourful weathered bare rock surfaces good survey targets. Motion blur, featureless areas (e.g. fresh snow) or highly complex or moving targets (e.g. vegetation, water) reduce the quality of the image matching, resulting in increased systematic error and noise in modelled surfaces. Since areas of strong shadow can present difficulties during processing, diffuse illumination from overcast weather is the preferred condition for imaging or photogrammetric surveys. Photogrammetric considerations such as overall imaging geometry (including image overlap) and the internal stability of the camera (i.e. how well all photographs can be represented using one camera model) also affect topographic measurement precision.

Processing photogrammetric survey data typically involves an automated camera calibration procedure [Luhmann et al. 2016] that aims to minimise systematic error in the resulting topographic model. Although camera calibration can be carried out separately from the survey [e.g. Harwin et al. 2015] the most reliable results are usually obtained if surveys are designed to facilitate the calibration process by acquiring some images over different ranges and angles [Harwin et al. 2015; James and Robson 2014; Nesbit and Hugenholtz 2019], and this is particularly important if there are limited or no external 'control' measurements to include in the processing. Inclusion of such convergent imagery in survey designs strengthens the photogrammetric image network by enabling surface points to be observed from multiple and highly varied viewing directions. This facilitates unique and accurate estimates of camera model parameters during processing [Fraser 2013] and helps avoid systematic error propagating into topographic results. Consequently, for nadir surveys, including some off-nadir images (~30° oblique) can strongly reduce systematic error in DEMs [James and Robson 2014; Nesbit and Hugenholtz 2019]. For topographic targets that are strongly 3-D with respect to the mean flight height above ground (e.g. domes or crater walls), using systems with a gimballed camera capable of being reoriented during flight enables better coverage and stronger image networks than conventional nadir survey styles. In some cases, circular flight paths can be adopted, in which the camera is constantly oriented at a central 'point of interest'.

For thermal and multispectral surveys, sensor and lens characteristics usually result in imagery with a lower spatial resolution than from visible-wavelength cameras flown at the same altitude. Thus, for comparable GSDs, thermal and multispectral surveys usually need to be flown at lower elevations above ground. Typically, such imagery are used only for orthomosaic products but, sometimes, thermal imagery can also provide useful 3-D data for areas occluded by condensing

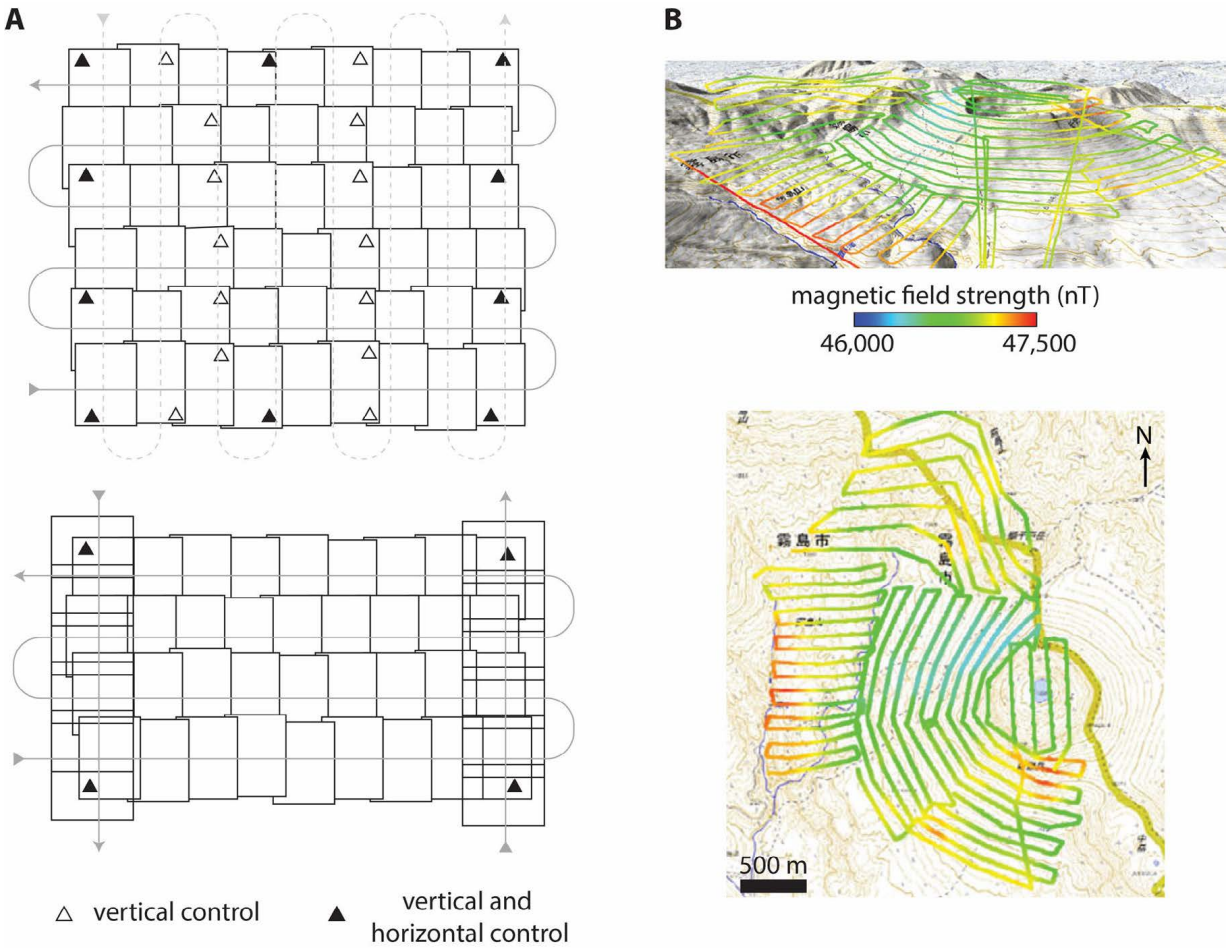

Figure 3: Survey flight paths. [A] Schematic of conventional flight paths (grey) for aerial photogrammetric surveys. Surveys comprise two orthogonal grids of parallel flight lines, shown (top) for only ground points (triangle symbols) used as control measurements, or for (bottom) when suitably accurate camera position data are also available. Only a selection of image outlines are shown for the horizontal lines; along-strip image overlap for UAS surveys are often 70–90 %. Adapted from James et al. [2017a]. [B] Visualisation of flight lines from a draped total magnetic field survey over Shinmoe-dake, Japan (2011), coloured by measured magnetic field intensity and viewed (top) obliquely or (bottom) in plan [Koyama et al. 2013].

gases, where results from visible-wavelength data have been compromised (e.g. Figure 4; [Thiele et al. 2017a]).

When compared with visible-wavelength surveys, thermal and multispectral surveys usually have more stringent radiometric requirements. For calibrated, quantitative analyses of multispectral data, repeat acquisitions of flight segments over a calibration surface of known reflective properties (or temperature) are required to account for changing light conditions. As for visible-light surveys, multispectral surveys are degraded by strong or moving shadows, so best practice is to fly on an overcast day during consistent illumination conditions. For thermal surveys, to avoid contamination from solar heating or reflection, pre-dawn missions are optimal.

Survey design should also consider georeferencing requirements (Subsection 3.4), and be linked to the deployment of ground control (if it is used). For detailed topographic work, considering photogrammetric and georeferencing contributions to measurement precision is important [James et al. 2017a; James et al. 2017b], for example, an image network capable of giving a strong focal length estimate during camera calibration is particularly important if ground control is weak or unavailable, and georeferencing is carried out by using measured camera positions instead. Recourse to the extensive photogrammetric literature will facilitate achieving the best survey accuracies if required [e.g. Kraus 1993; Kraus 2007; Luhmann et al. 2014; McGlone and Lee 2013; Mikhail et al. 2001].

3.3.2 *Geophysical surveys*

Many geophysical methods are in use in volcanology, e.g. magnetic, gravity, and active source electromagnetic surveys, of which only magnetic surveying has been explored from UAS [Hashimoto et al. 2014; Kaneko et al. 2011; Koyama et al. 2013; Rodgers et al. 2020; Rodgers et al. 2019]. Volcanic rocks are good tar-

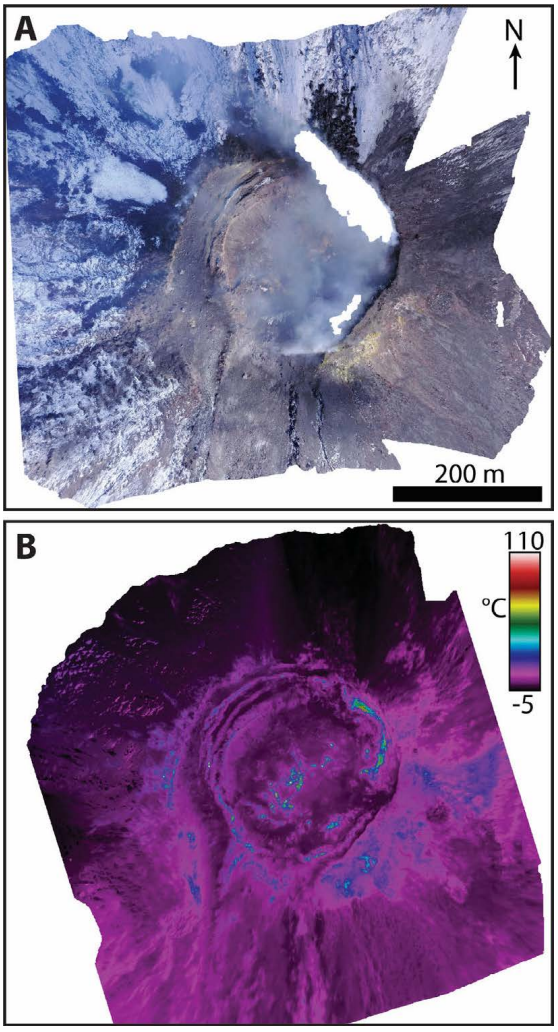

Figure 4: Vertical views of 3-D models of the summit lava dome at Volcán de Colima, Mexico constructed from quadcopter surveys (2018). [A] A visible-wavelength survey using 58 photographs acquired using a Mavic Pro and [B] 195 thermal images acquired with a FLIR TAU2 thermal camera on a Phantom 4 Pro. Both surveys were carried out at ~120 m above ground, with the higher-resolution visible data resulting in a model resolution of ~7.3 cm, compared to ~40 cm for the lower-resolution thermal data. Note that the visible data did not enable successful modelling of some areas which were obscured by degassing plumes (e.g. the NW-oriented white area of the NE crater wall area), whereas the thermal data provided full topographic coverage.

gets for magnetic surveying because they contain high concentrations of ferromagnetic minerals and, as they cool below their Curie point temperature, they acquire a remnant magnetisation aligned with the direction of the Earth's magnetic field at the time of cooling. Rocks heated above their Curie point lose magnetisation, thus it is possible to identify geothermal and hydrothermal areas, and subsurface changes in thermal state [Finn and Morgan 2002].

The signal of a magnetic body usually consists of a pair of positive-negative anomalies [Telford et al. 1990]. Single anomalies, however, dominate the magnetic signal close to the magnetic pole and equator. The anomaly will usually be in a north-south direction, unless significant deformation has rotated the body away from its original position after magnetization. Hence, if limited flight lines are available, it may be preferable to fly lines parallel to the direction of the anomaly pair to image both sides of the anomaly.

With the magnetic field strength of a magnetised body decreasing with the cube of the distance from the source, a significant advantage of UAS over traditional crewed aircraft is the ability to fly low to the ground (10–100 m), where anomaly magnitudes are greater. Flight planning should take into account the likely depth of the target, and it is highly recommended to fly a 'draped' or 'terrain-following' survey, maintaining a fixed altitude above ground. As with all potential fields, the magnetic field is continuous and varies smoothly. Thus, such data can be interpolated between points that are acquired on a spacing comparable with the wavelength of the anomaly [Reid 1980]. Survey line spacing will depend on the size and depth of the expected magnetic bodies. Small, shallow magnetic bodies will have shorter-wavelength anomalies and survey lines that are too widely separated may miss important details [Abdallatif et al. 2007]. Deeper magnetic bodies have longer-wavelength anomalies, so surveys must extend further to cover them fully, and may use a wider line spacing. In such scenarios, the relatively small changes in magnetic field measured across the anomaly mean that a narrow spacing of flight lines may not necessarily provide better constraints for modelling the subsurface body.

For small features, edge detection methods that use the field gradient can sometimes be more effective at locating an anomaly [Hood 1965]. For this, either flying dual sensors a fixed distance apart (i.e. as a gradiometer), or repeating a survey either at different elevations or line offsets can allow calculation of field gradient and provide more information than a single measurement [Grauch and Hudson 2011]. The sensor type and configuration will determine the need for such gradient methods.

3.3.3 In situ *measurement and sampling missions*

Missions for *in situ* measurement and sampling require different flight considerations depending on whether the target is atmospheric or on the surface. When targeting plumes, short-term variability in plume dispersal direction or altitude can render automated flight paths ineffective and somewhat restrictive, especially for long-range missions to narrow plumes. Therefore, manually controlled missions (or automated ascent to plume altitude followed by manual control) may be preferred, assisted by real-time telemetered sensor data

(e.g. SO_2 concentration) to provide a clear indication of when the UAS is within the plume. To maximise the sampling time, *a priori* spatial information on the region of densest plume concentrations should be obtained from either ground-based instruments (e.g. a scanning spectrometer) or coarse aerial mapping surveys using a smaller vehicle (with gas analyser), and used to directly inform subsequent flight paths. If the mission is over sufficiently long distances that a combustion-powered vehicle is required, flight planning of sampling or measurement paths must be designed to avoid contamination from CO_2 and H_2 in combustion exhaust gases [Kazahaya et al. 2019]. The type of sensor being used will determine whether the aircraft must be flown through the plume (e.g. for direct measurement of gas composition [Liu et al. 2019]) or at a particular orientation to the plume (e.g. for spectroscopic remote sensing of SO_2 flux [Stix et al. 2018b]). Missions may also include flight segments dedicated to wind speed estimation at plume altitude, either from the passive drift speed of the UAS with GNSS-position-hold disabled, and/or from calculations made based on the difference between ground and airspeed [e.g. Johansen et al. 2015].

For ground- or lake-sampling missions, planning must consider the additional positional precision required due to the proximity of the aircraft to the surface and this often involves incorporating some elements of manual piloting. In a similar manner as for aerial sampling flights, but at a much smaller scale, the UAS can automatically navigate to an optimal sampling location along a waypoint-programmed flight path, from which manual adjustments, guided by information from an observer at lake level or a real-time video feed, can ensure successful sampling whilst maintaining safety. Where a sampling location is surrounded by steep topography (e.g. a crater lake hosted in deep, steep walled crater), ground-level observations may not be possible and it can be difficult, from an elevated view point, for the pilot to judge vehicle height above the surface (e.g. at Irazu, Costa Rica; J. Stix [2019], personal communication). In such situations, the advantage of a remotely operated winch (or fixed length cable), to enable sampling from an easier vehicle altitude, may outweigh the disadvantages of reduced sampling time and operational range from the added payload weight. Additionally, it is strongly recommended that a dedicated visual observer, who can always maintain eyes on the aircraft and payload (using visual aids such as image stabilising binoculars), is used to help the pilot during such technical missions. In some cases, it can be helpful to have a second UAS to provide an additional visual perspective, whilst loitering well away from the flight path of the sampling vehicle to avoid airspace conflict. Limited lines of sight due to steep topography may also potentially disrupt the UAS radio link. Flight design to minimise the potential for loss of communication between the vehicle and the ground station (at which point most commercial UAS will attempt to return to home) is particularly important. During a mission, possible difficulties may manifest as a degradation in received signal strength indicators, which may require immediate ascent since this usually moves the aircraft to a position where line of sight is regained or improved.

3.4 Georeferencing

Georeferencing is usually an important component in planning UAS deployments, particularly when conducting repeat surveys for comparison (which may only require relative registration of sequential UAS-derived datasets to each other), or merging results with external data sources (e.g. lidar or satellite data, which requires georeferencing to a real-world coordinate system). Mission objectives will dictate the quality of georeferencing needed, for example, sub-metre- to metre-scale DEM accuracy may be required for detailed lava flow modelling, whereas gas sampling flights in dispersing plumes may only require absolute UAS positions to within a few tens of metres.

Most powered UAS use GNSS vehicle position information for navigation, and these location data can be used to georeference sensor data by time-stamping acquisitions or by direct integration of autopilot software and sensor data logging. Under most conditions, such data can provide accuracies of <10 m, although some care needs to be taken with systems that integrate altimeters for improved vertical precision because, by considering only change with respect to the estimated take-off altitude, they can add substantial bias (10s of metres) to the absolute elevation data recorded (e.g. as seen in some DJI systems). Systems that integrate RTK- or PPK-compatible GNSS receivers can, with suitable correction data and processing, deliver accuracies better than 0.1 m. As with all geodetic measurements, caution is required when transforming GNSS data between coordinate systems, noting in particular whether height values are relative to the ellipsoid or to a mean sea level.

Image-based surveys can also use observable features captured within the imagery as ground control for georeferencing; an approach that has been the mainstay of conventional photogrammetric surveying. For the highest accuracy work, the number and placement of ground control points (GCPs) is a key component of survey planning [e.g. James et al. 2017a; McGlone and Lee 2013] and can affect the resulting DEM in terms of absolute accuracy and systematic error within the model. A good quality survey can achieve a vertical precision of ~1 GSD [e.g. James et al. 2017b; Mosbrucker et al. 2017], and better horizontally. Achieving this usually requires dedicated, high-visibility targets to be deployed across the area, and their positions measured by ground-survey (e.g. by total station or survey-grade GNSS). Alternatively, natural features, if they can be distinguished in the imagery or in the final

orthomosaic or DEM products, can provide ground reference. The feature coordinates can be either directly surveyed in the field or (usually to lower accuracy and precision) estimated from pre-existing orthomosaic images, lidar point clouds, DEMs, or maps [e.g. Diefenbach et al. 2013; Diefenbach et al. 2012; James and Varley 2012; Kolzenburg et al. 2016; Zorn et al. 2019]. If there are areas of guaranteed negligible surface change in a reference dataset, then surface-to-surface optimisation [e.g. Besl and McKay 1992] can refine initial feature-based georeferencing. For cases in which repeated UAS-derived surveys are to be georeferenced, use of the same features, targets or areas will provide the strongest inter-survey registration for subsequent change detection analysis.

3.5 Image data processing: Orthomosaics, DEMs and multispectral products

The most common purpose for collecting aerial imagery is for generating georeferenced 2-D orthomosaic images or 3-D topographic products such as DEMs. With UAS-derived imagery usually collected with consumer-grade cameras at a variety of angles from nadir, it can be challenging to process using 'traditional' aerial photogrammetry software, designed for nadir photography from crewed aircraft with well-calibrated and minimal-distortion metric cameras. Consequently, structure-from-motion (SfM) photogrammetry software (e.g. PhotoScan [now Metashape], Pix4D, MicMac), which offer flexible and robust workflows that substantially automate photogrammetric processing and the generation of image-derived products, are generally used for processing. Processing procedures calculate relative camera positions, orientations and calibration data as well as surface information. Hence, camera location data are not required *a priori* for generating 3-D models, but additional 'control' information is required to transform such models into a geographic coordinate system.

Many UAS embed camera location information (derived from the on-board GNSS) into image metadata, and this can reduce photogrammetric processing time. It also reduces the likelihood of failed image alignments, and provides control data for georeferencing. If relatively low spatial accuracies are sufficient (e.g. multiple metres), then using standard GNSS measurements of camera position or relatively few ground control points (either dedicated targets or features identified in pre-existing imagery or DEMs) can suffice. In these cases, such control measurements will enable georeferencing, but are unlikely to be sufficient for improving the relative shape of the surface model derived from the image data, which may be subject to broad deformations or systematic error [James and Robson 2014].

If centimetric-precision control data are available (either from accurately surveyed GCPs or for camera positions from PPK- or RTK- enabled platforms [e.g. Eling et al. 2015; Turner et al. 2014]), then this information can be included within the photogrammetric processing in order to help reduce systematic error, as well as to provide accurate georeferencing. Even if high-accuracy camera position data are available, the use of at least one GCP is key to constraining vertical accuracy [Benassi et al. 2017; Forlani et al. 2018; Gerke and Przybilla 2016; Grayson et al. 2018; Tomaštík et al. 2019]. Furthermore, for all scenarios, in order to reliably quantify the accuracies achieved, some GCPs should be excluded from the processing, and used as independent check points for validation [Chandler 1999].

Thermal and multispectral data can often also be processed into 3-D models with SfM-photogrammetry (e.g. Figure 4; Hartmann et al. [2012]; Thiele et al. [2017b]; Walter et al. [2018a]. As for visible-wavelength imagery, surface shape is determined using the image texture, but software solutions are providing increasingly rigorous treatment of the additional radiometric considerations required for generating calibrated multispectral products.

3.6 Flight log analysis

After a completed mission, a thorough analysis of the flight logs (provided by nearly all autopilot systems) can provide additional measurements and can help inform future flight planning. Logs record time-stamped flight data such as image acquisitions, battery state, and airframe location and orientation. Such records allow identification of battery deterioration and estimates of wind speed (e.g. for fixed-wing vehicles, through comparison between GNSS-derived ground speed and the airspeed from a Pitot tube and, for hovering multirotors, from the roll and pitch orientation required to prevent drift of the airframe).

3.7 Incidents and failures

Being complex systems, UAS operations can and do go wrong, with underlying causes attributed to human error, mechanical, electrical, electronic or software failure, or to environmental conditions (or a combination of any or all of such factors). Issues experienced by the authors vary from the "fairly obvious if we'd thought about it properly or had more experience" to entirely unpredictable system failures, and all provide valuable lessons and experience (Table 4). Reducing the likelihood of failure requires training, experience and regular practice and system maintenance, and missions being carried out under minimum-risk conditions. The impact of incidents can be minimised by identifying issues in advance (e.g. during pre-survey on-site testing or by careful monitoring of system status during missions) and by ensuring that best practice deployment guidelines are followed, including the use of checklists.

Due to the nature of volcanic environments, low-

Table 4 – UAS incidents experienced by the authors.

Incident	Lessons learned
Piloting error (manual or automated)	
Whilst on autopilot, the aircraft suddenly started to oscillate out of control. We were able to land it by switching to completely manually piloted mode. This, and similar incidents have been attributed to on-board hardware failure or loss of or occlusion from GPS signal (e.g. flying close to or between large metallic structures).	Ensure that the pilot can fly manually if needed, and practice manual piloting procedures. Always use an experienced observer and use obstacle avoidance systems when available.
During a training flight, the trainee pilot and observer (trainer) were looking at the controller and not at the aircraft. When the observer looked up, the aircraft was already very close to a tree and an urgent avoidance command from the observer was not understood by the pilot, resulting in collision.	When training, the trainer should not be the observer too; train in areas free from obstacles such as trees.
Aircraft was accidentally flown into a hillside during first flight of an expedition.	Experience is needed to fully appreciate the difficulties of perceiving along-line-of-sight distances accurately. In unfamiliar terrain, familiarise yourself using sufficiently accurate topography data. Use terrain-enabled flight planning software where possible, but note the limited value of some topographic datasets (e.g. SRTM) unless flying >100 m above ground.
Aircraft modifications or payloads	
We strapped a hand-held SO_2 sensor to the landing gear… Shortly after take-off, the aircraft started vibrating, then drifted sideways and crashed into a tree, ultimately resulting in loss of the aircraft, camera and sensor.	Ensure that payloads are tightly secured with vibration-proof fixings.
A piece of tubing or rope under the aircraft came loose and hit a propeller, causing the propeller to break off completely. With only three propellers left, the aircraft spiralled downwards and pilot control could not be regained.	Secure payloads in a way that can not interfere with the propellers, and triple-check right before take-off.
When surveying ~1 km downwind from take-off, visual observers reported by radio that the aircraft (with payload) was struggling against strong winds in the upwind line directions. Survey was aborted with >50 % remaining battery (well before an automatic return to home would have initiated). The aircraft crawled home at max speed of 5 m s^{-1} and landed with <20% of battery remaining.	Automatic estimates of battery life may be substantial overestimates if custom payloads are used, particularly under windy conditions. Plan missions to take-off from the downwind side of survey block to facilitate aircraft return.
After successful previous long-range flights, a sensor payload was added. During aircraft return, strong headwinds and the extra aerodynamic drag from the sensor caused the drone to fly at a fraction of its normal ground speed. It ran out of battery and auto-landed away from us.	Particularly if pushing a UAS towards its endurance limits after a system change (e.g. addition of a new payload), incrementally build up to the final distance to fully explore UAS performance under the prevailing conditions.
Unexpected conditions	
A fairly large explosion took us by surprise and, before the aircraft could clear the area, a bomb hit either a propeller or the antenna. The aircraft began swerving and swirling rapidly, and the pilot could not regain control.	Avoid pressure to fly under sub-optimal conditions by including sufficient spare days during trip planning.
Within the crater, topographic shielding provided relatively benign wind conditions on the ground. However, after take-off, the aircraft ascended into the strong summit wind field and was taken into the crater wall.	Check wind forecast and assess conditions directly at site, keeping in mind that they can be highly variable in mountainous environments and forecasts will not include potentially strong local effects such as updrafts and turbulence. With rotor-based aircraft, if needing to descend quickly, avoid flying straight down within the prop wash.

Continued on next page.

Table 4: [cont.] – UAS incidents experienced by the authors.

Incident	Lessons learned
Unexpected conditions [cont.]	
When trying to descend from a volcano summit (~1500 m above the take-off point) the aircraft was significantly slower than during ascent, due to updrafts driven by topography and solar heating of the volcano flank. We only returned successfully by repeatedly moving fore- and backwards so that the tilt of the aircraft enabled more rapid descent, landing with ~5–10 % battery remaining.	Assess how accurately wind conditions can be estimated for the full flight path. Before operating larger vehicles, consider testing conditions thoroughly using a smaller (cheaper) aircraft. Note where any flight difficulties arise, and change or abort main mission flight plan as appropriate.
Miscellaneous	
The aircraft fell out of the sky mid-flight due to a total power failure. There were no warning messages or errors from the UAS at any time during the flight before failure. All pre-flight checks showed no issues with propellers, batteries or aircraft body. UAS was less than 6 months old and was returned to manufacturer, who were unable to determine the cause.	Sudden/unexplained equipment failures do happen. If field time is critical, have a backup UAS available if possible. Always ensure flights do not occur over people.
After take-off, the quadrotor aircraft hovered and would not start the mission plan or land; it had to be manually grabbed and an emergency motor shutdown command issued. Reliable functionality required reinstalling the ground station software and removing all previous mission information from the controlling tablet.	If using borrowed/shared equipment, flight test fully prior to each session to identify any changes that may have occurred due to automatic software updates or other user preferences etc.
Although battery initially appeared fine, during flight, battery level started to decrease more rapidly than expected, despite calm conditions. The mission was aborted and an immediate return to home and landing initiated. However, power failure led to an uncontrolled landing.	Ensure that a full flight and battery history is recorded, and batteries are used and stored appropriately. Prior to any flight, carefully consult the records for any recent anomalies. Battery failure can be very rapid, so replace batteries at the first indication of poor performance.
Crash during landing on an anchored ship: The aircraft was landed on deck by manual piloting to avoid issues with automated landing and drift of the ship since take-off. However, due to the motion of the boat, the aircraft did not recognise that it was safely landed and refused the command to turn off the motors. An emergency shut off was attempted but, in the process, the aircraft flipped and propellers were broken.	When operating from a boat, consider vehicle retrieval through catching by hand, rather than a landing command. Suitable only for the retrieval of small rotor-based aircraft.

risk missions (e.g. short, low-altitude surveys in warm, dry, and wind-free conditions) may be infrequent, and the benefits of any mission can be balanced against the potential risks such as loss of the vehicle. Having mission abort criteria that are defined before take-off and are continuously assessed in flight can help avoid encroaching into unacceptable scenarios. However, crisis management situations (e.g. surveys for emergency managers, observatory monitoring or forecasting needs) naturally increase the pressure to fly due to limited field access, amplified by the urgency of demands for observations and data. Under such conditions, the level of acceptable risk may be raised, for example, to enable night-time situational awareness observations through BVLOS missions, when conditions are otherwise dangerous for people. Communication with air traffic control and restrictions for crewed aircraft in operational areas are critical to being able to fly such missions safely, and when needed. During emergency operations, when UAS and crewed aircraft must share airspace, it is always necessary to have direct radio communication between all aviation users, as well as communicating flight plans with location and time of missions and with a pre-determined vertical separation of airspace. It should be noted that such communications themselves can be complex due to personnel with potentially different perspectives on the urgency of observations, field and aviation safety, and pilot fatigue.

In the USA, the Department of Interior agencies and the US Forest Service operate an Aviation Safety Communique (SAFECOM) database (https://www.safecom.gov/) to store reports of any issue with personnel, aircraft, circumstance, or conditions that has the potential to cause an aviation-related mishap (for occupied and unoccupied aircraft). A direct correlation has been found between the report-

ing of incidents, occurrences, and hazards which may impact aviation operations, and a reduction in mishap rate. The SAFECOM reports include a narrative that documents the issue as well as a corrective action; UAS users can search the database to learn from previous incidents and avoid issues that others have encountered.

4 Imaging and measurement applications

The synoptic views offered by aerial platforms, which provide image resolutions not possible from space and cover extents not accessible from the ground, result in many UAS missions acquiring imagery as either a primary or secondary data collection objective. Volcanology is no exception, and UAS-derived image capture (remote sensing) and direct measurement have provided valuable insight across a wide range of volcanic systems.

4.1 Lava flows, fissures and domes

Mapping and characterising eruptive fissures, lava flows, and lava domes is becoming increasingly common. The working environments involved are particularly challenging for ground-based data collection, with access on foot often not possible during activity, and being potentially dangerous for years afterwards due to loose and unstable surfaces. Only aerial approaches may be feasible to acquire detailed observations, but crewed helicopters, planes, or microlight aircraft may not be available at remote locations or during disasters and, with personnel on board, may have restricted access due to hazards such as airborne ash. Moreover, use of crewed aircraft requires reasonable advance planning and suitable meteorological conditions over the survey area and the approach route. During changeable weather conditions, UAS have the distinct advantage of requiring much shorter weather windows over much smaller areas within which to offer measurement opportunities.

4.1.1 *Crisis response*

One of the first uses of UAS during an effusive eruptive crisis was during the 2014–2015 Pāhoa eruption of Kīlauea volcano in Hawai'i. A team from the University of Hawai'i Hilo, located very close to the communities threatened by the flows, deployed UAS in coordination with the emergency response forces and supplied rapid information to civil defence. Post-analysis suggested that, for accurately forecasting pāhoehoe flow paths through such lowland tropical forest environments, optimal UAS imagery should enable DEMs with a resolution between 1 and 3 m [Turner et al. 2017b].

During the 2018 lower East Rift Zone eruption and summit collapse of Kīlauea volcano, UAS were routinely deployed for emergency response and scientific data collection tasks. The UAS provided continuous on-demand flight capability for situational awareness, tracking active lava flow fronts, overflows and caldera growth, gas monitoring with multi-GAS and DOAS, and assisting civil defence in identifying structures and people at risk [Diefenbach et al. 2018]. Real-time live-streaming video, rapidly uploaded field images, coordinates, and SfM-derived map products from the field were provided to emergency responders. During one incident, the UAS team identified a new outbreak of lava that was moving rapidly toward a residential area and notified emergency response of the immediate need for evacuation. UAS live-streaming video helped guide evacuation efforts and search teams to a stranded individual who was threatened by advancing lava flows. The individual was instructed to "follow the drone to safety" and was tracked as they moved through the jungle to meet the search teams*. DEMs and orthoimagery derived from daytime optical and night-time thermal surveys were particularly valuable for use during eruption response, especially for flow mapping and to update models of the changing topography for lava flow forecasting. Datasets collected at intervals of <1 hr to a week, at resolutions of 0.05–1 m over areas of 2–10 km^2 each, provided an unprecedented 4-D record of lava flow emplacement and caldera collapse over the three months of the eruption (Figure 5A). Rapid, low-quality processing using onboard RTK GNSS for georeferencing during the eruption provided products as quickly as possible, sacrificing higher resolution and accuracy for speed.

The UAS also provided an important tool for monitoring effusion rate changes. UAS acquired gimbal-stabilised overhead nadir videos along a defined set of channel site locations from the vent region to the zone of dispersed flow (10 km from vent) at intervals of hours to weeks. Particle velocimetry (PIVlab; Thielicke and Stamhuis [2014]) analyses of short (2–15 min) video segments provided timely measured flow rates within hours (Figure 5B). Results were then integrated with depth estimates to evaluate bulk flux through the channel at the vent, and within different flow branches [Dietterich et al. 2018]. These data enabled quantification of changing effusion rates (50–200 m^3s^{-1}) over the course of the eruption [Neal et al. 2019], an improved understanding of the driving forces of effusion rate fluctuation [Patrick et al. 2019], and provided a record of the down-flow evolution in channel dynamics. Such results were important for flow forecasting and assessing changes in activity for eruption response, in addition to representing a substantial dataset on lava flow emplacement.

UAS similarly enabled maps and lava volume es-

*For reports and video, see: https://www.usgs.gov/media/videos/k-lauea-volcano-uas-mission-aid-rescue, and https://www.doi.gov/aviation/uas/doi-uas-teams-supporting-volcano-monitoring-emergency-response-rescue

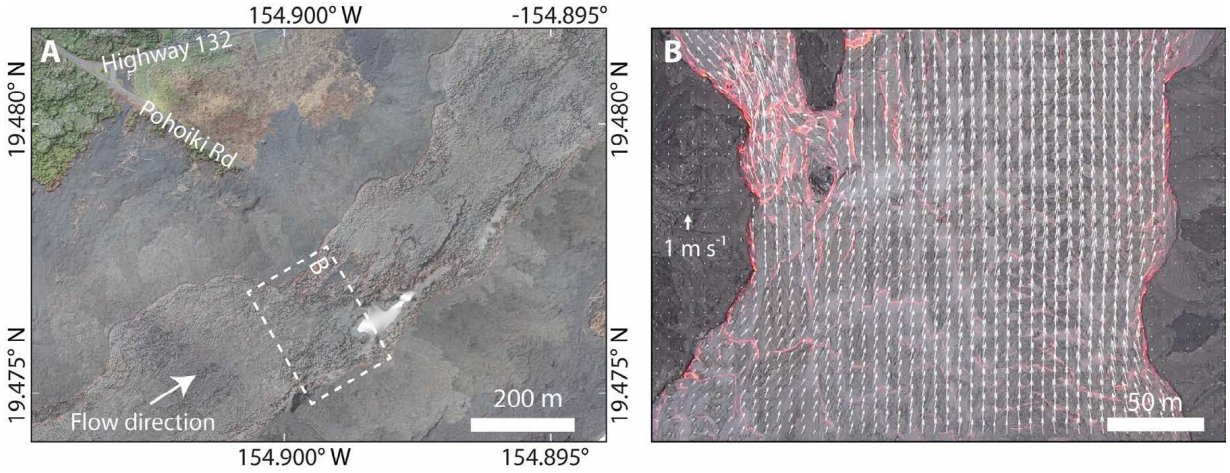

Figure 5: UAS imaging of active lava flows at Kīlauea volcano, Hawai'i. [A] Orthomosaic draped over a digital elevation model (DEM) of a section of the Fissure 8 channel of the 2018 Lower East Rift Zone eruption. UAS crew vehicles are visible on the road. Dashed rectangle outlines the location of [B], a segment of the Fissure 8 channel, overlaid by arrows indicating flow velocity magnitude and direction, computed using particle image velocimetry analysis on video acquired during UAS hover.

timates for supporting monitoring efforts during the 2017 eruption of Mt. Etna, Italy [De Beni et al. 2019]. Given the crisis, timely delivery of results (of order a day) covering >1 km^2 was prioritised over achieving high precision, so extensive ground control was not deployed. The issues encountered highlighted the importance of having sufficiently high quality pre-eruption baseline topographic data to enable surface-to-surface survey georeferencing when it was not feasible to distribute dedicated GCPs.

4.1.2 *Deposit mapping*

When mapping emplaced lava, spatial resolution usually takes precedence over temporal considerations, and UAS data can be sufficiently high resolution to provide insight into emplacement processes [Favalli et al. 2018]. For example, a UAS-derived visual orthomosaic (3-cm resolution) and DEM (20-cm resolution) covering 1.35 km^2 of the 1974 lava from Mt. Etna enabled mapping of sub-metre features such as folds, blocks and fractures. Spatial analysis of these results enabled parameterisation of structural, rheological and dynamic features and characterisation of different crustal regions across the lava surface that highlighted the fine structure of the flow's main channel. For example, the geometry, wavelength and amplitude of surface folding, can provide insight into rheological variations and the stress regime. For extensive, complex and spatially variable compound lava flow fields, recognizing important emplacement features and processes such as initial levee-formation, generation of lava channels and, eventually, lava tube formation, can be extremely valuable for lava flow hazard assessment and management [Favalli et al. 2018].

An alternative thermal-based approach to determining lava surface morphology has also been demonstrated using the rapid repeat capability of UAS surveys [Carr et al. 2019]. Four months after the 2018 eruption of Sierra Negra, Galapagos, repeat thermal imaging surveys captured the solar heating of the lava and tephra deposits over 3 hours following sunrise (Figure 6). The resulting time-series of 1 km^2 temperature maps (with 0.2 m resolution) was used to calculate heating rates proxies for surface roughness and grain size, which affect the relative thermal inertia for each pixel. The resulting heating rate map (Figure 6C) corresponds with the types of deposits, where the fastest heating rates represent the small particle sizes of tephra deposits, and the heating rate decreasing down the length of the lava as morphology transitions from pāhoehoe to channelised 'a'ā to blocky 'a'ā (slowest heating rate). Combined with measurements of surface roughness (Figure 6B), this method has the potential to be used to remotely characterise and classify lava flow morphology over expansive, difficult to traverse, terrain (Figure 6D).

The Icelandic 2014–2015 Holuhraun flood basalt eruption was sufficiently large (~85 km^2 [Gíslason et al. 2015]) that extensive UAS coverage was unfeasible. However, structural features and fractures could be identified through using a helikite and quadrotor UAS to provide high-resolution data of selected regions (e.g. <0.2 m per pixel over areas of up to 1 km^2 [Müller et al. 2017]). Over wider areas, the identification of larger features was also possible in terrestrial laser scanner (TLS) and satellite data. In combination, the results showed localised changes in fracture directions and offsets that may reflect geometric changes in the feeder dyke below [Müller et al. 2017]. The Holuhraun flow field also interacted with a river channel network and UAS enabled mapping of the hydrological impacts of the lava [Bonnefoy et al. 2017; Dundas et al. 2017].

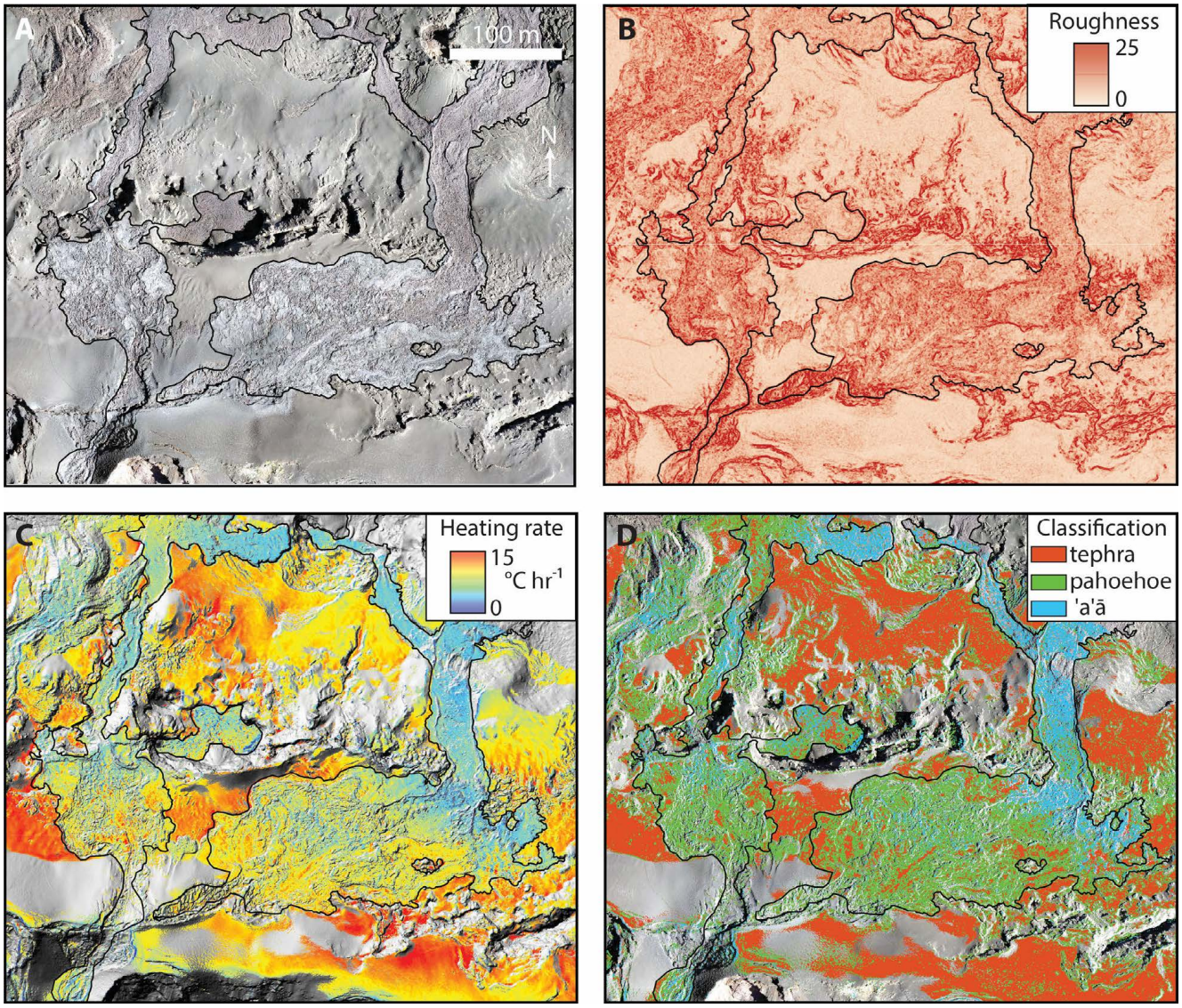

Figure 6: Remote classification of lava flow surface morphology using decimetric-resolution UAS data from Sierra Negra (Isla Isabela), Galapagos, Ecuador [Carr et al. 2019]. [A] A true-colour orthomosaic of a recent lava flow with both pāhoehoe and ʻaʻā morphologies, as well as tephra deposits. [B] Surface roughness (calculated as the standard deviation of DEM slopes in a 5 × 5-cell (1 m^2) moving window) and [C] the heating rate, derived from repeat thermal surveys, were used to identify typical values for each surface cover type and, hence, [D] remotely classify the distributions of eruption deposits.

For old, heavily vegetated, or buried lava deposits that cannot be directly observed, UAS-based magnetic surveying can facilitate mapping at sufficiently high spatial resolution to resolve structural details. For example, a UAS-derived magnetic map of partially buried volcanic cones in the Crater Flats distributed volcanic field, Nevada, USA, indicated that three different lavas, buried by desert alluvium, originate from one of the breached cinder cones (Figure 7; Rodgers et al. [2019]; Rodgers et al. [2020]). The magnetic results revealed lava lobes and channel structures, and enabled lava volumes and the emplacement sequence to be determined. Furthermore, comparing the magnetic data with the sub-aerial cone topography enables modelling of the internal structure of the cinder cones. A particular advantage of UAS platforms for aeromagnetic survey is that they facilitate repeated flight patterns at multiple elevations, enabling either the vertical magnetic gradient or the full 3-D field to be elucidated.

4.1.3 *Dome monitoring*

With lava domes usually forming in inaccessible summit regions and being associated with explosion or collapse hazards, UAS have proved advantageous for providing both timely and sufficiently high-resolution imagery to identify structural details such as fractures

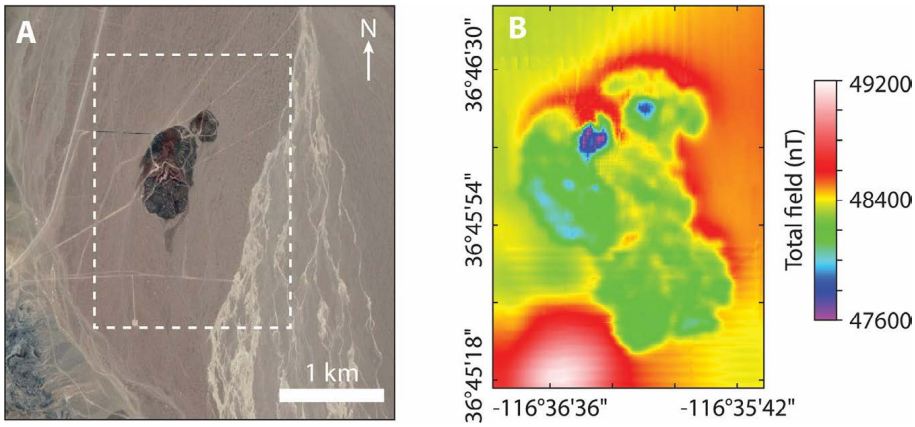

Figure 7: UAS magnetic survey data collected using a DJI Matrice 100 with dual triaxial fluxgate sensors (SENSYS MagDrone R3; Figure 1G). [A] Overview imagery (© 2020 Maxar Technologies, Google Earth) of the survey area (dashed box) of Little Cones, Amargosa Valley, Nevada, USA, illustrating the limited surface exposure of black volcanic rocks. [B] Interpolated magnetic map of preliminary field data prior to correction for UAS vehicle heading. Buried lava is revealed by the irregularly shaped central area of low total magnetic field (mainly green and blues) which result from the reverse polarisation of the volcanic rocks.

[Darmawan et al. 2018b] or rapid growth and collapse [von Aulock et al. 2016b; Watson et al. 2017]. For example, UAS-based visual images of the active lava dome at Mount Sinabung, Indonesia, resulted in SfM-based point cloud models (with data densities two orders of magnitude greater than those from an earlier ground-based survey [Carr and Lev 2018]). These data permitted estimates of the collapse volume removed from the dome and thus the corresponding volume, morphology, and grain size distribution of the resulting pyroclastic flow deposits [Carr et al. 2019]. At Mount Merapi, Indonesia, following the start of the current eruptive phase with an explosion in May 2018, a UAS enabled the first detection of dome growth in the summit crater (August 2018). Repeat UAS surveys have identified the growth of fracture networks and the excavated volume associated with phreatic explosions during 2012–2015 [Darmawan et al. 2018a]. The surveys enabled identification of areas of hydrothermal alteration and structural weakening along the dome structures, that may contribute to future instability and collapse (Figure 8A, B; Darmawan et al. [2018b]).

At consistently active domes, regular UAS survey results can be used to provide proximal observations of eruptions, assess dynamics, and integrate with other monitoring datasets. For example, visual and thermal UAS imagery have augmented seismic and geochemical data on Santiaguito volcano, Guatemala [Lamb et al. 2016]. Changes in the explosive and effusive activity at the dome and crater have been assessed using video and DEM construction to quantify eruptive behaviour, structural features, lava flow metrics, and ballistics distribution [von Aulock et al. 2016; von Aulock et al. 2016b]. At Santiaguito, UAS video footage of an explosion (see Supplementary Material) showed 20–30-m-long fractures, from which venting occurred during small outgassing events. These observations constrained inversions of acoustic infrasound signals and thus estimates of mass eruption rates during explosions [De Angelis et al. 2016]. At Volcán de Fuego, Guatemala, rapid extrusion rates of order 10^4 m^3 day^{-1} were measured in the days prior to a paroxysmal eruption on 1 March 2017, based on repeated photogrammetric UAS surveys of the growing dome (Figure 8C; Watson et al. [2017]).

4.2 Cones, craters and calderas

Volcanic cones, edifices, craters, and calderas are the continuously evolving results of both constructive and destructive processes. Studies of their morphology, structure, and composition can provide crucial information to understand the local geodynamic framework and volcanological settings, the style, frequency and evolution of eruptions, as well as the underlying magmatic and volcanic processes [Davidson and De Silva 2000; Kereszturi and Németh 2012; Lindsay 2015; Vespermann and Schmincke 2000]. The access provided by UAS enables measurement of areas that are otherwise not easily observable. These include vertical and overhanging walls—particularly difficult to view with the near-vertical lines of sight of conventional aerial or space-borne imagery—for which fully 3-D information can be acquired, augmented by video or thermal imagery if needed.

4.2.1 *Geological and geomorphological mapping*

UAS-based imaging with visible-wavelength or multispectral cameras enables classical geological remote

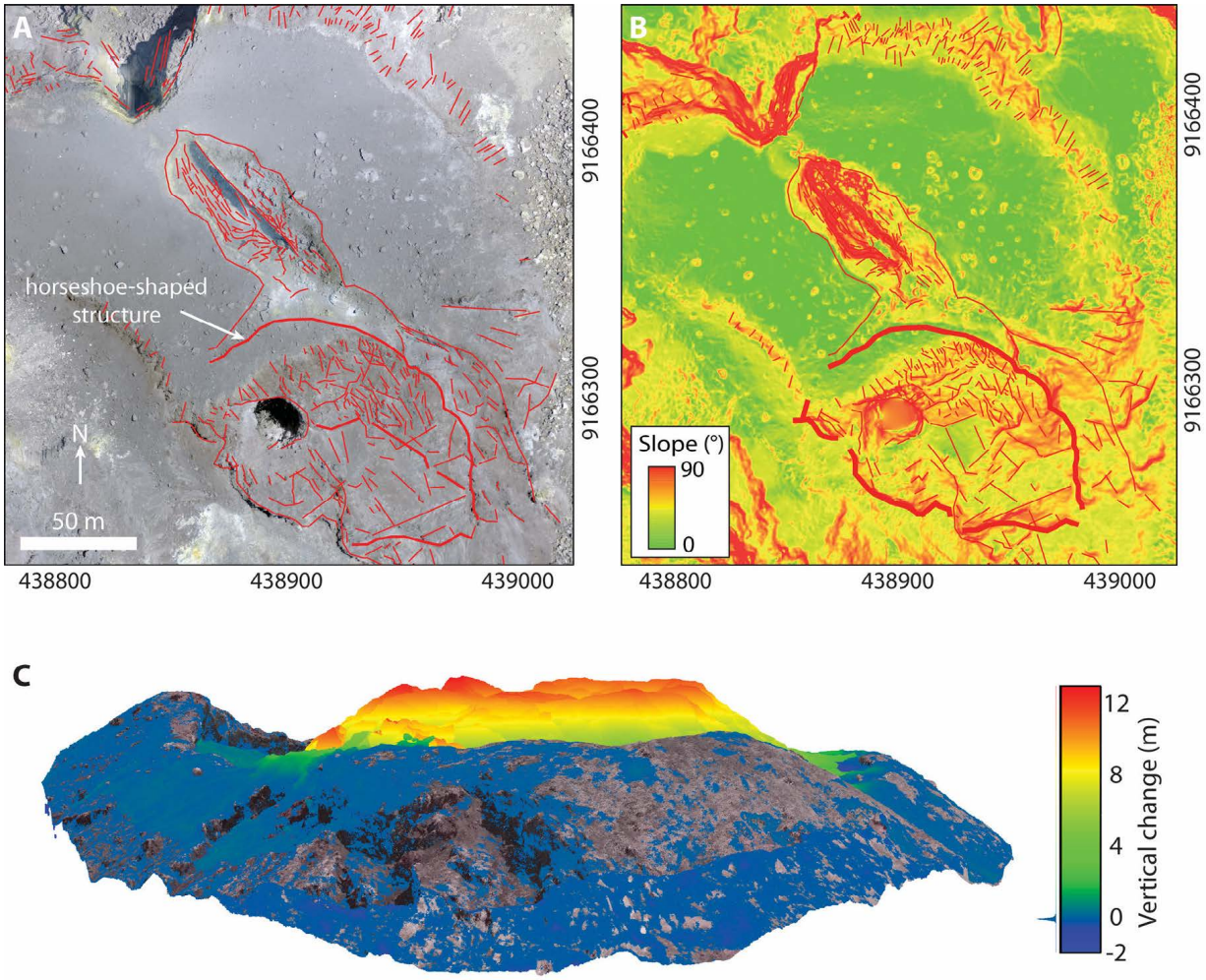

Figure 8: Lava domes surveyed by UAS. [A] and [B] The lava dome at Merapi, as mapped by combined UAS and TLS surveys (October 2015), showing a flat summit region, with highly fractured central fissure area, dome margins and southern flank. Red lines denote fractures and visible lineaments, and coordinates are in UTM. [A] Photomosaic of imagery collected by a DJI Phantom quadrotor from a height of 140 m above the ground. [B] Slope map from a 0.5-m-resolution DEM. The horseshoe-shaped structure bounds a fractured, southern-sloping region (descending >80 m at the map boundary) for which repeat UAS imaging in 2017 identified mechanical weakening, due to hydrothermal alteration at its northern boundary. Adapted from Darmawan et al. [2018b]. [C] Dome growth of Volcán de Fuego, captured by repeat flights of a DJI Phantom 3 Pro quadrotor in 2017 [Watson et al. 2017]. The oblique view shows two SfM-photogrammetry point clouds of the growing dome in the summit crater derived from imagery acquired on 19 (in true colour) and 23 (coloured by vertical change) February; the flat dome surface is approximately 40 m across. With GCP deployment not possible, the surveys were georeferenced using GNSS information embedded in the image metadata and their relative registration then refined using regions of unchanged surface on the flanks.

sensing techniques to be used to map features (e.g. magmatic intrusions, lava flows, pyroclastic deposits, faults and fissures) from derived data products. Primary output from SfM-photogrammetry processing is usually in the form of a coloured 3-D point cloud (i.e. a collection of points representing the 3-D surface), which does not have an inherent restriction for representing vertical and overhanging surfaces (unlike DEMs). Consequently, point clouds and associated textured meshes enable classification of steep or vertical surfaces using both 3-D textural and spectral information. As an example, dykes intruding volcanic tuff in the crater wall of Nyiragongo can be automatically identified and mapped from UAS-derived 3-D point cloud data (Figure 9). Extending such mapping over the whole crater would allow the detection of preferential orientations of magmatic intrusions and help decipher the complex history of the composite volcano. UAS-based imagery thus allows outcrop mapping at a level of spatial extent and detail that would not be

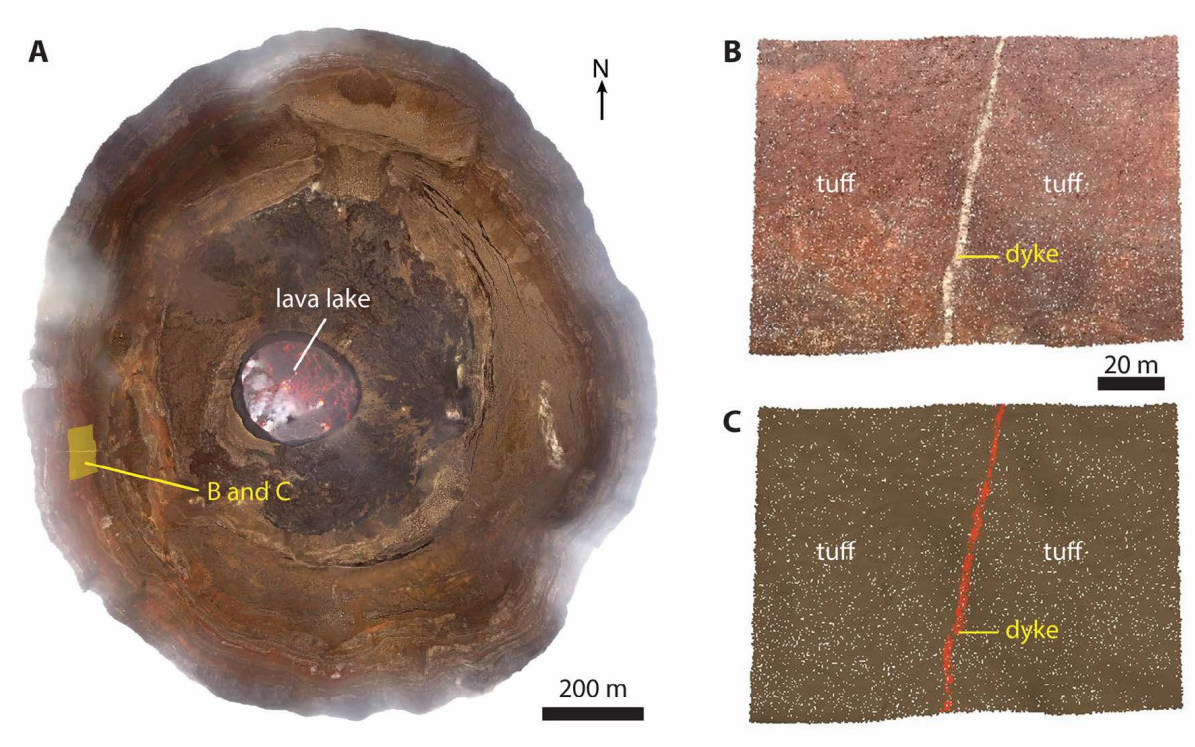

Figure 9: Example of dyke mapping on the SW inner flank of the Nyiragongo main crater, D. R. Congo, using RGB-based classification. Images collected by a DJI Phantom 4 quadcopter, with a ground sampling distance of ~10 cm. [A] Orthophoto of the main crater (August 2016), with the location of the target area shown in B and C. 3-D point cloud of the target area, [B] in true-colour and [C] classified into volcanic tuff (brown) and the nephelinite dyke (red).

possible using traditional field techniques [Dering et al. 2019], with structural information (e.g. dip magnitudes and orientations, and preferential alignments of faults, joints, dykes or strata) being extracted with increasingly automated methods from orthomosaics and DEMs [Dering et al. 2019]. The widening use of SfM-photogrammetry is driving parallel advances in analysis tools for 3-D point clouds (e.g. CloudCompare software `www.cloudcompare.org`, with plugins such as Facets [Dewez et al. 2016] and Compass [Thiele et al. 2017a] relevant to structural and morphological analyses).

UAS-based geophysical surveys can also be used for subsurface imaging of crustal geological features, with lower altitude deployments providing better signal-to-noise ratio and spatial resolution than from conventional survey aircraft. In addition, the lower cost of UAS surveys compared to crewed aircraft campaigns facilitates affordable time-series measurements, potentially opening up opportunities for detecting subsurface process dynamics. For example, a UAS-based aeromagnetic survey of Izu-Oshima volcano caldera, Japan, detected anomalies interpreted as putative dykes, hot magma, and cavities [Kaneko et al. 2011]. At Shinmoedake volcano (Kirishima, Japan) active magma pathways and magma cooling was detected following the January–April 2011 eruption, by comparing two aeromagnetic surveys acquired in May and October–November 2011 [Koyama et al. 2013].

At active eruption sites, UAS imagery enables mapping of vents, fumaroles, and active fissures and faults. Such maps permit the study of feature characteristics and distribution, including the dimensions of bombs [e.g. Konagai et al. 2016; Müller et al. 2017; Turner et al. 2017a]. 3-D topographic data allow detection of centimetre- to metre-scale topographic changes associated with ground deformation, accumulation of volcanic products and crater collapses, and quantification of the volumes involved (Figure 10). During the 2018 eruption of Kīlauea, Hawai'i, one of the primary missions of the United States Geological Survey (USGS) UAS team was mapping and measuring the collapse of the summit caldera, which occurred as the magma reservoir beneath it drained to supply the lava flows erupting in the lower East Rift Zone. Repeated flights resulted in 0.5-m-resolution DEMs and centimetre-resolution orthomosaics spanning 8–12 km^2 and quantification of topographic change at the summit area (Figure 10D, E; Diefenbach et al. [2018]). The USGS, the National Park Service, and civil defence were able to use these observations to track the rate of volume change with implications for understanding eruption

duration, as well as to identify unstable regions, new fractures and collapse locations, and their impact on nearby infrastructure.

4.2.2 *Mass movement and erosion processes*

Mass movements affect volcanic edifices over a variety of spatiotemporal scales ranging from edifice-scale flank instabilities and catchment-scale lahars to continuous surface erosion and individual block collapse. High resolution UAS imaging enables potential slip surfaces to be detected, volumes of vulnerable or displaced material to be determined, and areas of slow slip or creep identified. Events can be characterised, mechanisms determined and consequences quantified, e.g. debris flows and rock falls detected in the Nyiragongo main crater (Figure 11; Smets [2016]). Flow modelling can be highly sensitive to channel morphology, which can be one of the most difficult areas to assess from satellite imagery. Although mapping an entire edifice drainage system by UAS alone represents a considerable challenge, fusing DEMs from various sources (e.g. satellite, ground-based, and UAS) enables the production of composites that have the required coverage and resolution in these critical morphological areas [Deng et al. 2019].

4.2.3 *Geothermal systems*

Mud volcanoes, geysers, and fumaroles are dynamic surface expressions of geothermal systems that can change frequently and unpredictably in terms of their thermal output, degassing, and topography. The spatial distribution of such features is often clustered and related to local fractures and permeability contrasts (Figure 12). Due to high temperatures, strong degassing and muddy water, ground-based access to these sites is often challenging. UAS enable detection of fine structures, temperature anomalies, degassing and associated topographic features, often by observing from only a few metres above their targets. The quality and resolution of such measurements help to improve understanding of the heat source driving the system, the dynamics of heat and fluid flux associated with seasonal variations, and of changes in the shallow hydrothermal system potentially triggered by remote sources such as tectonic earthquakes. The types of useful UAS applications range from acquiring aerial photo perspectives of the ground [Zimmer et al. 2017], photogrammetric and geophysical assessment [Glen et al. 2012; Harvey et al. 2016] to infrared detection of thermal anomalies [Amici et al. 2013a; Walter et al. 2018a], gas plume measurement traverses [McGonigle et al. 2008; Pieri and Diaz 2015], and rock or water sampling [Di Stefano et al. 2018].

Visual photographs from UAS at geothermal sites and derived orthomosaics and DEMs provide valuable overviews of complex geothermal fields [Harvey et al. 2016; Zimmer et al. 2017] for field mapping, mission planning and identification of sites of degassing and hydrothermal alteration [Darmawan et al. 2018b]. The aerial perspective shows the spatial distribution of sub-metre-sized degassing features, mud pools, and fumaroles in a regional framework (e.g. Figure 12; Walter et al. [2018a]). Repeat surveys can reveal topographic change but, with the evolution of geothermal fields often being relatively slow, intervals of a few years may be required for change magnitudes to exceed measurement uncertainties.

For geothermal areas, thermal imaging via UAS has been used to record temperatures in places inaccessible from the ground [Amici et al. 2013a] and, through similar application of SfM-photogrammetry as for visual images, create high-resolution georeferenced temperature maps (Figure 13; [Di Felice et al. 2018; Harvey et al. 2016; Walter et al. 2018a]). Consumer-grade quadrotor systems (e.g. DJI's Phantom), equipped with an infrared camera (e.g. FLIR Tau), are suitable for mapping the temperature, appearance and location of geothermal features [Di Felice et al. 2018; Harvey et al. 2016; Walter et al. 2018a], and enable changes in apparent temperature and location to be monitored [Nishar et al. 2016]. However, the temperature, size, and temperature variations of geothermal features are often much smaller compared to the general trends and patterns observed in volcanic systems, which increases the importance of accurate temperature and spatial calibration of the data products. Various methodologies to address these issues and quantify error are described at length in Harvey et al. [2016], Nishar et al. [2016], Chio and Lin [2017] and Di Felice et al. [2018].

The detail provided by high-resolution thermal image products can help quantify the dynamics of geothermal systems. For example, a DEM (with comparable accuracy to lidar surveys) and a calibrated thermal orthophoto enabled calculation of the total heat loss of 43 ± 12 MW for 2.2 km^2 of thermal lakes and streams in the Waikite geothermal area, New Zealand [Harvey et al. 2016]. At the LUSI mud volcano (East Java, Indonesia), multiple years of UAS surveys indicated a generally consistent heat flux of ~700 W m^{-2} from the vent area, and concentric temperature patterns mapped around the vent enabled identification of convection cells in the shallow subsurface (Figure 14; [Di Felice et al. 2018]).

4.3 Volcanic plumes

Volcanoes and geothermal areas are often associated with persistent plumes that ascend from source regions (either main magmatic vents or subsidiary fissures and fractures) before dispersing downwind. Plumes emitted during passive, effusive, and explosive activity, are composed of variable amounts of volcanic gases (mainly H_2O, CO_2, and SO_2), and silicate ash and aerosols, depending on pre-eruptive magmatic pro-

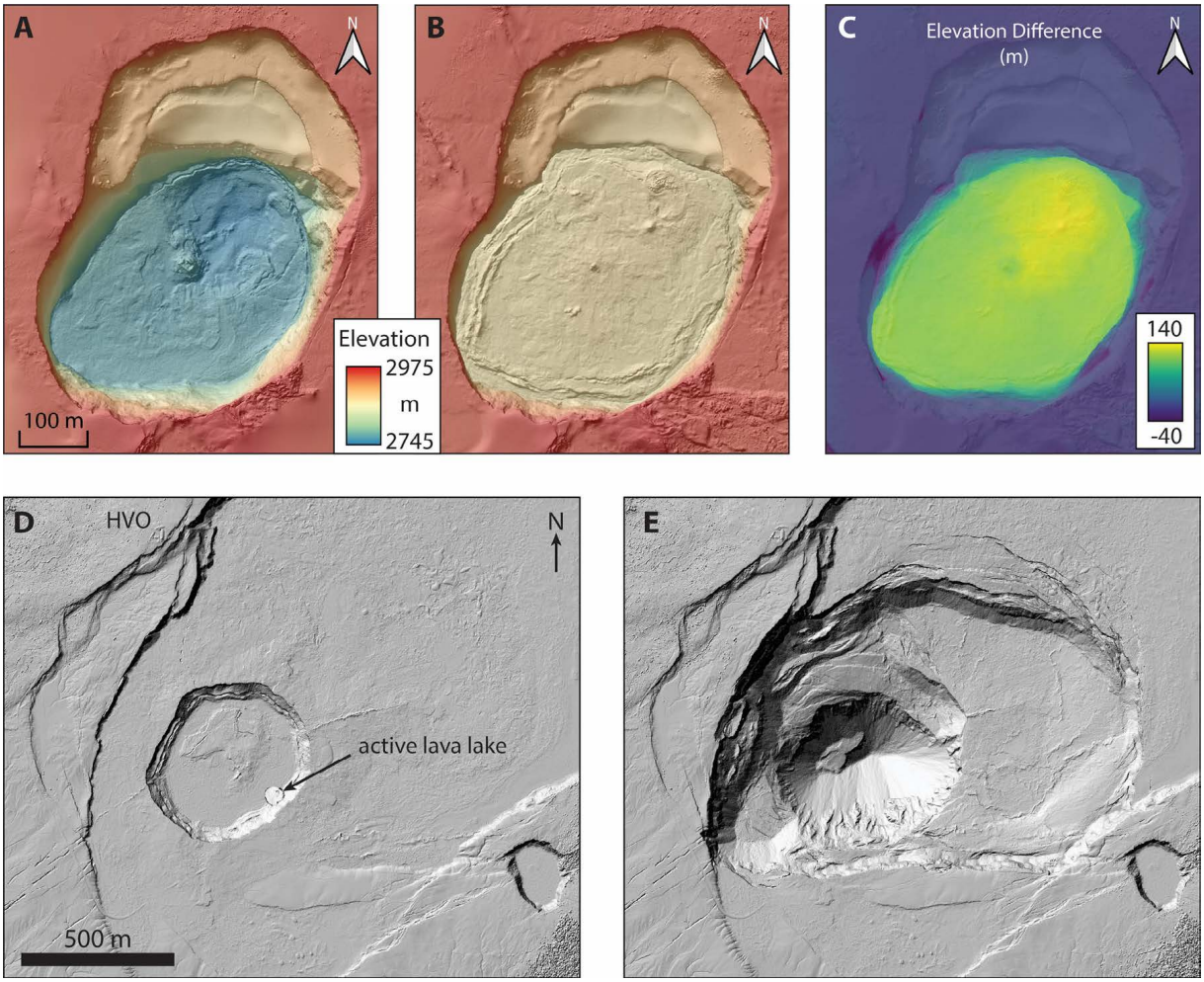

Figure 10: Topographic change due to crater filling [A–C] and caldera collapse [D–E]. 8-cm resolution DEMs of the pit crater in the NE part of the Nyamulagira summit caldera, D. R. Congo, in [A] June 2017 and [B] October 2018, capture an elevation change [C] due to a lava accumulation of ~2.3 × 10^6 m^3 [Smets et al. 2018]. DEMs were derived from SfM-based photogrammetry, with images captured using DJI Phantom 4 (2017) and 4-PRO (2018) quadcopters. Reproduced from Smets et al. [2018]. The summit caldera collapse at Kīlauea, 2018, is illustrated by shaded relief images from a [D] 2009 LiDAR survey (1-m resolution) and [E] post-collapse UAS photogrammetry survey (11 August 2018, 15-cm resolution). HVO marks the Hawaiian Volcano Observatory buildings and infrastructure, now closed. UAS surveys provided unprecedented monitoring of caldera growth including sequential DEMs bracketing a single collapse event. The summit underwent ~825 × 10^6 m^3 of volume loss (~12.4 × 10^6 m^3 per day), with maximum subsidence exceeding 500 m in the central part of the caldera [Diefenbach et al. 2018].

cesses and syn-eruptive dynamics [Carey and Bursik 2015]. The quantification of gas emissions in terms of both composition and flux is critical to volcanic hazard assessment, through the identification of geochemical eruptive precursors (e.g. in gas ratios such as CO_2/SO_2), and for constraining regional and global volatile budgets at actively degassing volcanoes [e.g. Aiuppa et al. 2017b; Burton et al. 2013]. The importance of frequent, regular measurements is underscored by abrupt changes in gas composition occurring immediately prior to significant shifts in eruptive behaviour, such as the initiation of large 'paroxysmal' eruptions [Aiuppa et al. 2017a; Aiuppa et al. 2007; Werner et al. 2013], or as precursors to otherwise unanticipated phreatic/phreatomagmatic eruptions [de Moor et al. 2019]. UAS equipped with miniaturised gas sensing instrumentation (see Subsection 2.2.3; Figure 2A, Figure 15) are now bridging the gap between direct measurements and remote sensing observations, enabling repeatable, proximal measurements from ranges >5 km [Di Stefano et al. 2018; Diaz et al. 2015; Kazahaya et al. 2019; Liu et al. 2019; Mori et al. 2016; Pieri et al. 2013a; Rüdiger et al. 2018; Schellenberg et al. 2019; Shinohara 2013; Stix et al. 2018b; Syahbana et al. 2019; Xi et al. 2016].

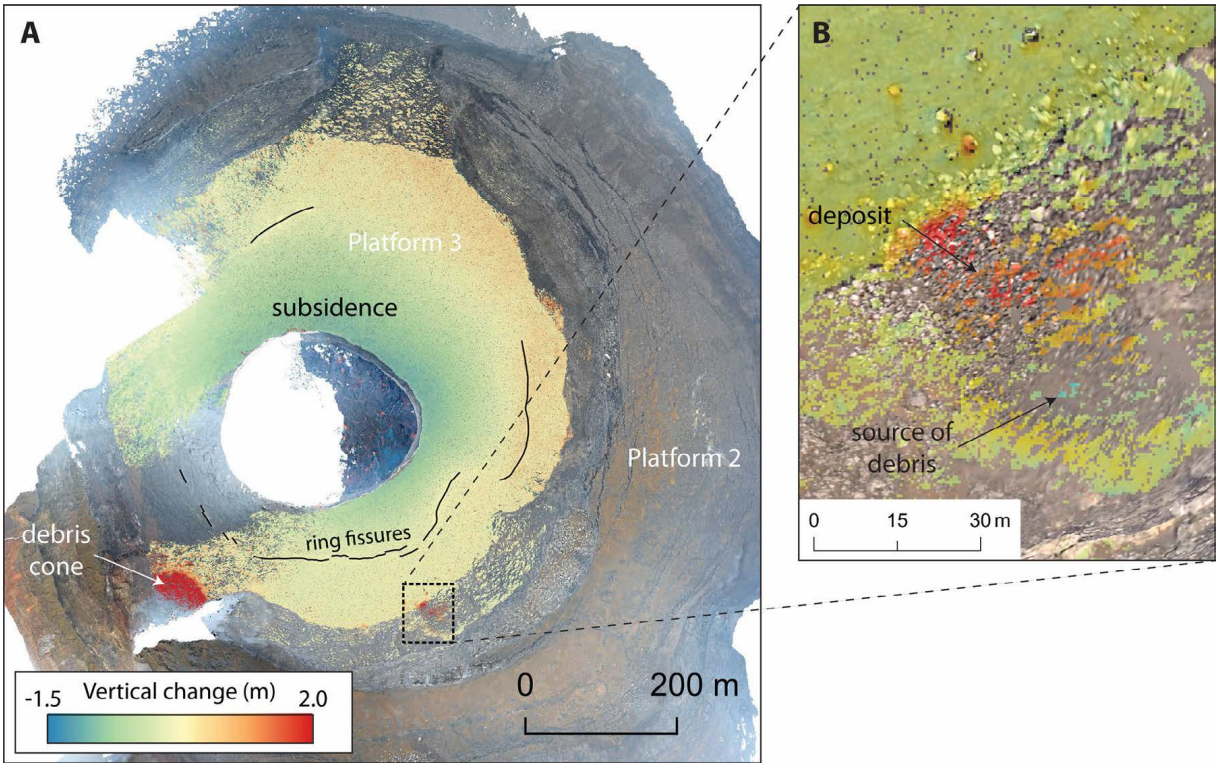

Figure 11: Topographic evolution of the Nyiragongo main crater, D. R. Congo, between March 2013 and July 2014, based on images collected with Nikon D3 and Nikon D7000 cameras, during helicopter and UAS flights. The ground sampling distance is ~30 cm. [A] Point cloud difference superimposed on the July 2014 crater orthophoto. Topographic changes include a ground subsidence associated with a long-term lava lake level drop during that period and cones of debris located at the foot of gullies and cliffs. [B] Enlargement of a cliff region between Platform 2 and 3 in the crater, with evidence of the fallen debris deposit and its source area. Reproduced from Smets [2016].

4.3.1 *Degassing rates*

The determination of SO_2 flux based on differential optical absorption spectroscopy (DOAS) plume traverses is well-suited to UAS deployment. The aerial approach not only reduces the measurement distance to the plume, thus minimising scattering errors, but also removes the constraint of having to follow roads or paths, which can limit ground-based surveys. Flexibility to select an optimal transect on a flight-by-flight basis is especially advantageous in regions where wind fields vary on timescales of hours to days. At Turrialba volcano, Costa Rica, SO_2 concentrations measured by UAS in the dilute distal plume (0.3–20 ppm SO_2, up to 3 km from the vent) were used to derive estimates of SO_2 emission rates using an inverse Bayesian modelling approach that incorporated meteorological wind fields [Xi et al. 2016]. When calculating flux values, the greatest errors usually stem from the assumed plume velocity [Burton et al. 2009; Conde et al. 2014], which is often extrapolated from ground-based wind speed measurements. By enabling wind speed measurements at plume altitude and thus, critically, accounting for low altitude topographic controls on local wind fields, UAS approaches have been able to address one of the most significant sources of uncertainty in SO_2 flux calculations [D'Arcy et al. 2018; Stix et al. 2018b].

4.3.2 *Near-vent measurement*

Simultaneous measurements of CO_2/SO_2 molar ratios by UAS and proximal ground-based instruments highlight that, although time-averaged ratios agree well, plume dilution and homogenisation rapidly reduces the temporal fidelity of degassing time series and results in larger uncertainties on ratios obtained in more distal plumes [Liu et al. 2019; Pieri et al. 2018; Rüdiger et al. 2018]. Accounting for plume dilution and entrainment processes between source and detection is critical to the correct interpretation of measured gas ratios [Chosson et al. 2008; Kelly et al. 2013; von Glasow et al. 2003]. Furthermore, early 'aerial' attempts to measure CO_2/SO_2 molar ratios by traversing instruments through a plume along a metal cable over a vent, revealed significant differences to measurements taken at the crater rim, due to excluding contributions from soil gas and fumaroles [Giuffrida et al. 2015]. At Villarrica, Chile, UAS-derived SO_2 concentrations mea-

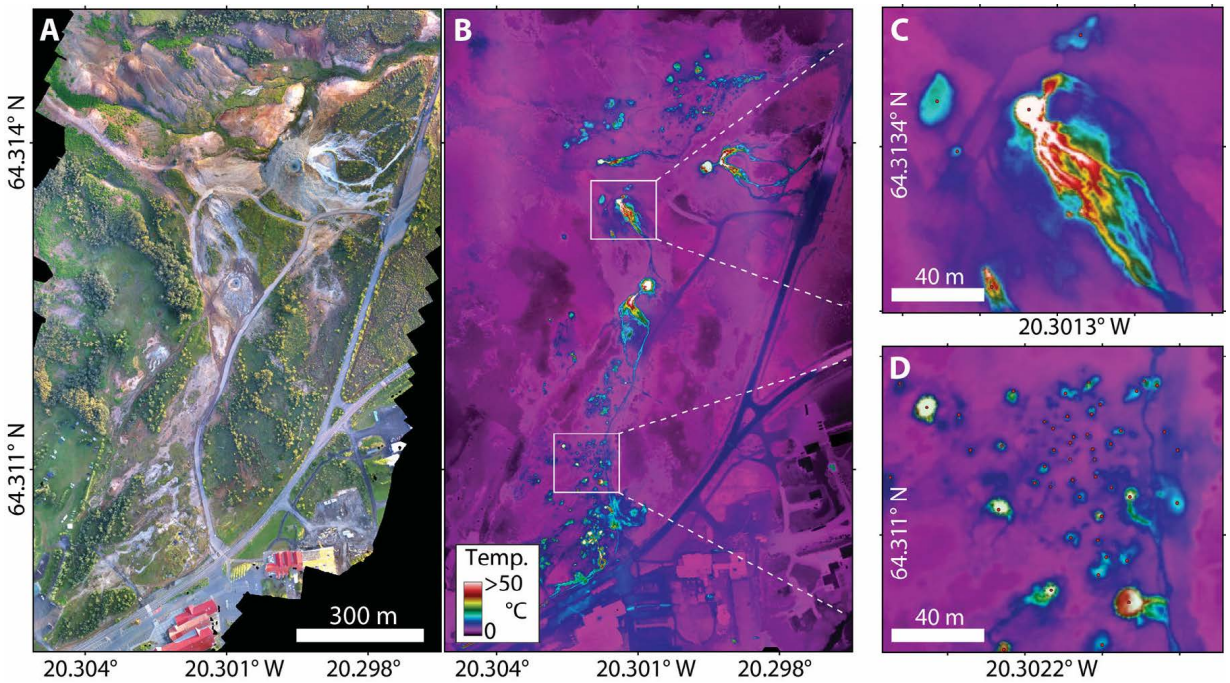

Figure 12: Thermal and visible-wavelength imaging identifying hot-pot features within the Geysir geothermal field, Iceland [Walter et al. 2018a]. The results represent example regions from full datasets of >7000 infrared and 1500 visible-wavelength images covering ~1.01 km^2, collected from 80–140 m above the ground with a DJI Matrice 100 multi-rotor UAS. [A] Visible-wavelength orthomosaic from imagery collected with a DJI Zenmuse X5R. [B] The same region as a thermal orthomosaic (with boxed areas enlarged in [C] and [D]), from imagery collected under atmospheric temperatures of ~2 °C (03:00 local time), with a FLIR Tau 2 (giving a mean GSD of ~17 cm).

sured whilst hovering directly over the central vent (<120 ppm) were found to be an order of magnitude greater than measured at the crater rim after only 150 m of downwind transport (<10 ppm). The degassing time series exhibited regular cyclicity on timescales of 30–50 s (i.e. from bubble bursts at the lake surface) that was entirely absent from the crater-rim time series (Figure 16; [Liu et al. 2019]). Quantification of cyclicity in volcanic outgassing, particularly over timescales of seconds to minutes, provides valuable insights into the fluid dynamics and permeability of shallow magmatic systems [Lev et al. 2019; Moussallam et al. 2016; Pering et al. 2019]. The enhanced temporal resolution of proximal UAS sampling, coupled with the more limited opportunity for overprinting of the signal by atmospheric processes, enables identification of short timescale periodicity that might otherwise be missed.

4.3.3 *Supporting monitoring during unrest and activity*

Reactive deployments of UAS-based instrumentation are increasingly integrated into volcano monitoring procedures. They maintain continuity in time-series data when ground-based stations are rendered non-operational due to volcanic activity (e.g. Poás volcano, Costa Rica [de Moor et al. 2019]) and/or complement simultaneous ground measurements (e.g. 2018 Kīlauea eruption [Mason et al. 2019; Nadeau et al. 2018; Neal et al. 2019]). Following the 2014 eruption of Mt Ontake, Japan, UAS gas measurements flown from outside the 1–2 km exclusion zone revealed a dominantly hydrothermal degassing source (low SO_2/H_2S molar ratios, combined with SO_2 concentrations <1 ppm). This indicated a phreatic origin for the explosive activity [Mori et al. 2016]. Similarly, during a period of unrest between 2014 and 2016 at Kuchinoerabujima volcano, Japan, airborne Multi-GAS measurements using UAS documented a decline in SO_2/H_2S molar ratio from 10 in December 2014 to 1.9 in March 2016 [Kazahaya et al. 2019]. This gas ratio time-series reflected progressive conduit sealing and a return to a background degassing regime characterised by strong hydrothermal interaction [Kazahaya et al. 2019]. The work also combined UAS surveys with conventional aircraft flights and found the UAS platforms to be more spatially versatile for plume measurements [Kazahaya et al. 2019].

5 Sample retrieval and instrument deployment

Sample collection is arguably at the forefront of UAS applications in volcanology, with samples including

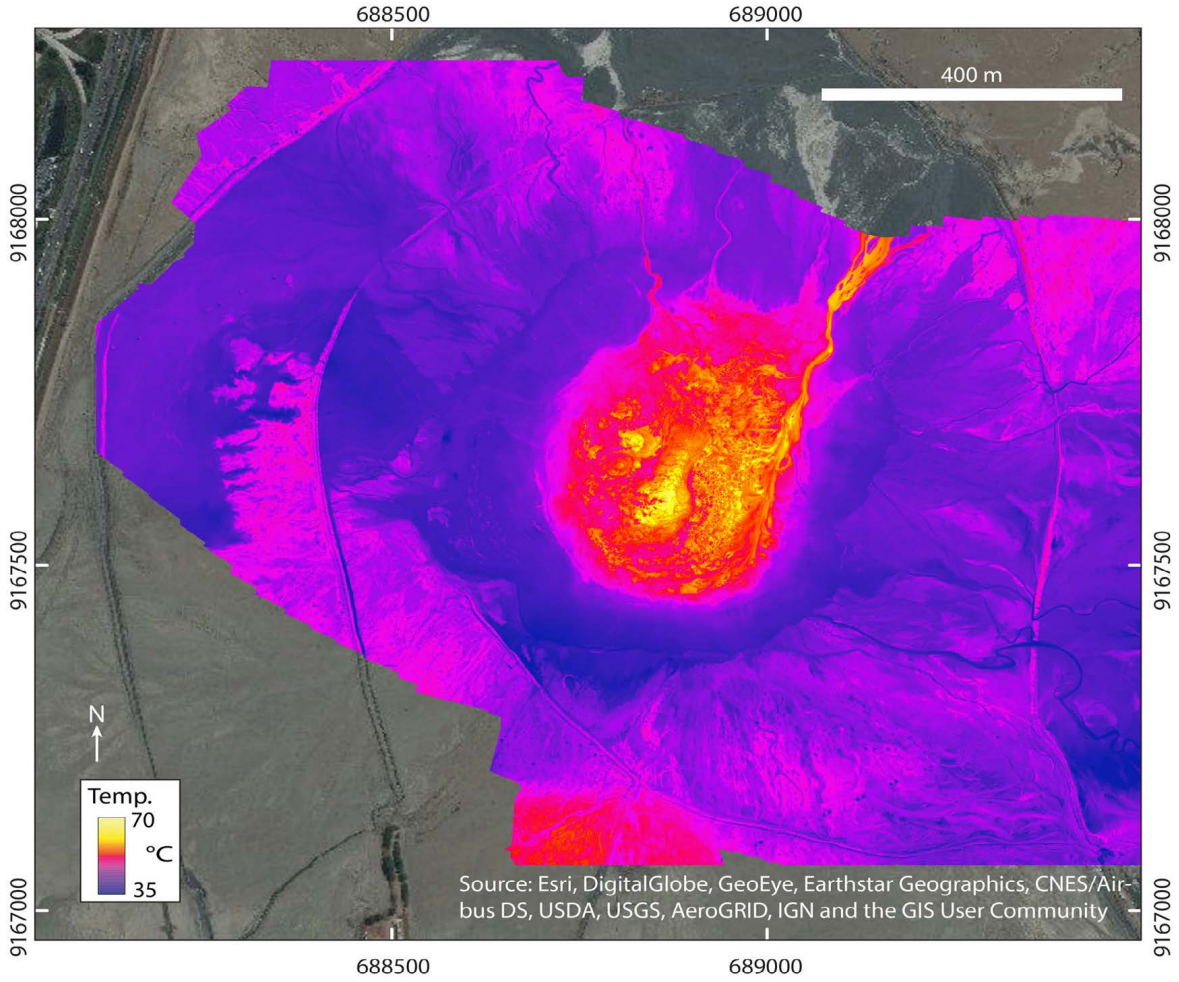

Figure 13: A thermal orthomosaic of the LUSI mud volcano collected by a DJI Matrice 210 in 2018, superimposed over web-sourced visible-wavelength imagery. The thermal data (approximately 445 images) were collected with a DJI Zenmuse XT from ~200 m above ground. The final orthomosaic (DOI: 10.5069/G9Q81B6D) has a spatial resolution of 0.3 m, and shows the ~300-m-diameter hot central area surrounding the vent region, and associated warm outflow channels.

gas, water, and ash retrieved for detailed laboratory geochemical and other analyses.

5.1 Volcanic gas sampling

Sampling volcanic gas is perhaps the most challenging of all direct sampling techniques due to the dynamic nature of plumes. While portable instrumentation enables *in situ* analysis of gas concentrations, other geochemical analyses—such as stable isotope analysis of CO_2—are only possible using laboratory-based instruments, so require the return of a physical sample that is chemically isolated from the atmosphere (Figure 17). Samples of several hundred millilitres are usually necessary to obtain accurate isotopic ratios, requiring pumped sampling over several tens of seconds. Traditional ground-based methods of direct sampling involve filling glass vials or bottles from fumaroles [Giggenbach 1996] but, more recently, lightweight Tedlar® or ALTEF gas bags (Figure 2A) have also provided adequate sampling volumes from horizontally dispersing dilute ground-level plumes [Malowany et al. 2017] or high altitude plumes by airborne sampling from a helicopter [Fischer and Lopez 2016]. A dilute ascending plume at Stromboli volcano has also been successfully sampled using such bags deployed via UAS [Stix et al. 2018a]. These various sampling approaches enable the reconstruction of volcanic CO_2 $\delta^{13}C$ values by extrapolating back to the source composition using a Keeling plot populated with a range of mixing fractions with the background air [McGee 1992]. While development of this technique using UAS

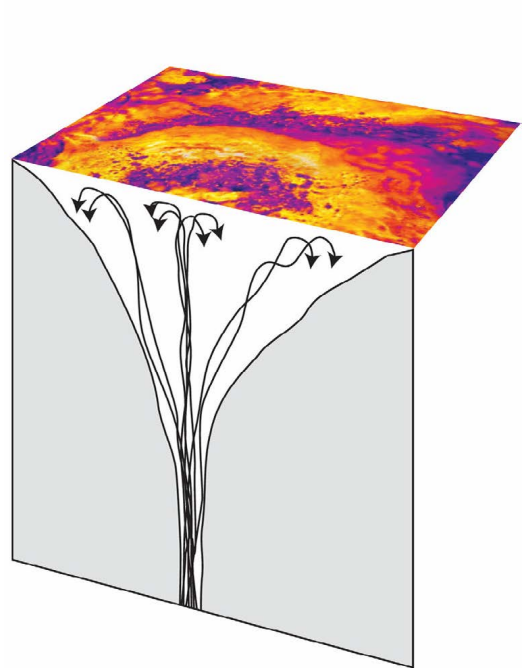

Figure 14: A thermal orthomosaic (2015) of the crater area of the LUSI mud eruption, projected on a 3-D cartoon depicting the envisaged subsurface convection cells (not to scale). The concentric rings observed in the central zone illustrate hotter regions (orange and yellow) alternating with colder (purple colour) areas. Diameter of the clear hotter ring is ~100 m. Data were acquired with a FLIR I7 thermal camera mounted on the LUSI drone (a DJI Spreading Wings S800 hexacopter [Di Stefano et al. 2018]). Redrawn from Di Felice et al. [2018].

is ongoing, there is no doubt that past studies on carbon isotope systematics in volcanic and geothermal areas [Hilton et al. 2010; Lucic et al. 2014; Venturi et al. 2017] highlight the potential.

5.2 Airborne particulate (ash and aerosol) sampling

Particulate material within volcanic plumes is usually dominated by silicate tephra (ash and scoria), with the smallest size fractions (aerosol) also comprising halides and their trace element compounds. The capability for particle sampling within plumes provides an interesting comparison to established methods for reconstructing in-plume ash size distributions from ground-based samples and theoretical particle settling laws [Schellenberg et al. 2019] and for understanding in-plume chemical reactions related to aerosol condensation and deposition [Mason et al. 2019]. The composition and size distribution of volcanic aerosol in the near-vent plume of Fissure 8 during the 2018 eruption of Kīlauea, Hawai'i, was measured using optical particle counters (OPCs) and sampled with aerial filter packs [Mason et al. 2019]. These samples provide a valuable source composition to inform interpretation of ground-based samples acquired downwind, and thus determine rates of sulphur-to-sulphate conversion and aerosol deposition [Mason et al. 2019]. For the coarser fractions of silicate ash particles, grain size distributions can only be determined by the return of a representative sample for laboratory analysis (which also permits geochemical and petrological study). Adhesive-based collectors were used to obtain a bulk sample of ash from the plume producing by small Strombolian explosions at Volcan de Fuego, Guatemala [Schellenberg et al. 2019], although further work is needed to prevent fractionation of the particle size distribution during sampling. Obtaining ground-based samples after large eruptions is relatively straightforward, but such sampling is more challenging for smaller events with a reduced fallout area, and particularly for phreatic and phreatomagmatic eruptions with little juvenile material output. However, obtaining ash samples from the full spectrum of eruptive intensities is arguably critical to reconstructing the contrasting pre-eruptive conduit conditions prior to different eruptive styles, and thus understanding effusive to explosive transitions in more detail.

5.3 Water and sediment sampling

The association of crater lake systems with phreatic explosions, as well as their usually inaccessible locations, highlights the applicability of remote sampling to such an environment. Crater lake chemistry can be crucial for detecting changes in magmatic degassing prior to and during eruptive phases, through variations in rock-forming elements, anion and cation concentrations, stable isotopes of water, and pH [e.g. Agusto et al. 2017; Hernández et al. 2017; Rouwet et al. 2017]. With lakes and geothermal waters potentially being acidic or capable of eruption, close sampling may be limited for the protection of the vehicle, with sampling carried out via long-distance holders, ropes, and/or winches [Di Stefano et al. 2018; Terada et al. 2018]. For example, a water sampling bottle (Figure 2B) tethered 30 m below a multi-rotor was used to successfully collect 250 mL from Yugama crater lake without the requirement for a heavy winch (Figure 18A; [Terada et al. 2018]). The rope tether not only maintained the aircraft at a safe distance from the lake surface during sampling, but also allowed an observer to secure the sample prior to landing.

At Kīlauea, following the 2018 eruption and summit collapse, UAS surveys have been employed (Figure 18B) to collect water samples for chemical and isotopic analyses from the growing summit crater lake within Halema'uma'u. A hydrasleeve (water sample bag) and temperature probe payload is attached to the hexacopter (DJI M600 Pro) via a ~7.5 m paracord, marked by different coloured ribbon at ~1.5 m intervals, with a release mechanism enabled through the

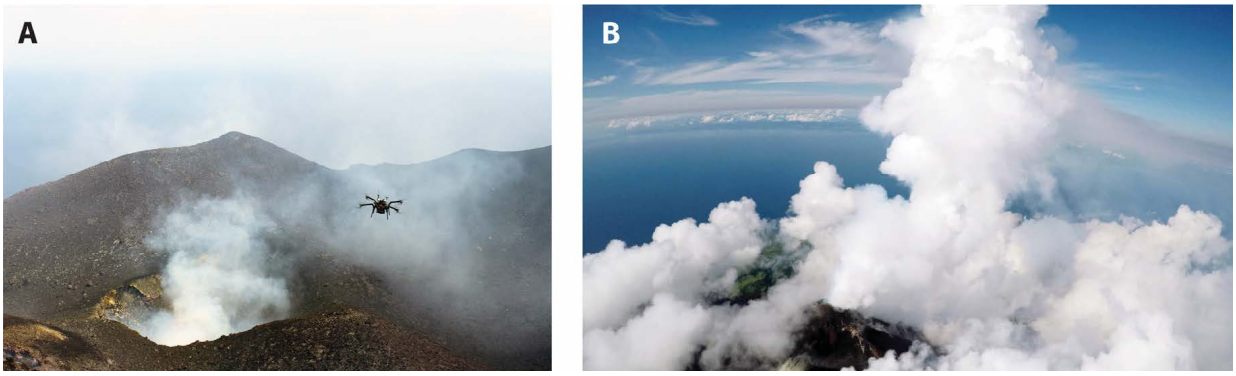

Figure 15: Aerial gas measurements using drone-mounted Multi-GAS analyser. [A] Short-range but long time-series measurements using multi-rotor platform at Stromboli, Italy, in June 2017, and [B] long-range but short time-series measurements using fixed-wing platforms at Manam, Papua New Guinea, May 2019.

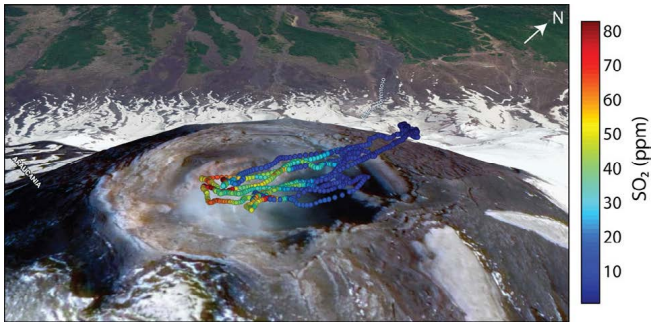

Figure 16: Aerial survey of gas concentrations in the volcanic plume of Villarrica, Chile (20 March 2018); for scale, the crater rim is ~200 m in diameter. Data acquired using a multi-rotor UAS mounted with Aeris sensor unit (Air Quality Innovations Ltd, Australia), sampling at a frequency of 1.25 Hz. Symbols indicate sampling locations, coloured according to the measured SO_2 concentration in parts per million (ppm). Data from Liu et al. [2019], image © 2019 Maxar Technologies, Google Earth.

Figure 17: CO_2 sampling from the plume at Poás volcano, Costa Rica (2019). The gas sampling payload (550 g) is suspended 1.5 m below the DJI Inspire 1 as it is flown into the plume. The sample is procured by a remotely operated pump which fills gas bags for isotopic analysis in the laboratory.

UAS controller. The UAS enables routine monitoring of the evolving summit lake whilst eliminating the risk of crewed aircraft entering an environment with dangerously steep terrain where volcanic gas concentrations may be lethal.

5.4 Deployment of ground-based instruments

Providing direct support for ground-based measurements is an emerging application that fully embraces UAS capabilities for safe, rapid and affordable access to remote and hazardous environments. Missions can deploy temporary ground-based instrument networks or densify an existing monitoring network, including installing sensors in proximal vent regions (Figure 19). The advantages of rapid aerial deployment of ground-based sensors were illustrated during the 2004–2005 eruption of Mount St. Helens when remote sensor packages enabled telemetered seismic and deformation data to be acquired from regions proximal to, and on, the growing lava spine [LaHusen et al. 2008; McChesney et al. 2008]. However, at ~70 kg per package, these sensors were deployed slung under a crewed helicopter, and were too heavy for UAS.

The deployment of smaller seismometer systems was successfully carried out by UAS in 2009, within the otherwise un-instrumented 2-km exclusion zone surrounding the active Showa crater, Sakurajima, Japan. These proximal instruments demonstrated their value in 2011 by recording increasing signals magnitudes associated with explosions, interpreted as upward migration of the explosion source [Ohminato et al. 2011]. Further UAS-compatible mobile instruments were subsequently designed and deployed during the 2014–2015 eruptions of Kuchinoerabujima (Kyushu, Japan). Following two explosions that destroyed geophysical instrumentation in the summit region, and de-

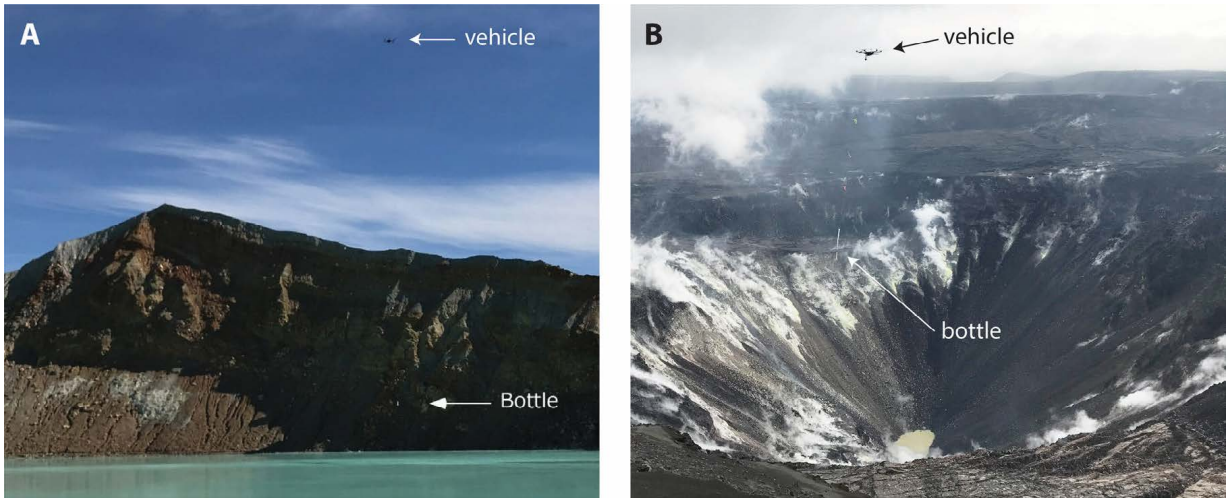

Figure 18: Water sampling, [A] at Yugama crater lake (reproduced from [Terada et al. 2018] under the Creative Commons Attribution 4.0 International License) and [B] at Halema'uma'u, Kīlauea, 2019.

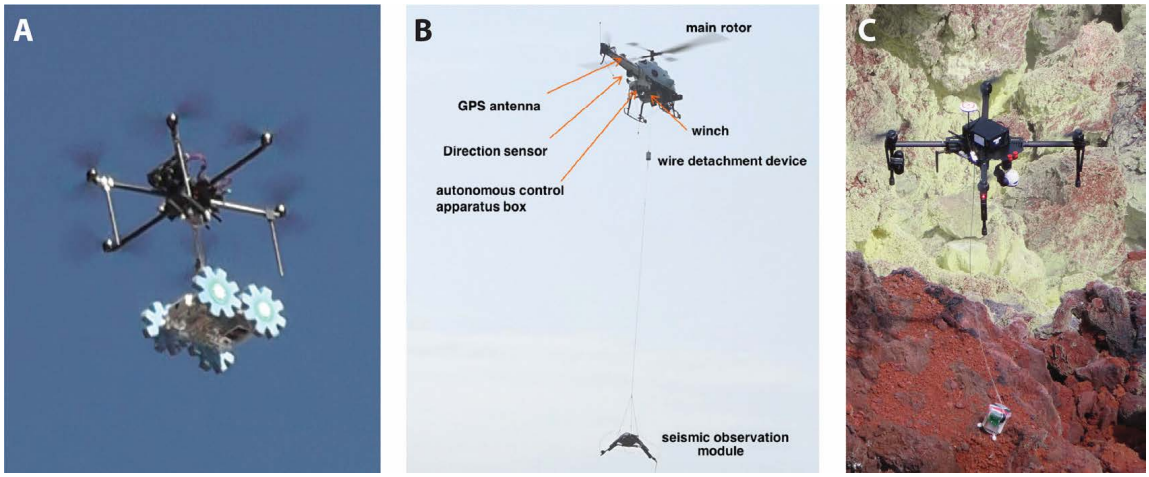

Figure 19: Instrument deployments. [A] A small mobile robot ('CLOVER', <3 kg and <0.5 m long) for ground-based sampling and observation being transported by a ZionPro800 hexa-rotor at Mt. Asama, during operational tests [Nagatani et al. 2014]. [B] Deployment of a 5-kg seismic observation module slung under a RMAX-G1 single-rotor vehicle at Kuchinoerabujima, Japan, 2015 (adapted from Ohminato et al. [2017]). [C] A sensor pod being deployed on Tavurvur, Papua New Guinea, (2018) using a quadrotor. The pod measures surface temperature via thermocouples in the base, and any significant vibrations via a MEMS accelerometer, and then wirelessly telemeters the measurements to a recording ground station [Wood et al. 2018].

spite access restrictions of up to 3 km, a UAS successfully reinstated the summit seismic network with ~5 kg seismometers (Figure 19B; [Ohminato et al. 2017]). Near-real-time telemetered data from the network contributed to the decision-making process that enabled evacuated communities to return in December 2015. The substantial payload and range requirements required the use of a large, combustion-powered UAS (RMAX-G1 helicopter; Figure 19B), and work on smaller sensor packages, suitable for deployment by smaller electric-powered quadrotor UAS is ongoing (Figure 19C; [Wood et al. 2018]).

6 Discussion

Applications of UAS within volcanology have already advanced from the limited use of a few, relatively large aircraft prior to circa 2010, to a diverse range of systems being regularly deployed globally, to support a broad range of volcanological work. Their advantages in providing cost effective and responsive data acquisition, along with increased access to difficult and hazardous environments have led to:

- *Decimetric-resolution DEMs of lava flows and domes from high resolution (centimetre-scale) visible-wavelength imaging.* Such products can be more

than two orders of magnitude better resolution than widely available space-based products, and have enabled analysis of surface morphology (reflecting emplacement dynamics) and structural assessment, with implications for hazard assessment.

- *High resolution fully 3-D models of vertical or overhanging surfaces (e.g. caldera cliffs).* Rotor-based UAS can collect close-range oblique imagery that is not possible from space-based platforms or regularly available from conventional aerial systems (e.g. crewed helicopters), and provides unique access for modelling vertical faces for mapping or quantifying mass movements.

- *Centimetric-resolution thermal imagery for detailed analysis of heat loss and thermal structure.* In line with advantages for visible-imaging operations, UAS-compatible thermal cameras provide a two-order-of magnitude step change in the resolution of airborne thermal imaging data, enhancing feature identification and change detection at sites such as geothermal fields.

- *Remote measurement and sampling of hazardous environments* such as plumes and surface hydrothermal regions. With personnel able to remain at safe locations, the use of UAS have provided measurement and sampling opportunities in otherwise inaccessible areas. These are often proximal to activity, and hence, the data acquired (e.g. gas geochemistry, particle size distributions, surface temperatures) are particularly valuable for initialising (e.g. plume dispersal) or validating (e.g. cooling) models.

- *Instrument deployment into difficult to access or hazardous environments.* Enabling the installation of seismic stations in near-vent regions within exclusion zones has provided insight into evolving magmatic processes and provided valuable data that have contributed to crisis-response decision-making.

- *Rapid, responsive and regular mission capabilities* (for all points above). Short deployment timescales and efficient data processing enables UAS use not only for scientific research, but also for generating sufficiently timely data products to support crisis management (e.g. video footage and high-resolution georectified orthomosaics disseminated within minutes to hours). Thus, importantly, UAS demonstrate strong value for both scientific investigation and for monitoring applications, for which requirements in terms of data quantity, quality and timeliness can vary substantially.

6.1 Current limitations

While future possibilities for UAS applications are extensive, current operations are often limited by legislative restrictions, which will most likely increase, mainly due to public privacy and safety concerns. Import and export between countries, particularly for larger vehicles, can be slow and require extensive prior paperwork. This can hinder research activities, but can also effectively prevent rapid UAS support within international responses to volcanic crises. Further delays can result from navigating varying legal frameworks for UAS operations, especially where there are inefficient bureaucratic procedures and no direct previous experience in the practicalities and logistics for a specific location. Obtaining necessary permissions, in particular for relatively unusual or challenging work such as BVLOS missions, can take weeks to months. Although areas of volcanological interest are usually in remote areas, they can still be protected regions subject to permitting (for example, UAS can only be used in National Parks of the USA under a Special Use Permit). Until fully autonomous systems are available, skilled personnel must still be present in the field and on-site human expertise is a key component of successful UAS deployments.

For scientific applications, as measurement opportunities expand and become increasingly accessible, there is a risk that data volume and availability may result in their associated uncertainties being insufficiently considered. Investigators must ensure the appropriate use of data through maintaining rigorous processing standards and accounting for new and UAS-specific sources of uncertainty. For example, necessary compromises in lightweight instrument design, as well as short sampling times, can result in reduced signal to noise ratios when compared with near-equivalent ground-based instruments. It should be noted that the accuracy and precision of specialised airborne systems designed for conventional aircraft (e.g. Volcano Emissions Research Package; [Kelly et al. 2013]) exceed those of both ground-based and UAS-mounted Multi-GAS systems, but at the expense of considerable size and weight. Maintaining sensor calibration is important and, because some flight capabilities exceed altitudes of 3.5 km above sea level [e.g. Schellenberg et al. 2019], the need exists for the extension of pressure and temperature calibration curves. For gas measurements, species-specific differences in sensor response times introduces uncertainties in derived ratios for ground-based measurements [e.g. Roberts et al. 2017], and this effect is amplified for UAS-based instruments. With sensor response times of order 10 s or more [Liu et al. 2019; Roberts et al. 2017], and fixed-wing platforms flying at 15–25 m s^{-1}, UAS-based measurements represent spatially averaged concentrations with potential location uncertainties of up to order 100 m in the direction of travel. Accounting for such effects requires de-

convolution of the sensor response (based on quantitative sensor-specific characterisation and platform motion information) to reconstruct the real signal [Liu et al. 2019; Roberts et al. 2017; Rüdiger et al. 2018]. Similarly, for multi-rotor platforms, rotor-driven atmospheric mixing results in spatially averaged sampling of poorly constrained plume volumes [Rüdiger et al. 2018; Villa et al. 2016; Yeo et al. 2015], with implications for the discrimination of closely spaced emission sources and for representative sampling of particle and aerosol size distributions.

With imaging applications, ease of data capture and processing should not circumvent the use of established remote sensing and photogrammetry protocols. In the broader geomorphology community, the wide availability of imagery and the use of straightforward 'black box' processing (which typifies the application of SfM-photogrammetry for generating topographic models) motivated a reminder of requirements for maintaining the quality of data collection, processing and dissemination [James et al. 2019]. When assessing topographic change, and particularly when anticipated magnitudes approach the expected measurement quality, results should be supported by rigorous tests of precision and accuracy [e.g. Höhle and Höhle 2009; James et al. 2017b]. Increasing data volumes require enhanced efforts to ensure that quality, utility and discoverability is maintained. Best practices strongly suggest that users should provide full metadata and open access wherever possible.

6.2 Future prospects and opportunities

To maximise the benefits of UAS use, the volcanology community should take all opportunities to help streamline legislative requirements and their implementation. Regulation and scrutiny may increase if the accelerating use of UAS across all sectors leads to more incidents (including crashes), and could potentially offset flexible deployment advantages over using crewed aircraft. Hopefully, as authorities become increasingly familiar with mission requests, procedures will become more efficient and timescales for obtaining permission to fly will decrease. The wider use of approaches such as annual permits (where appropriate) could substantially reduce paperwork and delays. Extended and documented track records of good practice, adherence to local restrictions, and demonstrations of positive use-cases for UAS will be key contributors to maintaining and broadening access. Nevertheless, regulations are continuously updated and as onboard safety systems evolve (to include collision avoidance systems for example) restrictions may be relaxed, particularly for smaller, lightweight UAS categories. As commercial UAS use increases, consultation with UAS user groups is helping to streamline policy and provide positive changes to regulations, e.g. improvements in the FAA Waiver process within the USA. Wider international recognition of pilot qualifications, increased harmonisation of UAS regulations (as is occurring within the EU), along with improved ease of international UAS transport (particularly for large UAS) would all enhance opportunities, whilst maintaining safety standards.

Application of UAS technologies in volcanology is likely to continue expanding as sensors become smaller and system flight times, payload capabilities, and ease of use increase. Modular designs, integrated telemetry and flexible UAS frameworks are increasingly enabling customised and effective solutions for research-, monitoring- or response-focussed missions. With the development of affordable, fully autonomous systems (or, prior to that, the widespread use of BVLOS missions), UAS could become essential tools for daily to sub-daily observatory-based monitoring of difficult-to-access or dangerous environments. Consequently, automated data processing, integration with existing data streams and assimilation with models and decision-making procedures will become priorities.

The introduction of new sensors will enhance measurement capabilities. Some lidar systems are now sufficiently lightweight to be UAS-mounted (e.g. <4 kg), and have already been used in applications such as forestry [e.g. Sankey et al. 2017; Wallace et al. 2012]. Deployment of such systems in volcanology will widen options for topographic data collection, with particular potential in areas that are challenging for photogrammetric methods, such as where vegetation or gas emissions partially obscure the surface, or over water bodies where image alignment can fail. Multispectral sensors have the potential to measure surface composition with, for example, implications for analysis of hydrothermal deposits and alteration, and of the thermophilic organisms that live in these environments [e.g. Hellman and Ramsey 2004; Reath and Ramsey 2013]. The development of UAS-portable mass balances and spectrometers for *in situ* particle and gas analysis is ongoing [Airey et al. 2017; Diaz et al. 2015]. Development of lightweight gravity sensors such as the MEMS gravimeter [Middlemiss et al. 2016] may open the door to future geophysical applications with UAS. It is likely that commercial exploration for resources will drive such developments but, as sensors become available and affordable, they will represent valuable tools for volcanology.

Regular UAS use will promote the generation of detailed time-series data on a wide range of volcanic processes. For example, high-resolution thermal data of geothermal areas offer potential to illuminate details of the dynamics of fluid, gas, and heat flux in these systems. For active lava flows, imagery and topographic data, updated hourly to daily, enable early detection of breakouts, overflows and tumulus formation, are critical for forecasting changes in flow direction. 3-D models from photogrammetric processing are required to be generated within the few-hours timescales for cri-

sis monitoring and civil protection purposes [De Beni et al. 2019; Favalli et al. 2018; Turner et al. 2017b], and regular measurements such as lava channel dimensions and discharge rates will be assimilated into flow models to update maximum flow length estimates. Realising the potential of 'swarm' systems, which involve multiple cooperating vehicles, will accelerate data collection, increase resilience and provide novel distributed measurement opportunities such as distributed atmospheric data [Pieri et al. 2013b]. Looking forward, the possibilities are endless for sampling applications at volcanoes, from the retrieval of volcanic bombs for petrological study to enabling regular, automated *in situ* measurements from plumes. Increased automation of sampling missions will accelerate sample collection, and the development of on-board 'plume finding' algorithms will enhance the repeatability and precision of UAS-based strategies for gas measurement.

Intensive use of UAS could evolve ground-based monitoring systems into truly agile sensor networks, with rapid instrument deployments at the earliest signs of unrest. Enhancement of minimal-coverage seismic arrays for background monitoring into high-density resilient networks for delivering continuous and detailed data streams is expected. Affordable and lightweight sensor packages [Wood et al. 2018] will enable unprecedented proximal data collection during critical periods of rapidly evolving activity, where, currently, the system dynamics that are key to robust forecasting are the most poorly constrained. The potential for mobile sensor deployments will enable the rapid addressing of any instrument failures or sensor network weaknesses identified through modelling or data analysis and, ultimately, for networks to develop self-healing capabilities.

7 Conclusion

The hazardous environments and spatial scales associated with volcanic processes mean that technologies providing remote and automated measurements will always be highly valued. Consequently, the broad (and rapidly increasing) capabilities of UAS are seeing their application and development within volcanological research, monitoring and crisis response. Critically, the use of UAS enables the addressing of existing gaps in temporal and spatial data resolution, both through facilitating physical access and by offering practical and affordable alternatives to expensive crewed systems. Increasing automation and sensor development will continue to enhance UAS capabilities, and seamless integration with existing systems and data streams is likely to be one of the main challenges ahead. Legislation is a critical contributor to ongoing safety but inefficiencies can also lead it to be a limiting factor for rapid deployments. Harmonising regulations and streaming flight permission procedures represent key areas for maximising future UAS utility, particularly for international crisis response. UAS have already provided unique insight into volcanic processes, and are set to represent an invaluable tool for volcanologists and associated hazard managers.

Acknowledgements

We are indebted to the following for generously providing materials for figures: Takayuki Nakano (Figure 1B), Adriano Mazzini (Figure 2C, Figure 14), Herlan Darmawan (Figure 8) and Keiji Nagatani Figure 19A). The paper was substantially improved following constructive and insightful reviews from Peter Kelly and two anonymous reviewers, to whom we are very grateful. EJL acknowledges an Early Career Fellowship from the Leverhulme Trust, and funding from the Alfred P. Sloan Foundation through their support of the Deep Carbon Observatory. BS acknowledges support from the Belgian Science Policy Office and the STEREO-III Programme, through the RESIST (SR/00/305), MUZUBI (SR/00/324) and VeRSUS (SR/00/382) projects. EL is supported by USA NSF award EAR-1654588. BBC acknowledges support from NSF EAR PF Award #1725768. Work by DP is supported under contract to NASA at the Jet Propulsion Laboratory of the California Institute of Technology. Any use of trade, firm, or product names is for descriptive purposes only, and does not imply endorsement by the United States government or any other party.

Author contributions

This review was conceived and coordinated by MRJ, with all authors contributing to the design and writing of the manuscript.

Author affiliations

α Lancaster Environment Centre, Lancaster University, Lancaster, LA1 4YQ UK.
β Lancaster Intelligent Robotic & Autonomous Systems Centre, Lancaster University, Lancaster, LA1 4WA UK.
γ Lamont-Doherty Earth Observatory, Columbia University, 61 Route 9W, Palisades, NY, USA 10964.
δ Department of Earth and Planetary Sciences, McGill University, 3450 University Street, Montreal H3A 0E8, Quebec, Canada.
ε Volcano Disaster Assistance Program, U.S. Geological Survey, Vancouver, WA 98683 USA.
ζ U.S. Geological Survey, Alaska Volcano Observatory, Anchorage, AK 99508 USA.
η Istituto Nazionale di Geofisica e Vulcanologia, Sezione di Pisa, Italy.
ϑ Earth Sciences, University College London, London, WC1E 6BS, UK.

ι Jet Propulsion Laboratory, California Institute of Technology, Pasadena, CA, USA.
ϰ School of Geosciences, University of South Florida, Tampa, FL, USA.
λ Natural Hazards Service, Royal Museum for Central Africa, B-3080 Tervuren, Belgium.
μ Volcanic Fluid Research Center, School of Science, Tokyo Institute of Technology, 2-12-1 Ookayama, Meguro-ku, Tokyo, 152-8551, Japan.
ν School of Environmental Sciences, University of Liverpool, Jane Herdman Building, 4 Brownlow Street, Liverpool L69 3GP, UK.
ξ GFZ German Research Centre for Geosciences, Potsdam, Germany.
ο Department of Aerospace Engineering, University of Bristol, Bristol, BS8 1TR UK.

Data availability

No new data were generated during this review. Where data are freely available, a DOI is provided. Supporting information is available as Supplementary Material alongside the online version of this article.

Copyright notice

References

Abdallatif, T. F., M. Suh, J. Oh, and K. K. Hyun (2007). "Impact of magnetic survey design on the imaging of small archeological objects: Practicability in gradiometer surveying". *The Leading Edge* 26.5, pp. 571–577. doi: 10.1190/1.2737095.

Abdullah, Q., J. Bethel, M. Hussain, and R. Munjy (2013). "Photogrammetric project and mission planning". *Manual of Photogrammetry*. American Society for Photogrammetry and Remote Sensing, pp. 1187–1220.

Agusto, M. R., A. Caselli, R. Daga, J. Varekamp, A. Trinelli, M. D. Afonso, M. L. Velez, P. Euillades, and S. Ribeiro Guevara (2017). "The crater lake of Copahue volcano (Argentina): geochemical and thermal changes between 1995 and 2015". *Geochemistry and geophysics of active volcanic lakes*. Ed. by T. Ohba, B. Capaccioni, and C. Caudron. Vol. 437. Geological Society of London, pp. 107–130. doi: 10.1144/sp437.16.

Airey, M. W., R. G. Harrison, K. A. Nicoll, P. D. Williams, and G. J. Marlton (2017). "Note: A miniature oscillating microbalance for sampling ice and volcanic ash from a small airborne platform". *Review of Scientific Instruments* 88.8, p. 086108. doi: 10.1063/1.4998971.

Aiuppa, A., S. Inguaggiato, A. McGonigle, M. O'Dwyer, C. Oppenheimer, M. Padgett, D. Rouwet, and M. Valenza (2005). "H2S fluxes from Mt. Etna, Stromboli, and Vulcano (Italy) and implications for the sulfur budget at volcanoes". *Geochimica et Cosmochimica Acta* 69.7, pp. 1861–1871. doi: 10.1016/j.gca.2004.09.018.

Aiuppa, A., M. Bitetto, V. Francofonte, G. Velasquez, C. Bucarey Parra, G. Giudice, M. Liuzzo, R. Moretti, Y. Moussallam, N. Peters, G. Tamburello, O. A. Valderrama, and A. Curtis (2017a). "A CO_2-gas precursor to the March 2015 Villarrica volcano eruption". *Geochemistry, Geophysics, Geosystems* 18.6, pp. 2120–2132. doi: 10.1002/2017gc006892.

Aiuppa, A., T. P. Fischer, T. Plank, P. Robidoux, and R. Di Napoli (2017b). "Along-arc, inter-arc and arc-to-arc variations in volcanic gas CO_2/S_T ratios reveal dual source of carbon in arc volcanism". *Earth-Science Reviews* 168, pp. 24–47. doi: 10.1016/j.earscirev.2017.03.005.

Aiuppa, A., R. Moretti, C. Federico, G. Giudice, S. Gurrieri, M. Liuzzo, P. Papale, H. Shinohara, and M. Valenza (2007). "Forecasting Etna eruptions by real-time observation of volcanic gas composition". *Geology* 35.12, pp. 1115–1118. doi: 10.1130/g24149a.1.

Ambrosia, V., S. Wegener, J. Brass, and E. Hinkley (2005). "Use of unmanned aerial vehicles for fire detection". *Proceedings of the 5th International Workshop on Remote Sensing and GIS Applications to Forest Fire Management: Fire Effects Assessment*, 9–17.

Amici, S., M. Turci, F. Giulietti, S. Giammanco, M. F. Buongiorno, A. La Spina, and L. Spampinato (2013b). "Volcanic environments monitoring by drones mud volcano case study". *ISPRS - International Archives of the Photogrammetry, Remote Sensing and Spatial Information Sciences* XL-1/W2, pp. 5–10. doi: 10.5194/isprsarchives-xl-1-w2-5-2013.

Amici, S., M. Turci, S. Giammanco, L. Spampinato, and F. Giulietti (2013a). "UAV Thermal Infrared Remote Sensing of an Italian Mud Volcano". *Advances in Remote Sensing* 02.04, pp. 358–364. doi: 10.4236/ars.2013.24038.

Andaru, R. and J. Rau (2019). "Lava dome changes detection at Agung mountain during high level of volcanic activity using UAV photogrammetry." *ISPRS - International Archives of the Photogrammetry, Remote Sensing and Spatial Information Sciences* XLII-2, pp. 173–179.

Anderson, R., S. Gathman, J. Hughes, S. Bjornsson, S. Jonasson, D. C. Blanchard, C. B. Moore, H. J. Survilas, and B. Vonnegut (1965). "Electricity in Volcanic Clouds: Investigations show that lightning can result from charge-separation processes in a volcanic

crater". *Science* 148.3674, pp. 1179–1189. DOI: 10.1126/science.148.3674.1179.

Aurell, J., W. Mitchell, V. Chirayath, J. Jonsson, D. Tabor, and B. Gullett (2017). "Field determination of multipollutant, open area combustion source emission factors with a hexacopter unmanned aerial vehicle". *Atmospheric Environment* 166, pp. 433–440. DOI: 10.1016/j.atmosenv.2017.07.046.

Ball, J. L., E. S. Calder, B. E. Hubbard, and M. L. Bernstein (2013). "An assessment of hydrothermal alteration in the Santiaguito lava dome complex, Guatemala: implications for dome collapse hazards". *Bulletin of Volcanology* 75.1. DOI: 10.1007/s00445-012-0676-z.

Bares, J. E. and D. S. Wettergreen (1999). "Dante II: Technical Description, Results, and Lessons Learned". *The International Journal of Robotics Research* 18.7, pp. 621–649. DOI: 10.1177/02783649922066475.

Belousov, A. and M. Belousova (2004). "First attempt to sample eruptive cloud with tethered balloon". *Priroda* 4, pp. 42–54. [In Russian].

Benassi, F., E. Dall'Asta, F. Diotri, G. Forlani, U. Morra di Cella, R. Roncella, and M. Santise (2017). "Testing Accuracy and Repeatability of UAV Blocks Oriented with GNSS-Supported Aerial Triangulation". *Remote Sensing* 9.2, p. 172. DOI: 10.3390/rs9020172.

Berni, J., P. Zarco-Tejada, L. Suarez, and E. Fereres (2009). "Thermal and Narrowband Multispectral Remote Sensing for Vegetation Monitoring From an Unmanned Aerial Vehicle". *IEEE Transactions on Geoscience and Remote Sensing* 47.3, pp. 722–738. DOI: 10.1109/tgrs.2008.2010457.

Besl, P. and N. D. McKay (1992). "A method for registration of 3-D shapes". *IEEE Transactions on Pattern Analysis and Machine Intelligence* 14.2, pp. 239–256. DOI: 10.1109/34.121791.

Bhardwaj, A., L. Sam, Akanksha, F. J. Martín-Torres, and R. Kumar (2016). "UAVs as remote sensing platform in glaciology: Present applications and future prospects". *Remote Sensing of Environment* 175, pp. 196–204. DOI: 10.1016/j.rse.2015.12.029.

Bonnefoy, L. E., C. W. Hamilton, S. P. Scheidt, J. Voigt, A. Hoskuldsson, I. Jonsdottir, and T. Thordarson (2017). "Landscape Evolution After the 2014-2015 Lava Flow at Holuhraun, Iceland". *Lunar and Planetary Science Conference*, 1652.

Brady, J. M., M. D. Stokes, J. Bonnardel, and T. H. Bertram (2016). "Characterization of a Quadrotor Unmanned Aircraft System for Aerosol-Particle-Concentration Measurements". *Environmental Science & Technology* 50.3, pp. 1376–1383. DOI: 10.1021/acs.est.5b05320.

Burton, M. R., G. M. Sawyer, and D. Granieri (2013). "Deep Carbon Emissions from Volcanoes". *Reviews in Mineralogy and Geochemistry* 75.1, pp. 323–354. DOI: 10.2138/rmg.2013.75.11.

Burton, M., T. Caltabiano, F. Murè, G. Salerno, and D. Randazzo (2009). "SO_2 flux from Stromboli during the 2007 eruption: Results from the FLAME network and traverse measurements". *Journal of Volcanology and Geothermal Research* 182.3-4, pp. 214–220. DOI: 10.1016/j.jvolgeores.2008.11.025.

Caltabiano, D. and G. Muscato (2005). "A Robotic System for Volcano Exploration". *Cutting Edge Robotics*. Ed. by V. Kordic, A. Lazinica, and M. Mer. Pro Literatur Verlag, Germany, pp. 499–518. DOI: 10.5772/4666.

Caltabiano, D., G. Muscato, A. Orlando, C. Federico, G. Giudice, and S. Guerrieri (2005). "Architecture of a UAV for volcanic gas sampling". *2005 IEEE Conference on Emerging Technologies and Factory Automation*. Vol. 1, 739–744. DOI: 10.1109/ETFA.2005.1612599.

Campion, R. (2014). "New lava lake at Nyamuragira volcano revealed by combined ASTER and OMI SO_2 measurements". *Geophysical Research Letters* 41.21, pp. 7485–7492. DOI: 10.1002/2014gl061808.

Campion, R., G. G. Salerno, P.-F. Coheur, D. Hurtmans, L. Clarisse, K. Kazahaya, M. Burton, T. Caltabiano, C. Clerbaux, and A. Bernard (2010). "Measuring volcanic degassing of SO_2 in the lower troposphere with ASTER band ratios". *Journal of Volcanology and Geothermal Research* 194.1-3, pp. 42–54. DOI: 10.1016/j.jvolgeores.2010.04.010.

Cao, Z. and Y. Zhang (2014). "Analysis and Design of Electromagnetic Compatibility Techniques for Unmanned Aerial Vehicle Power in Aeromagnetic Survey". *Electric Power Components and Systems* 42.13, pp. 1409–1418. DOI: 10.1080/15325008.2014.933370.

Carey, S. and M. Bursik (2015). "Volcanic Plumes". *The Encyclopedia of Volcanoes*. Ed. by H. Sigurdsson, B. Houghton, S. McNutt, H. Rymer, and J. Stix. Elsevier, pp. 571–585. DOI: 10.1016/b978-0-12-385938-9.00015-8.

Carn, S. A., V. E. Fioletov, C. A. McLinden, C. Li, and N. A. Krotkov (2017). "A decade of global volcanic SO_2 emissions measured from space". *Scientific Reports* 7.1. DOI: 10.1038/srep44095.

Carr, B. B., K. A. Bennett, E. Lev, and C. S. Edwards (2019). "Utilization of an sUAS-Based Thermal Camera to Determine Relative Thermal Inertia of Volcanic Deposits". *Lunar and Planetary Science Conference*, 3129.

Carr, B. B. and E. Lev (2018). "Activity and hazards of the ongoing eruption of Sinabung Volcano, Indonesia, evaluated using UAS-derived datasets". *AGU Fall Meeting Abstracts*. Vol. 2018. AGU, V23D–0108.

Cashman, K. V., R. C. Kerr, and R. W. Griffiths (2006). "A laboratory model of surface crust formation and disruption on lava flows through non-uniform channels". *Bulletin of Volcanology* 68.7-8, pp. 753–770. DOI: 10.1007/s00445-005-0048-z.

Catalán, M., Y. M. Martos, J. Galindo-Zaldívar, and M. Funaki (2014). "Monitoring the evolution of Deception Island volcano from magnetic anomaly data

(South Shetland Islands, Antarctica)". *Global and Planetary Change* 123, pp. 199–212. doi: 10.1016/j.gloplacha.2014.07.018.

Chandler, J. (1999). "Effective application of automated digital photogrammetry for geomorphological research". *Earth Surface Processes and Landforms* 24.1, pp. 51–63. doi: 10.1002/(sici)1096-9837(199901)24:1<51::aid-esp948>3.0.co;2-h.

Chang, C.-C., J.-L. Wang, C.-Y. Chang, M.-C. Liang, and M.-R. Lin (2016). "Development of a multicopter-carried whole air sampling apparatus and its applications in environmental studies". *Chemosphere* 144, pp. 484–492. doi: 10.1016/j.chemosphere.2015.08.028.

Chio, S.-H. and C.-H. Lin (2017). "Preliminary Study of UAS Equipped with Thermal Camera for Volcanic Geothermal Monitoring in Taiwan". *Sensors* 17.7, p. 1649. doi: 10.3390/s17071649.

Chosson, F., R. Paoli, and B. Cuenot (2008). "Ship plume dispersion rates in convective boundary layers for chemistry models". *Atmospheric Chemistry and Physics* 8.16, pp. 4841–4853. doi: 10.5194/acp-8-4841-2008.

Colomina, I. and P. Molina (2014). "Unmanned aerial systems for photogrammetry and remote sensing: A review". *ISPRS Journal of Photogrammetry and Remote Sensing* 92, pp. 79–97. doi: 10.1016/j.isprsjprs.2014.02.013.

Conde, V., S. Bredemeyer, E. Duarte, J. F. Pacheco, S. Miranda, B. Galle, and T. H. Hansteen (2014). "SO2 degassing from Turrialba Volcano linked to seismic signatures during the period 2008–2012". *International Journal of Earth Sciences* 103.7, pp. 1983–1998. doi: 10.1007/s00531-013-0958-5.

D'Arcy, F., J. Stix, J. de Moor, J. Rüdiger, J. Diaz, A. Alan, and E. Corrales (2018). "Drones Swoop in to Measure Gas Belched from Volcanoes". *Eos* 99. doi: 10.1029/2018eo102329.

Darmawan, H., T. R. Walter, K. S. Brotopuspito, Subandriyo, and I. Gusti Made Agung Nandaka (2018a). "Morphological and structural changes at the Merapi lava dome monitored in 2012–15 using unmanned aerial vehicles (UAVs)". *Journal of Volcanology and Geothermal Research* 349, pp. 256–267. doi: 10.1016/j.jvolgeores.2017.11.006.

Darmawan, H., T. R. Walter, V. R. Troll, and A. Budi-Santoso (2018b). "Structural weakening of the Merapi dome identified by drone photogrammetry after the 2010 eruption". *Natural hazards and earth system sciences* 18.12, pp. 3267–3281. doi: 10.5194/nhess-18-3267-2018.

Davidson, J. and S. De Silva (2000). "Composite volcanoes". *Encyclopedia of volcanoes*. Ed. by B. Houghton, H. Rymer, S. McNutt, and J. Stix. Vol. 1. Academic Press, pp. 663–681.

De Angelis, S., O. D. Lamb, A. Lamur, A. J. Hornby, F. W. von Aulock, G. Chigna, Y. Lavallée, and A. Rietbrock (2016). "Characterization of moderate ash-and-gas explosions at Santiaguito volcano, Guatemala, from infrasound waveform inversion and thermal infrared measurements". *Geophysical Research Letters* 43.12, pp. 6220–6227. doi: 10.1002/2016gl069098.

De Beni, E., M. Cantarero, and A. Messina (2019). "UAVs for volcano monitoring: A new approach applied on an active lava flow on Mt. Etna (Italy), during the 27 February–02 March 2017 eruption". *Journal of Volcanology and Geothermal Research* 369, pp. 250–262. doi: 10.1016/j.jvolgeores.2018.12.001.

de Moor, J. M., J. Stix, G. Avard, C. Muller, E. Corrales, J. A. Diaz, A. Alan, J. Brenes, J. Pacheco, A. Aiuppa, and T. P. Fischer (2019). "Insights on Hydrothermal-Magmatic Interactions and Eruptive Processes at Poás Volcano (Costa Rica) From High-Frequency Gas Monitoring and Drone Measurements". *Geophysical Research Letters* 46.3, pp. 1293–1302. doi: 10.1029/2018gl080301.

Deng, F., M. Rodgers, S. Xie, T. H. Dixon, S. Charbonnier, E. A. Gallant, C. M. L. Vélez, M. Ordoñez, R. Malservisi, N. K. Voss, and J. A. Richardson (2019). "High-resolution DEM generation from spaceborne and terrestrial remote sensing data for improved volcano hazard assessment — A case study at Nevado del Ruiz, Colombia". *Remote Sensing of Environment* 233.111348. doi: 10.1016/j.rse.2019.111348.

Dering, G. M., S. Micklethwaite, S. T. Thiele, S. A. Vollgger, and A. R. Cruden (2019). "Review of drones, photogrammetry and emerging sensor technology for the study of dykes: Best practises and future potential". *Journal of Volcanology and Geothermal Research* 373, pp. 148–166. doi: 10.1016/j.jvolgeores.2019.01.018.

Dewez, T. B., D. Girardeau-Montaut, C. Allanic, and J. Rohmer (2016). "FACETS : A Cloudcompare plugin to extract geological planes from unstructured 3d point clouds". *ISPRS - International Archives of the Photogrammetry, Remote Sensing and Spatial Information Sciences* XLI-B5, pp. 799–804. doi: 10.5194/isprsarchives-xli-b5-799-2016.

Di Felice, F., A. Mazzini, G. Di Stefano, and G. Romeo (2018). "Drone high resolution infrared imaging of the Lusi mud eruption". *Marine and Petroleum Geology* 90, pp. 38–51. doi: 10.1016/j.marpetgeo.2017.10.025.

Di Stefano, G., G. Romeo, A. Mazzini, A. Iarocci, S. Hadi, and S. Pelphrey (2018). "The Lusi drone: A multidisciplinary tool to access extreme environments". *Marine and Petroleum Geology* 90, pp. 26–37. doi: 10.1016/j.marpetgeo.2017.07.006.

Diaz, J. A. et al. (2015). "Unmanned Aerial Mass Spectrometer Systems for In-Situ Volcanic Plume Analysis". *Journal of The American Society for Mass Spectrometry* 26.2, pp. 292–304. doi: 10.1007/s13361-014-1058-x.

Diefenbach, A. K., J. Adams, T. Burton, B. Koeckeritz, J. Sloan, and S. Stroud (2018). "The 2018 U.S. Geological Survey-Department of Interior UAS Kılauea Eruption Response". *AGU Fall Meeting Abstracts*. Vol. 2018. AGU, V23D–0107.

Diefenbach, A. K., K. F. Bull, R. L. Wessels, and R. G. McGimsey (2013). "Photogrammetric monitoring of lava dome growth during the 2009 eruption of Redoubt Volcano". *Journal of Volcanology and Geothermal Research* 259, pp. 308–316. DOI: 10.1016/j.jvolgeores.2011.12.009.

Diefenbach, A. K., J. G. Crider, S. P. Schilling, and D. Dzurisin (2012). "Rapid, low-cost photogrammetry to monitor volcanic eruptions: an example from Mount St. Helens, Washington, USA". *Bulletin of Volcanology* 74.2, pp. 579–587. DOI: 10.1007/s00445-011-0548-y.

Dietterich, H. R. and K. V. Cashman (2014). "Channel networks within lava flows: Formation, evolution, and implications for flow behavior". *Journal of Geophysical Research: Earth Surface* 119.8, pp. 1704–1724. DOI: 10.1002/2014jf003103.

Dietterich, H. R., K. V. Cashman, A. C. Rust, and E. Lev (2015). "Diverting lava flows in the lab". *Nature Geoscience* 8.7, pp. 494–496. DOI: 10.1038/ngeo2470.

Dietterich, H. R., M. R. Patrick, A. K. Diefenbach, C. Parcheta, E. Lev, and N. L. Foks (2018). "Lava flow hazard modeling and the assessment of effusion rates and topographic change with UAS and lidar during the 2018 Kilauea lower East Rift Zone eruption". *AGU Fall Meeting Abstracts*. AGU, V21B–03.

Doukas, M. P. and K. A. McGee (2007). *A Compilation of Gas Emission-Rate Data from Volcanoes of Cook Inlet (Spurr, Crater Peak, Redoubt, Iliamna, and Augustine) and Alaska Peninsula (Douglas, Fourpeaked, Griggs, Mageik, Martin, Peulik, Ukinrek Maars, and Veniaminof), Alaska, from 1995-2006*. Tech. rep. US Geological Survey. DOI: 10.3133/ofr20071400.

Dundas, C. M., L. Keszthelyi, C. W. Hamilton, L. E. Bonnefoy, S. P. Scheidt, E. Lev, M. E. Rumpf, T. Thordarson, A. Hoskuldsson, I. Jonsdottir, A. L. Keske, and M. M. Sori (2017). "The Hydrothermal System of the 2014-2015 lava Flows at Holuhraun, Iceland: An Analog for Martian Lava-Water Interactions". *Lunar and Planetary Science Conference*, 2470.

Eldering, A., T. E. Taylor, C. W. O'Dell, and R. Pavlick (2019). "The OCO-3 mission: measurement objectives and expected performance based on 1 year of simulated data". *Atmospheric Measurement Techniques* 12.4, pp. 2341–2370. DOI: 10.5194/amt-12-2341-2019.

Eling, C., M. Wieland, C. Hess, L. Klingbeil, and H. Kuhlmann (2015). "Development and Evaluation of a UAV Based Mapping System for Remote Sensing and Surveying Applications". *ISPRS - International Archives of the Photogrammetry, Remote Sensing and Spatial Information Sciences* XL1, pp. 233–239. DOI: 10.5194/isprsarchives-XL-1-W4-233-2015.

Eltner, A., P. Baumgart, H.-G. Maas, and D. Faust (2015). "Multi-temporal UAV data for automatic measurement of rill and interrill erosion on loess soil". *Earth Surface Processes and Landforms* 40.6, pp. 741–755. DOI: 10.1002/esp.3673.

Favalli, M., A. Fornaciai, F. Mazzarini, A. Harris, M. Neri, B. Behncke, M. T. Pareschi, S. Tarquini, and E. Boschi (2010). "Evolution of an active lava flow field using a multitemporal LIDAR acquisition". *Journal of Geophysical Research* 115.B11203. DOI: 10.1029/2010jb007463.

Favalli, M., A. Fornaciai, L. Nannipieri, A. Harris, S. Calvari, and C. Lormand (2018). "UAV-based remote sensing surveys of lava flow fields: a case study from Etna's 1974 channel-fed lava flows". *Bulletin of Volcanology* 80.29, pp. 1192–1196. DOI: 10.1007/s00445-018-1192-6.

Federico, C., M. Liuzzo, G. Giudice, G. Capasso, A. Pisciotta, and M. Pedone (2019). "Variations in CO_2 emissions at a mud volcano at the southern base of Mt Etna: are they due to volcanic activity interference or a geyser-like mechanism?" *Bulletin of Volcanology* 81.2. DOI: 10.1007/s00445-018-1261-x.

Finn, C. A. and L. A. Morgan (2002). "High-resolution aeromagnetic mapping of volcanic terrain, Yellowstone National Park". *Journal of Volcanology and Geothermal Research* 115.1-2, pp. 207–231. DOI: 10.1016/s0377-0273(01)00317-1.

Fischer, T. P. and T. M. Lopez (2016). "First airborne samples of a volcanic plume for $\delta^{13}C$ of CO_2 determinations". *Geophysical Research Letters* 43.7, pp. 3272–3279. DOI: 10.1002/2016gl068499.

Forlani, G., E. Dall'Asta, F. Diotri, U. Morra di Cella, R. Roncella, and M. Santise (2018). "Quality Assessment of DSMs Produced from UAV Flights Georeferenced with On-Board RTK Positioning". *Remote Sensing* 10.311, pp. 1–22. DOI: 10.3390/rs10020311.

Fraser, C. S. (2013). "Automatic Camera Calibration in Close Range Photogrammetry". *Photogrammetric Engineering & Remote Sensing* 79.4, pp. 381–388. DOI: 10.14358/pers.79.4.381.

Gerke, M. and H. Przybilla (2016). "Accuracy Analysis of Photogrammetric UAV Image Blocks: Influence of Onboard RTK-GNSS and Cross Flight Patterns". *Photogrammetrie - Fernerkundung - Geoinformation* 2016.1, pp. 17–30. DOI: 10.1127/pfg/2016/0284.

Gerlach, T. M., H. Delgado, K. A. McGee, M. P. Doukas, J. J. Venegas, and L. Cárdenas (1997). "Application of the LI-COR CO_2 analyzer to volcanic plumes: A case study, volcán Popocatépetl, Mexico, June 7 and 10, 1995". *Journal of Geophysical Research: Solid Earth* 102.B4, pp. 8005–8019. DOI: 10.1029/96jb03887.

Gerlach, T. M., K. A. McGee, and M. P. Doukas (2008). "Emission rates of CO_2, SO_2, and $H2_2S$, scrubbing, and preeruption excess volatiles at Mount St. Helens, 2004-2005". *A Volcano Rekindled: The Renewed Eruption of Mount St. Helens*. Ed. by D. R. Sherrod, W. E.

Scott, and P. H. Stauffer. U.S. Geological Survey Professional Paper 1750, pp. 543–571. doi: 10.3133/pp175026.

Gerlach, T. M., K. A. McGee, A. J. Sutton, and T. Elias (1998). "Rates of volcanic CO_2 degassing from airborne determinations of SO_2 emission rates and plume CO_2/SO_2: test study at Puu Ōō Cone, Kilauea Volcano, Hawaii". *Geophysical Research Letters* 25.14, pp. 2675–2678. doi: 10.1029/98gl02030.

Giggenbach, W. F. (1996). "Chemical Composition of Volcanic Gases". *Monitoring and Mitigation of Volcano Hazards*. Ed. by R. Scarpa and R. I. Tilling. Springer Berlin Heidelberg, pp. 221–256. doi: 10.1007/978-3-642-80087-0_7.

Giordan, D., Y. Hayakawa, F. Nex, F. Remondino, and P. Tarolli (2018). "Review article: the use of remotely piloted aircraft systems (RPASs) for natural hazards monitoring and management". *Natural Hazards and Earth System Sciences* 18.4, pp. 1079–1096. doi: 10.5194/nhess-18-1079-2018.

Gíslason, S. et al. (2015). "Environmental pressure from the 2014–15 eruption of Bárðarbunga volcano, Iceland". *Geochemical Perspectives Letters* 1.1, pp. 84–93. doi: 10.7185/geochemlet.1509.

Giuffrida, G., S. Calabrese, N. Bobrowski, H. Finkenzeller, G. Pecoraino, and S. Scaglione (2015). "The flight of Arcadia: spatial CO_2/SO_2 variations in a cross section above the Nord East crater of Etna volcano". *EGU General Assembly Conference Abstracts*. Vol. 17. EGU2015-6648.

Glen, J. M., A. E. Egger, C. Ippolito, G. A. Phelps, R. Berthold, R. Lee, J. M. Spritzer, and M. Tchernychev (2012). "The application of unmanned aerial systems (UAS) in geophysical investigations of geothermal systems". *AGU Fall Meeting Abstracts*. Vol. 2012. AGU, V23F–03.

Gomez, C. and B. Kennedy (2018). "Capturing volcanic plumes in 3D with UAV-based photogrammetry at Yasur Volcano – Vanuatu". *Journal of Volcanology and Geothermal Research* 350, pp. 84–88. doi: 10.1016/j.jvolgeores.2017.12.007.

Granshaw, S. I. (2018). "RPV, UAV, UAS, RPAS ... or just drone?" *The Photogrammetric Record* 33.162, pp. 160–170. doi: 10.1111/phor.12244.

Grauch, V. J. S. and M. R. Hudson (2011). "Aeromagnetic anomalies over faulted strata". *The Leading Edge* 30.11, pp. 1242–1252. doi: 10.1190/1.3663396.

Grayson, B., N. T. Penna, J. P. Mills, and D. S. Grant (2018). "GPS precise point positioning for UAV photogrammetry". *The Photogrammetric Record* 33.164, pp. 427–447. doi: 10.1111/phor.12259.

Greco, F., S. Giammanco, R. Napoli, G. Currenti, A. Vicari, A. La Spina, G. Salerno, L. Spampinato, A. Amantia, M. Cantarero, A. Messina, and A. Sicali (2016). "A multidisciplinary strategy for in-situ and remote sensing monitoring of areas affected by pressurized fluids: Application to mud volcanoes: A multidisciplinary environmental monitoring strategy". *2016 IEEE Sensors Applications Symposium (SAS)*. IEEE. doi: 10.1109/sas.2016.7479861.

Gregg, T. K. P. and J. H. Fink (1995). "Quantification of submarine lava-flow morphology through analog experiments". *Geology* 23.1, p. 73. doi: 10.1130/0091-7613(1995)023<0073:qoslfm>2.3.co;2.

Hartmann, W., S. Tilch, H. Eisenbeiss, and K. Schindler (2012). "Determination of the UAS position by automatic processing of thermal images". *ISPRS - International Archives of the Photogrammetry, Remote Sensing and Spatial Information Sciences* XXXIX-B6, pp. 111–116. doi: 10.5194/isprsarchives-xxxix-b6-111-2012.

Harvey, M., J. Rowland, and K. Luketina (2016). "Drone with thermal infrared camera provides high resolution georeferenced imagery of the Waikite geothermal area, New Zealand". *Journal of Volcanology and Geothermal Research* 325, pp. 61–69. doi: 10.1016/j.jvolgeores.2016.06.014.

Harwin, S., A. Lucieer, and J. Osborn (2015). "The Impact of the Calibration Method on the Accuracy of Point Clouds Derived Using Unmanned Aerial Vehicle Multi-View Stereopsis". *Remote Sensing* 7.9, pp. 11933–11953. doi: 10.3390/rs70911933.

Hashimoto, T., T. Koyama, T. Kaneko, T. Ohminato, T. Yanagisawa, M. Yoshimoto, and E. Suzuki (2014). "Aeromagnetic survey using an unmanned autonomous helicopter over Tarumae Volcano, northern Japan". *Exploration Geophysics* 45.1, pp. 37–42. doi: 10.1071/eg12087.

Hatakeyama, H. (1943). "On the Variation of the Atmospheric Potential Gradient caused by the Cloud of Smoke of the Volcano Asama. The Second Report". *Journal of the Meteorological Society of Japan. Ser. II* 21.9, pp. 420–426. doi: 10.2151/jmsj1923.21.9_420.

Heap, M. J., R. Coats, C.-f. Chen, N. Varley, Y. Lavallée, J. Kendrick, T. Xu, and T. Reuschlé (2018). "Thermal resilience of microcracked andesitic dome rocks". *Journal of Volcanology and Geothermal Research* 367, pp. 20–30. doi: 10.1016/j.jvolgeores.2018.10.021.

Hellman, M. J. and M. S. Ramsey (2004). "Analysis of hot springs and associated deposits in Yellowstone National Park using ASTER and AVIRIS remote sensing". *Journal of Volcanology and Geothermal Research* 135.1-2, pp. 195–219. doi: 10.1016/j.jvolgeores.2003.12.012.

Hernández, P. A., G. V. Melián, L. Somoza, M. C. Arpa, N. M. Pérez, E. Bariso, H. Sumino, E. Padrón, J. C. Varekamp, J. Albert-Beltran, and R. Solidum (2017). "The acid crater lake of Taal Volcano, Philippines: hydrogeochemical and hydroacoustic data related to the 2010–11 volcanic unrest". *Geochemistry and geophysics of active volcanic lakes*. Ed. by T. Ohba, B. Capaccioni, and C. Caudron. Vol. 437. Geological Society of London, pp. 131–152. doi: 10.1144/sp437.17.

Hilton, D. R., C. J. Ramırez, R. A. Mora-Amador, T. P. Fischer, E. Füri, P. Barry, and A. Shaw (2010). "Monitoring of temporal and spatial variations in fumarole

helium and carbon dioxide characteristics at Poás and Turrialba volcanoes, Costa Rica (2001–2009)". *Geochemical Journal* 44.5, pp. 431–440. DOI: 10.2343/geochemj.1.0085.

Hisbaron, D. R., H. Wijayanti, M. Iffani, R. Winastuti, and M. Yudinugroho (2018). "Vulnerability mapping in Kelud volcano based on village information". *IOP Conference Series: Earth and Environmental Science* 148.012008. DOI: 10.1088/1755-1315/148/1/012008.

Höhle, J. and M. Höhle (2009). "Accuracy assessment of digital elevation models by means of robust statistical methods". *ISPRS Journal of Photogrammetry and Remote Sensing* 64.4, pp. 398–406. DOI: 10.1016/j.isprsjprs.2009.02.003.

Hood, P. (1965). "Gradient measurements in aeromagnetic surveying". *Geophysics* 30.5, pp. 891–902. DOI: 10.1190/1.1439666.

Iarocci, A., G. Romeo, A. Mazzini, G. Di Stefano, and P. Benedetti (2014). "UAV: A multidisciplinary tool to access extreme enviroments". *2014 6th Workshop on Hyperspectral Image and Signal Processing: Evolution in Remote Sensing (WHISPERS)*. IEEE. DOI: 10.1109/whispers.2014.8077571.

Ikegami, F., J. McPhie, R. Carey, R. Mundana, A. Soule, and M. Jutzeler (2018). "The Eruption of Submarine Rhyolite Lavas and Domes in the Deep Ocean – Havre 2012, Kermadec Arc". *Frontiers in Earth Science* 6.147. DOI: 10.3389/feart.2018.00147.

Ilyinskaya, E., S. Mobbs, R. Burton, M. Burton, F. Pardini, M. A. Pfeffer, R. Purvis, J. Lee, S. Bauguitte, B. Brooks, et al. (2018). "Globally significant CO_2 emissions from Katla, a subglacial volcano in Iceland". *Geophysical Research Letters* 45.19, pp. 10–332. DOI: 10.1029/2018GL079096.

Immerzeel, W., P. Kraaijenbrink, J. Shea, A. Shrestha, F. Pellicciotti, M. Bierkens, and S. de Jong (2014). "High-resolution monitoring of Himalayan glacier dynamics using unmanned aerial vehicles". *Remote Sensing of Environment* 150, pp. 93–103. DOI: 10.1016/j.rse.2014.04.025.

International Civil Aviation Organization (2015). *Manual on Remotely Piloted Aircraft Systems (RPAS)*. Doc 10019 AN/507. International Civil Aviation Organization.

James, M. R., J. H. Chandler, A. Eltner, C. Fraser, P. E. Miller, J. P. Mills, T. Noble, S. Robson, and S. N. Lane (2019). "Guidelines on the use of structure-from-motion photogrammetry in geomorphic research". *Earth Surface Processes and Landforms* 44.10, pp. 2081–2084. DOI: 10.1002/esp.4637.

James, M. R., S. J. Lane, and J. S. Gilbert (1998). "Volcanic plume monitoring using atmospheric electric potential gradients". *Journal of the Geological Society* 155.4, pp. 587–590. DOI: 10.1144/gsjgs.155.4.0587.

James, M. R. and S. Robson (2014). "Mitigating systematic error in topographic models derived from UAV and ground-based image networks". *Earth Surface Processes and Landforms* 39.10, pp. 1413–1420. DOI: 10.1002/esp.3609.

James, M. R., S. Robson, S. d'Oleire-Oltmanns, and U. Niethammer (2017a). "Optimising UAV topographic surveys processed with structure-from-motion: Ground control quality, quantity and bundle adjustment". *Geomorphology* 280, pp. 51–66. DOI: 10.1016/j.geomorph.2016.11.021.

James, M. R., S. Robson, and M. W. Smith (2017b). "3-D uncertainty-based topographic change detection with structure-from-motion photogrammetry: precision maps for ground control and directly georeferenced surveys". *Earth Surface Processes and Landforms* 42.12, pp. 1769–1788. DOI: 10.1002/esp.4125.

James, M. R. and N. R. Varley (2012). "Identification of structural controls in an active lava dome with high resolution DEMs: Volcán de Colima, Mexico". *Geophysical Research Letters* 39.22, p. L22303. DOI: 10.1029/2012gl054245.

Johansen, T. A., A. Cristofaro, K. Sorensen, J. M. Hansen, and T. I. Fossen (2015). "On estimation of wind velocity, angle-of-attack and sideslip angle of small UAVs using standard sensors". *2015 International Conference on Unmanned Aircraft Systems (ICUAS)*. IEEE. DOI: 10.1109/icuas.2015.7152330.

Jordan, B. R. (2019). "Collecting field data in volcanic landscapes using small UAS (sUAS)/drones". *Journal of Volcanology and Geothermal Research* 385, pp. 231–241. DOI: 10.1016/j.jvolgeores.2019.07.006.

Kaneko, T., T. Koyama, A. Yasuda, M. Takeo, T. Yanagisawa, K. Kajiwara, and Y. Honda (2011). "Low-altitude remote sensing of volcanoes using an unmanned autonomous helicopter: an example of aeromagnetic observation at Izu-Oshima volcano, Japan". *International Journal of Remote Sensing* 32.5, pp. 1491–1504. DOI: 10.1080/01431160903559770.

Kazahaya, R., H. Shinohara, T. Ohminato, and T. Kaneko (2019). "Airborne measurements of volcanic gas composition during unrest at Kuchinoerabujima volcano, Japan". *Bulletin of Volcanology* 81.2. DOI: 10.1007/s00445-018-1262-9.

Kelly, P. J., C. Kern, T. J. Roberts, T. Lopez, C. Werner, and A. Aiuppa (2013). "Rapid chemical evolution of tropospheric volcanic emissions from Redoubt Volcano, Alaska, based on observations of ozone and halogen-containing gases". *Journal of Volcanology and Geothermal Research* 259, pp. 317–333. DOI: 10.1016/j.jvolgeores.2012.04.023.

Kereszturi, G. and K. Németh (2012). "Monogenetic Basaltic Volcanoes: Genetic Classification, Growth, Geomorphology and Degradation". *Updates in Volcanology - New Advances in Understanding Volcanic Systems*. Ed. by K. Németh. InTech. DOI: 10.5772/51387.

Kolzenburg, S., M. Favalli, A. Fornaciai, I. Isola, A. J. L. Harris, L. Nannipieri, and D. Giordano (2016). "Rapid Updating and Improvement of Airborne LIDAR DEMs Through Ground-Based SfM 3-D Model-

ing of Volcanic Features". *IEEE Transactions on Geoscience and Remote Sensing* 54.11, pp. 6687–6699. doi: 10.1109/tgrs.2016.2587798.

Konagai, K., T. Kiyota, M. Shiga, H. Tomita, H. Okuda, and K. Kajihara (2016). "Ground fissures that appeared in aso caldera basin in the 2016 kumamoto earthquake, Japan". *JSCE Journal of Disaster Fact-Sheets* FS2016-E-0003.

Koyama, T., T. Kaneko, T. Ohminato, T. Yanagisawa, A. Watanabe, and M. Takeo (2013). "An aeromagnetic survey of Shinmoe-dake volcano, Kirishima, Japan, after the 2011 eruption using an unmanned autonomous helicopter". *Earth, Planets and Space* 65.6, pp. 657–666. doi: 10.5047/eps.2013.03.005.

Kraus, K. (1993). *Photogrammetry, Vol. 1. Fundamentals and Standard Processes*. Ferdinand Dümmels.

– (2007). *Photogrammetry: Geometry from Images and Laser Scans*. Vol. 1. Walter de Gruyter.

Krotkov, E., J. Bares, L. Katragadda, R. Simmons, and R. Whittaker (1994). "Lunar rover technology demonstrations with Dante and Ratler". *Proceedings of the Third International Symposium on Artificial Intelligence, Robotics, and Automation for Space*. N95-23672 07-63, 113–116.

LaHusen, R. G., K. J. Swinford, M. Logan, and M. Lisowski (2008). "Instrumentation in remote and dangerous settings examples using data from GPS "spider" deployments during the 2004-2005 eruption of Mount St. Helens, Washington". *A Volcano Rekindled: The Renewed Eruption of Mount St. Helens, 2004–2006*. Ed. by D. R. Sherrod, W. E. Scott, and P. H. Stauffer. US Geological Survey, pp. 335–345. doi: 10.3133/pp175016.

Lai, C.-J., J.-K. Liu, W.-C. Hsu, K.-S. Li, M.-C. Wu, and K.-T. Chang (2018). "An Experiment of Geothermal Exploration with an Uas-Tir in Xiaoyoukeng Area of Tatun Volcanoes, Taiwan". *IGARSS 2018 - 2018 IEEE International Geoscience and Remote Sensing Symposium*. IEEE. doi: 10.1109/igarss.2018.8518437.

Lamb, O. D., Y. Lavallée, S. De Angelis, A. Lamur, A. J. Hornby, F. W. von Aulock, J. E. Kendrick, G. Chigna, and A. Rietbrock (2016). "Changes in long-term eruption dynamics at Santiaguito, Guatemala: Observations from seismic data". *AGU Fall Meeting Abstracts*. Vol. 2016. AGU, V43A–3127.

Lane, S. J. and J. S. Gilbert (1992). "Electric potential gradient changes during explosive activity at Sakurajima volcano, Japan". *Bulletin of Volcanology* 54.7, pp. 590–594. doi: 10.1007/bf00569942.

Lelong, C., P. Burger, G. Jubelin, B. Roux, S. Labbé, and F. Baret (2008). "Assessment of Unmanned Aerial Vehicles Imagery for Quantitative Monitoring of Wheat Crop in Small Plots". *Sensors* 8.5, pp. 3557–3585. doi: 10.3390/s8053557.

Lev, E., P. Ruprecht, C. Oppenheimer, N. Peters, M. Patrick, P. A. Hernández, L. Spampinato, and J. Marlow (2019). "A global synthesis of lava lake dynamics". *Journal of Volcanology and Geothermal Research* 381, pp. 16–31. doi: 10.1016/j.jvolgeores.2019.04.010.

Lindsay, S. d. J. M. (2015). "Primary Volcanic Landforms". *The Encyclopedia of Volcanoes*. Ed. by H. Sigurdsson, B. Houghton, S. McNutt, H. Rymer, and J. Stix. Elsevier, pp. 273–297. doi: 10.1016/b978-0-12-385938-9.00015-8.

Liu, E. J. et al. (2019). "Dynamics of Outgassing and Plume Transport Revealed by Proximal Unmanned Aerial System (UAS) Measurements at Volcán Villarrica, Chile". *Geochemistry, Geophysics, Geosystems* 20.2, pp. 730–750. doi: 10.1029/2018gc007692.

Lucic, G., J. Stix, B. S. Lollar, G. Lacrampe-Couloume, A. Muñoz, and M. I. Carcache (2014). "The degassing character of a young volcanic center: Cerro Negro, Nicaragua". *Bulletin of Volcanology* 76.9. doi: 10.1007/s00445-014-0850-6.

Lucieer, A., S. M. de Jong, and D. Turner (2014). "Mapping landslide displacements using Structure from Motion (SfM) and image correlation of multi-temporal UAV photography". *Progress in Physical Geography: Earth and Environment* 38.1, pp. 97–116. doi: 10.1177/0309133313515293.

Luhmann, T., C. Fraser, and H.-G. Maas (2016). "Sensor modelling and camera calibration for close-range photogrammetry". *ISPRS Journal of Photogrammetry and Remote Sensing* 115, pp. 37–46. doi: 10.1016/j.isprsjprs.2015.10.006.

Luhmann, T., S. Robson, S. Kyle, and J. Boehm (2014). *Close-range photogrammetry and 3D imaging*. Walter de Gruyter GmbH.

Malehmir, A., L. Dynesius, K. Paulusson, A. Paulusson, H. Johansson, M. Bastani, M. Wedmark, and P. Marsden (2017). "The potential of rotary-wing UAV-based magnetic surveys for mineral exploration: A case study from central Sweden". *The Leading Edge* 36.7, pp. 552–557. doi: 10.1190/tle36070552.1.

Malowany, K. S., J. Stix, J. M. de Moor, K. Chu, G. Lacrampe-Couloume, and B. S. Lollar (2017). "Carbon isotope systematics of Turrialba volcano, Costa Rica, using a portable cavity ring-down spectrometer". *Geochemistry, Geophysics, Geosystems* 18.7, pp. 2769–2784. doi: 10.1002/2017gc006856.

Mancini, F., C. Castagnetti, P. Rossi, M. Dubbini, N. Fazio, M. Perrotti, and P. Lollino (2017). "An Integrated Procedure to Assess the Stability of Coastal Rocky Cliffs: From UAV Close-Range Photogrammetry to Geomechanical Finite Element Modeling". *Remote Sensing* 9.12, p. 1235. doi: 10.3390/rs9121235.

Mandon, C. L., B. W. Christenson, C. I. Schipper, T. M. Seward, and E. Garaebiti (2019). "Metal transport in volcanic plumes: A case study at White Island and Yasur volcanoes". *Journal of Volcanology and Geothermal Research* 369, pp. 155–171. doi: 10.1016/j.jvolgeores.2018.11.024.

Mason, E., E. Ilyinskaya, R. C. W. Whitty, P. Wieser, E. J. Liu, M. Edmonds, T. Mather, T. Elias, P. A. Nadeau, C. Kern, D. J. Schneider, and C. Oppenheimer (2019).

"Aerosol chemistry of the 2018 Kılauea Lower East Rift Zone eruption - following major and trace elements from source to exposed communities". *EGU General Assembly Conference Abstracts*. EGU2019-13557.

McChesney, P. J., M. R. Couchman, S. C. Moran, A. B. Lockhart, K. J. Swinford, and R. G. LaHusen (2008). "Seismic-monitoring changes and the remote deployment of seismic stations (seismic spider) at Mount St. Helens, 2004-2005". *A Volcano Rekindled: The Renewed Eruption of Mount St. Helens, 2004–2006*. Ed. by D. R. Sherrod, W. E. Scott, and P. H. Stauffer. US Geological Survey, pp. 129–140. DOI: 10.3133/pp17507.

McCormick, B. T., M. Edmonds, T. A. Mather, and S. A. Carn (2012). "First synoptic analysis of volcanic degassing in Papua New Guinea". *Geochemistry, Geophysics, Geosystems* 13.3. DOI: 10.1029/2011gc003945.

McGee, K. (1992). "The structure, dynamics, and chemical composition of noneruptive plumes from Mount St. Helens, 1980–1988". *Journal of Volcanology and Geothermal Research* 51.3, pp. 269–282. DOI: 10.1016/0377-0273(92)90127-y.

McGlone, J. and G. Lee (2013). *Manual of Photogrammetry, Sixth*. ASPRS. [6th edition].

McGonigle, A. J. S., A. Aiuppa, G. Giudice, G. Tamburello, A. J. Hodson, and S. Gurrieri (2008). "Unmanned aerial vehicle measurements of volcanic carbon dioxide fluxes". *Geophysical Research Letters* 35.L06303. DOI: 10.1029/2007gl032508.

Meier, L., P. Tanskanen, F. Fraundorfer, and M. Pollefeys (2011). "PIXHAWK: A system for autonomous flight using onboard computer vision". *2011 IEEE International Conference on Robotics and Automation*. IEEE. DOI: 10.1109/icra.2011.5980229.

Middlemiss, R. P., A. Samarelli, D. J. Paul, J. Hough, S. Rowan, and G. D. Hammond (2016). "Measurement of the Earth tides with a MEMS gravimeter". *Nature* 531.7596, pp. 614–617. DOI: 10.1038/nature17397.

Mikhail, E. M., J. S. Bethel, and J. C. McGlone (2001). *Introduction to modern photogrammetry*. John Wiley & Sons, Inc., p. 19.

Miura, T., T. Koyaguchi, and Y. Tanaka (1995). "Simultaneous measurement of the changing of the atmospheric electric field and the relative electric charge on ash caused by the eruption of Sakurajima Volcano". *8th Report of Geophysical and Geochemical Observations at Sakurajima Volcano*, 89–104. [In Japanese].

Mori, T., T. Hashimoto, A. Terada, M. Yoshimoto, R. Kazahaya, H. Shinohara, and R. Tanaka (2016). "Volcanic plume measurements using a UAV for the 2014 Mt. Ontake eruption". *Earth, Planets and Space* 68.1. DOI: 10.1186/s40623-016-0418-0.

Mosbrucker, A. R., J. J. Major, K. R. Spicer, and J. Pitlick (2017). "Camera system considerations for geomorphic applications of SfM photogrammetry". *Earth Surface Processes and Landforms* 42.6, pp. 969–986. DOI: 10.1002/esp.4066.

Moussallam, Y., P. Bani, A. Curtis, T. Barnie, M. Moussallam, N. Peters, C. I. Schipper, A. Aiuppa, G. Giudice, Á. Amigo, G. Velasquez, and C. Cardona (2016). "Sustaining persistent lava lakes: Observations from high-resolution gas measurements at Villarrica volcano, Chile". *Earth and Planetary Science Letters* 454, pp. 237–247. DOI: 10.1016/j.epsl.2016.09.012.

Müller, D., T. R. Walter, A. Schöpa, T. Witt, B. Steinke, M. T. Gudmundsson, and T. Dürig (2017). "High-Resolution Digital Elevation Modeling from TLS and UAV Campaign Reveals Structural Complexity at the 2014/2015 Holuhraun Eruption Site, Iceland". *Frontiers in Earth Science* 5. DOI: 10.3389/feart.2017.00059.

Muscato, G., D. Caltabiano, S. Guccione, D. Longo, M. Coltelli, A. Cristaldi, E. Pecora, V. Sacco, P. Sim, G. Virk, P. Briole, A. Semerano, and T. White (2003). "ROBOVOLC: a robot for volcano exploration result of first test campaign". *Industrial Robot: An International Journal* 30.3, pp. 231–242. DOI: 10.1108/01439910310473942.

Nadeau, P. A., T. Elias, C. Kern, A. H. Lerner, C. A. Werner, M. Cappos, L. E. Clor, P. J. Kelly, A. J. Sutton, and S. A. Carn (2018). "The 2018 Eruption of Kılauea Volcano: Tales from a Gas Perspective". *AGU Fall Meeting Abstracts*. Vol. 2018. AGU, V21B–07.

Nagatani, K., K. Akiyama, G. Yamauchi, H. Otsuka, T. Nakamura, S. Kiribayashi, K. Yoshida, Y. Hada, S. Yuta, K. Fujino, T. Izu, and R. Mackay (2013). "Volcanic ash observation in active volcano areas using teleoperated mobile robots - Introduction to our robotic-volcano-observation project and field experiments". *2013 IEEE International Symposium on Safety, Security, and Rescue Robotics (SSRR)*. IEEE. DOI: 10.1109/ssrr.2013.6719324.

Nagatani, K., K. Akiyama, G. Yamauchi, K. Yoshida, Y. Hada, S. Yuta, T. Izu, and R. Mackay (2014). "Development and field test of teleoperated mobile robots for active volcano observation". *2014 IEEE/RSJ International Conference on Intelligent Robots and Systems*. IEEE. DOI: 10.1109/iros.2014.6942818.

Nagatani, K., S. Kiribayashi, R. Yajima, Y. Hada, T. Izu, A. Zeniya, H. Kanai, H. Kanasaki, J. Minagawa, and Y. Moriyama (2018). "Micro-unmanned aerial vehicle-based volcano observation system for debris flow evacuation warning". *Journal of Field Robotics* 35.8, pp. 1222–1241. DOI: 10.1002/rob.21834.

Nakano, T., I. Kamiya, M. Tobita, J. Iwahashi, and H. Nakajima (2014). "Landform monitoring in active volcano by UAV and SfM-MVS technique". *ISPRS - International Archives of the Photogrammetry, Remote Sensing and Spatial Information Sciences* XL-8, pp. 71–75. DOI: 10.5194/isprsarchives-xl-8-71-2014.

NASA (2012). *Style Guide for NASA History Authors and Editors*. URL: https://history.nasa.gov/styleguide.html (visited on 03/13/2020).

National Academies of Sciences, Engineering, and Medicine (2017). *Volcanic eruptions and their repose, unrest, precursors, and timing*. Washington, D.C.: National Academies Press.

Neal, C. A. et al. (2019). "The 2018 rift eruption and summit collapse of Kılauea Volcano". *Science* 363.6425, pp. 367–374. DOI: 10.1126/science.aav7046.

Nesbit, P. and C. Hugenholtz (2019). "Enhancing UAV–SfM 3D Model Accuracy in High-Relief Landscapes by Incorporating Oblique Images". *Remote Sensing* 11.3, p. 239. DOI: 10.3390/rs11030239.

Nex, F. and F. Remondino (2014). "UAV for 3D mapping applications: a review". *Applied Geomatics* 6.1, pp. 1–15. DOI: 10.1007/s12518-013-0120-x.

Nicoll, K., M. Airey, C. Cimarelli, A. Bennett, G. Harrison, D. Gaudin, K. Aplin, K. L. Koh, M. Knuever, and G. Marlton (2019). "First In Situ Observations of Gaseous Volcanic Plume Electrification". *Geophysical Research Letters* 46.6, pp. 3532–3539. DOI: 10.1029/2019gl082211.

Niethammer, U., S. Rothmund, M. James, J. Travelletti, and M. Joswig (2010). "UAV-based Remote Sensing Of Landslides". *Proceedings of the ISPRS Commission V Mid-Term Symposium 'Close Range Image Measurement Techniques'*. Vol. 38. 5, 496–501.

Nishar, A., S. Richards, D. Breen, J. Robertson, and B. Breen (2016). "Thermal infrared imaging of geothermal environments and by an unmanned aerial vehicle (UAV): A case study of the Wairakei – Tauhara geothermal field, Taupo, New Zealand". *Renewable Energy* 86, pp. 1256–1264. DOI: 10.1016/j.renene.2015.09.042.

O'Connor, J., M. J. Smith, and M. R. James (2017). "Cameras and settings for aerial surveys in the geosciences". *Progress in Physical Geography: Earth and Environment* 41.3, pp. 325–344. DOI: 10.1177/0309133317703092.

Ohminato, T., T. Kaneko, T. Koyama, A. Watanabe, M. Takeo, and M. Iguchi (2011). "Upward migration of the explosion sources at Sakurajima volcano, Japan, revield by a seismic network in the close vocinity of the summit crater". *AGU Fall Meeting Abstracts*. Vol. 2011, V41H–07.

Ohminato, T., T. Kaneko, T. Koyama, A. Watanabe, W. Kanda, T. Tameguri, and R. Kazahaya (2017). "Observations using an unmanned aerial vehicle in an area in danger of volcanic eruptions at Kuchinoerabujima Volcano, southern Kyushu, Japan". *Journal of Natural Disaster Science* 38.1, pp. 85–104. DOI: 10.2328/jnds.38.85.

Oshima, S., M. Tsuchide, S. Kato, S. Okubo, K. Watanabe, K. Kudo, and J. Osaka (1991). "Birth of a Submarine Volcano "Teisi Knoll"". *Journal of Physics of the Earth* 39.1, pp. 1–19.

Parcheta, C. E., C. A. Pavlov, N. Wiltsie, K. C. Carpenter, J. Nash, A. Parness, and K. L. Mitchell (2016). "A robotic approach to mapping post-eruptive volcanic fissure conduits". *Journal of Volcanology and Geothermal Research* 320, pp. 19–28. DOI: 10.1016/j.jvolgeores.2016.03.006.

Patrick, M. R., H. R. Dietterich, J. J. Lyons, A. K. Diefenbach, C. Parcheta, K. R. Anderson, A. Namiki, I. Sumita, B. Shiro, and J. P. Kauahikaua (2019). "Cyclic lava effusion during the 2018 eruption of Kılauea Volcano". *Science* 366.6470, eaay9070. DOI: 10.1126/science.aay9070.

Peppa, M. V., J. P. Mills, P. Moore, P. E. Miller, and J. E. Chambers (2017). "Brief communication: Landslide motion from cross correlation of UAV-derived morphological attributes". *Natural Hazards and Earth System Sciences* 17.12, pp. 2143–2150. DOI: 10.5194/nhess-17-2143-2017.

Pering, T., T. Ilanko, and E. J. Liu (2019). "Periodicity in Volcanic Gas Plumes: A Review and Analysis". *Geosciences* 9.9, p. 394. DOI: 10.3390/geosciences9090394.

Pieri, D. C., J. A. Diaz, G. Bland, M. M. Fladeland, and J. M. Schumann (2013b). "Near-vent measurements of volcanic gases and aerosols with multiple small unmanned aerial vehicles". *AGU Fall Meeting Abstracts*. Vol. 2013, V43B–2883.

Pieri, D. C. et al. (2018). "UAS based in-situ volcanic plume characterization for airborne and satellite retrieval validation: VEREX mission results at Kilauea Volcano". *AGU Fall Meeting Abstracts*. Vol. 2018. AGU, NH23D–0869.

Pieri, D. and J. A. Diaz (2015). "In Situ Sampling of Volcanic Emissions with a UAV Sensorweb: Progress and Plans". *Dynamic Data-Driven Environmental Systems Science*. Ed. by S. Ravela and A. Sandu. Springer International Publishing, pp. 16–27. DOI: 10.1007/978-3-319-25138-7_3.

Pieri, D., J. A. Diaz, G. Bland, M. Fladeland, Y. Madrigal, E. Corrales, O. Alegria, A. Alan, V. Realmuto, T. Miles, and A. Abtahi (2013a). "In situ observations and sampling of volcanic emissions with NASA and UCR unmanned aircraft, including a case study at Turrialba Volcano, Costa Rica". *Remote Sensing of Volcanoes and Volcanic Processes: Integrating Observation and Modelling*. Ed. by D. M. Pyle, T. A. Mather, and J. Biggs. Vol. 380. Geological Society of London, pp. 321–352. DOI: 10.1144/sp380.13.

Pounds, P., R. Mahony, P. Hynes, and J. M. Roberts (2002). "Design of a four-rotor aerial robot". *Proceedings of the 2002 Australasian Conference on Robotics and Automation (ACRA 2002)*. Australian Robotics & Automation Association, 145–150.

Reath, K. A. and M. S. Ramsey (2013). "Exploration of geothermal systems using hyperspectral thermal infrared remote sensing". *Journal of Volcanology and Geothermal Research* 265, pp. 27–38. DOI: 10.1016/j.jvolgeores.2013.08.007.

Reid, A. B. (1980). "Aeromagnetic survey design". *GEOPHYSICS* 45.5, pp. 973–976. DOI: 10.1190/1.1441102.

Roberts, T. J., T. Lurton, G. Giudice, M. Liuzzo, A. Aiuppa, M. Coltelli, D. Vignelles, G. Salerno, B. Couté, M. Chartier, R. Baron, J. R. Saffell, and B. Scaillet (2017). "Validation of a novel Multi-Gas sensor for volcanic HCl alongside H2S and SO2 at Mt. Etna". *Bulletin of Volcanology* 79.5. DOI: 10.1007/s00445-017-1114-z.

Rodgers, M., C. Connor, R. Malservisi, L. Connor, and R. Van Alphen (2020). "High-Resolution Magnetic Surveys Using UAVs Reveal New Eruptive Details About Long-Studied Volcanoes: Little Cones (NV)." *AGU Chapman Conference on Distributed Volcanism and Distributed Volcanic Hazards*. 659440. AGU.

Rodgers, M., R. Malservisi, C. Connor, P. Wang, L. Connor, R. Van Alphen, M. Vallée, M. S. Hastings, and J. McIlrath (2019). "From beaches to volcanoes: UAV applications in geoscience using high-resolution topography and aerial magnetic surveys." *AGU Fall Meeting Abstracts*. Vol. 2019, EP11C–2127.

Rokhmana, C. A. and R. Andaru (2017). "Some technical notes on using UAV-based remote sensing for post disaster assessment". *AIP Conference Proceedings*. Vol. 1857. 1. AIP Publishing LLC. DOI: 10.1063/1.4987115.

Rosa, M., G. O'Brien, and V. Vermeiren (2018). "Spain–UK–Belgium Comparative Legal Framework: Civil Drones for Professional and Commercial Purposes". *Ethics and Civil Drones: European Policies and Proposals for the Industry*. Ed. by M. de Miguel Molina and V. S. Campos. Springer International Publishing, pp. 43–75. DOI: 10.1007/978-3-319-71087-7_4.

Rouwet, D., R. Mora-Amador, C. J. Ramırez-Umaña, G. González, and S. Inguaggiato (2017). "Dynamic fluid recycling at Laguna Caliente (Poás, Costa Rica) before and during the 2006–ongoing phreatic eruption cycle (2005–10)". *Geochemistry and geophysics of active volcanic lakes*. Ed. by T. Ohba, B. Capaccioni, and C. Caudron. Vol. 437. 1. Geological Society of London, 73–96. DOI: 10.1144/sp437.11.

Rüdiger, J., J.-L. Tirpitz, J. M. de Moor, N. Bobrowski, A. Gutmann, M. Liuzzo, M. Ibarra, and T. Hoffmann (2018). "Implementation of electrochemical, optical and denuder-based sensors and sampling techniques on UAV for volcanic gas measurements: examples from Masaya, Turrialba and Stromboli volcanoes". *Atmospheric Measurement Techniques* 11.4, pp. 2441–2457. DOI: 10.5194/amt-11-2441-2018.

Rumpf, M. E., E. Lev, and R. Wysocki (2018). "The influence of topographic roughness on lava flow emplacement". *Bulletin of Volcanology* 80.7. DOI: 10.1007/s00445-018-1238-9.

Saito, H., S. Uchiyama, Y. S. Hayakawa, and H. Obanawa (2018). "Landslides triggered by an earthquake and heavy rainfalls at Aso volcano, Japan, detected by UAS and SfM-MVS photogrammetry". *Progress in Earth and Planetary Science* 5.1. DOI: 10.1186/s40645-018-0169-6.

Samson, C., P. Straznicky, J. Laliberté, R. Caron, S. Ferguson, and R. Archer (2010). "Designing and building an unmanned aircraft system for aeromagnetic surveying". *SEG Technical Program Expanded Abstracts 2010*. Society of Exploration Geophysicists. DOI: 10.1190/1.3513051.

Sankey, T., J. Donager, J. McVay, and J. B. Sankey (2017). "UAV lidar and hyperspectral fusion for forest monitoring in the southwestern USA". *Remote Sensing of Environment* 195, pp. 30–43. DOI: 10.1016/j.rse.2017.04.007.

Santagata, T. (2017). "Monitoring of the Nirano Mud Volcanoes Regional Natural Reserve (North Italy) using Unmanned Aerial Vehicles and Terrestrial Laser Scanning". *Journal of Imaging* 3.4, p. 42. DOI: 10.3390/jimaging3040042.

Sato, A. (2003). *The RMAX helicopter UAV*. URL: http://www.dtic.mil/dtic/tr/fulltext/u2/a427393.pdf (visited on 03/13/2020).

Schellenberg, B., T. Richardson, M. Watson, C. Greatwood, R. Clarke, R. Thomas, K. Wood, J. Freer, H. Thomas, E. Liu, F. Salama, and G. Chigna (2019). "Remote sensing and identification of volcanic plumes using fixed-wing UAVs over Volcán de Fuego, Guatemala". *Journal of Field Robotics* 36.7, pp. 1192–1211. DOI: 10.1002/rob.21896.

Schilling, S. P., R. A. Thompson, J. A. Messerich, and E. Y. Iwatsubo (2008). "Use of digital aerophotogrammetry to determine rates of lava dome growth, Mount St. Helens, Washington, 2004-2005". *A Volcano Rekindled: The Renewed Eruption of Mount St. Helens*. Ed. by D. R. Sherrod, W. E. Scott, and P. H. Stauffer. U.S. Geological Survey Professional Paper 1750, pp. 145–167. DOI: 10.3133/pp17508.

Schwandner, F. M. et al. (2017). "Spaceborne detection of localized carbon dioxide sources". *Science* 358.6360, eaam5782. DOI: 10.1126/science.aam5782.

Shinohara, H. (2005). "A new technique to estimate volcanic gas composition: plume measurements with a portable multi-sensor system". *Journal of Volcanology and Geothermal Research* 143.4, pp. 319–333. DOI: 10.1016/j.jvolgeores.2004.12.004.

– (2013). "Composition of volcanic gases emitted during repeating Vulcanian eruption stage of Shinmoedake, Kirishima volcano, Japan". *Earth, Planets and Space* 65.6, pp. 667–675. DOI: 10.5047/eps.2012.11.001.

Shinohara, H., K. Kazahaya, G. Saito, K. Fukui, and M. Odai (2003). "Variation of CO_2/SO_2 ratio in volcanic plumes of Miyakejima: Stable degassing deduced from heliborne measurements". *Geophysical Research Letters* 30.5, p. 1208. DOI: 10.1029/2002gl016105.

Smets, B. (2016). "Dynamics of Volcanic Activity in a Youthful Extensional Setting Studied by Means of Remote Sensing and Ground-based Monitoring Techniques: Nyiragongo and Nyamulagira Volcanoes

(North Kivu, DR Congo)". PhD thesis. Vrije Universiteit Brussel.

Smets, B., C. Wauthier, A. Dille, R. Paris, D. Samyn, N. d'Oreye, and F. Kervyn (2018). "Monitoring ground deformation and lava accumulation in volcanic craters using UAS image acquisitions and 4D photogrammetry". *AGU Fall Meeting Abstracts*. Vol. 2018. V23D-0106. AGU.

Stix, J., F. D'Arcy, F. Grassa, A. Aiuppa, and A. L. Rizzo (2018a). "Near real-time isotopic measurements of CO_2 sampled by drone at Stromboli, Italy". *AGU Fall Meeting Abstracts*. Vol. 2018. V23D-0110. AGU.

Stix, J., J. M. de Moor, J. Rüdiger, A. Alan, E. Corrales, F. D'Arcy, J. A. Diaz, and M. Liotta (2018b). "Using Drones and Miniaturized Instrumentation to Study Degassing at Turrialba and Masaya Volcanoes, Central America". *Journal of Geophysical Research: Solid Earth* 123.8, pp. 6501–6520. doi: 10.1029/2018jb015655.

Stöcker, C., R. Bennett, F. Nex, M. Gerke, and J. Zevenbergen (2017). "Review of the Current State of UAV Regulations". *Remote Sensing* 9.5, p. 459. doi: 10.3390/rs9050459.

Syahbana, D. K. et al. (2019). "The 2017–19 activity at Mount Agung in Bali (Indonesia): Intense unrest, monitoring, crisis response, evacuation, and eruption". *Scientific Reports* 9.1. doi: 10.1038/s41598-019-45295-9.

Telford, W. M., W. Telford, L. Geldart, R. E. Sheriff, and R. Sheriff (1990). *Applied geophysics*. Cambridge university press.

Terada, A., Y. Morita, T. Hashimoto, T. Mori, T. Ohba, M. Yaguchi, and W. Kanda (2018). "Water sampling using a drone at Yugama crater lake, Kusatsu-Shirane volcano, Japan". *Earth, Planets and Space* 70.1. doi: 10.1186/s40623-018-0835-3.

Thiele, S. T., L. Grose, A. Samsu, S. Micklethwaite, S. A. Vollgger, and A. R. Cruden (2017a). "Rapid, semi-automatic fracture and contact mapping for point clouds, images and geophysical data". *Solid Earth* 8.6, pp. 1241–1253. doi: 10.5194/se-8-1241-2017.

Thiele, S. T., N. Varley, and M. R. James (2017b). "Thermal photogrammetric imaging: A new technique for monitoring dome eruptions". *Journal of Volcanology and Geothermal Research* 337, pp. 140–145. doi: 10.1016/j.jvolgeores.2017.03.022.

Thielicke, W. and E. J. Stamhuis (2014). "PIVlab – Towards User-friendly, Affordable and Accurate Digital Particle Image Velocimetry in MATLAB". *Journal of Open Research Software* 2. doi: 10.5334/jors.bl.

Tomaštík, J., M. Mokroš, P. Surový, A. Grznárová, and J. Merganič (2019). "UAV RTK/PPK Method—An Optimal Solution for Mapping Inaccessible Forested Areas?" *Remote Sensing* 11.6, p. 721. doi: 10.3390/rs11060721.

Turner, D., A. Lucieer, and L. Wallace (2014). "Direct Georeferencing of Ultrahigh-Resolution UAV Imagery". *IEEE Transactions on Geoscience and Remote Sensing* 52.5, pp. 2738–2745. doi: 10.1109/tgrs.2013.2265295.

Turner, I. L., M. D. Harley, and C. D. Drummond (2016). "UAVs for coastal surveying". *Coastal Engineering* 114, pp. 19–24. doi: 10.1016/j.coastaleng.2016.03.011.

Turner, N. R., R. L. Perroy, and K. Hon (2017b). "Lava flow hazard prediction and monitoring with UAS: a case study from the 2014–2015 Pāhoa lava flow crisis, Hawai'i". *Journal of Applied Volcanology* 6.17. doi: 10.1186/s13617-017-0068-3.

Turner, N., B. Houghton, J. Taddeucci, J. von der Lieth, U. Kueppers, D. Gaudin, T. Ricci, K. Kim, and P. Scalato (2017a). "Drone Peers into Open Volcanic Vents". *Eos*. doi: 10.1029/2017eo082751.

Venturi, S., F. Tassi, G. Bicocchi, J. Cabassi, F. Capecchiacci, G. Capasso, O. Vaselli, A. Ricci, and F. Grassa (2017). "Fractionation processes affecting the stable carbon isotope signature of thermal waters from hydrothermal/volcanic systems: The examples of Campi Flegrei and Vulcano Island (southern Italy)". *Journal of Volcanology and Geothermal Research* 345, pp. 46–57. doi: 10.1016/j.jvolgeores.2017.08.001.

Vespermann, D. and H.-U. Schmincke (2000). "Scoria cones and tuff rings". *Encyclopedia of volcanoes*. Ed. by B. Houghton, H. Rymer, S. McNutt, and J. Stix. Vol. 1. Academic Press, pp. 683–694.

Villa, T., F. Gonzalez, B. Miljievic, Z. Ristovski, and L. Morawska (2016). "An Overview of Small Unmanned Aerial Vehicles for Air Quality Measurements: Present Applications and Future Prospectives". *Sensors* 16.7, p. 1072. doi: 10.3390/s16071072.

von Aulock, F. W., Y. Lavallée, A. J. Hornby, O. D. Lamb, B. J. Andrews, and J. E. Kendrick (2016). "Observing changes at Santiaguito Volcano, Guatemala with an Unmanned Aerial Vehicle (UAV)". *EGU General Assembly Conference Abstracts*, EPSC2016–11080.

von Aulock, F. W., Y. Lavallée, A. J. Hornby, O. D. Lamb, B. J. Andrews, and J. E. Kendrick (2016b). "Observing changes at Santiaguito Volcano, Guatemala with an Unmanned Aerial Vehicle (UAV)". *AGU Fall Meeting Abstracts*. Vol. 2016. AGU, V43A–3130.

von Glasow, R., M. G. Lawrence, R. Sander, and P. J. Crutzen (2003). "Modeling the chemical effects of ship exhaust in the cloud-free marine boundary layer". *Atmospheric Chemistry and Physics* 3.1, pp. 233–250. doi: 10.5194/acp-3-233-2003.

Wallace, L., A. Lucieer, C. Watson, and D. Turner (2012). "Development of a UAV-LiDAR System with Application to Forest Inventory". *Remote Sensing* 4.6, pp. 1519–1543. doi: 10.3390/rs4061519.

Walter, T. R., P. Jousset, M. Allahbakhshi, T. Witt, M. T. Gudmundsson, and G. P. Hersir (2018a). "Underwater and drone based photogrammetry reveals structural control at Geysir geothermal field in Iceland". *Journal of Volcanology and Geothermal Research*

391.106282. DOI: 10.1016/j.jvolgeores.2018.01.010.

Walter, T. R., J. Salzer, N. Varley, C. Navarro, R. Arámbula-Mendoza, and D. Vargas-Bracamontes (2018b). "Localized and distributed erosion triggered by the 2015 Hurricane Patricia investigated by repeated drone surveys and time lapse cameras at Volcán de Colima, Mexico". *Geomorphology* 319, pp. 186–198. DOI: 10.1016/j.geomorph.2018.07.020.

Watanabe, A., M. Kuri, and K. Nagatani (2016). "Field report: Autonomous lake bed depth mapping by a portable semi-submersible USV at Mt. Zao Okama Crater lake". *2016 IEEE International Symposium on Safety, Security, and Rescue Robotics (SSRR)*. IEEE. DOI: 10.1109/ssrr.2016.7784301.

Watson, M., G. Chigna, K. Wood, T. Richardson, E. Liu, B. Schellenberg, H. Thomas, and A. Naismith (2017). "On the use of UAVs at active volcanoes: a case study from Volcan de Fuego, Guatemala". *AGU Fall Meeting Abstracts*. Vol. 2017. AGU, NH31C–03.

Werner, C. A., M. P. Doukas, and P. J. Kelly (2011). "Gas emissions from failed and actual eruptions from Cook Inlet Volcanoes, Alaska, 1989–2006". *Bulletin of Volcanology* 73.2, pp. 155–173. DOI: 10.1007/s00445-011-0453-4.

Werner, C., P. J. Kelly, M. Doukas, T. Lopez, M. Pfeffer, R. McGimsey, and C. Neal (2013). "Degassing of CO2, SO_2, and H_2S associated with the 2009 eruption of Redoubt Volcano, Alaska". *Journal of Volcanology and Geothermal Research* 259, pp. 270–284. DOI: 10.1016/j.jvolgeores.2012.04.012.

Werner, C., C. Kern, D. Coppola, J. J. Lyons, P. J. Kelly, K. L. Wallace, D. J. Schneider, and R. L. Wessels (2017). "Magmatic degassing, lava dome extrusion, and explosions from Mount Cleveland volcano, Alaska, 2011–2015: Insight into the continuous nature of volcanic activity over multi-year timescales". *Journal of Volcanology and Geothermal Research* 337, pp. 98–110. DOI: 10.1016/j.jvolgeores.2017.03.001.

Wigmore, O. and B. Mark (2017). "Monitoring tropical debris-covered glacier dynamics from high-resolution unmanned aerial vehicle photogrammetry, Cordillera Blanca, Peru". *The Cryosphere* 11.6, pp. 2463–2480. DOI: 10.5194/tc-11-2463-2017.

Williams, W. and M. Harris (2003). "Determination of the Operational Effectiveness of UAV's for Mining Exploration". *Proceedings of UAV Asia-Pacific Conference, Melbourne, Australia*.

Witt, T., T. R. Walter, D. Müller, M. T. Guðmundsson, and A. Schöpa (2018). "The Relationship Between Lava Fountaining and Vent Morphology for the 2014–2015 Holuhraun Eruption, Iceland, Analyzed by Video Monitoring and Topographic Mapping". *Frontiers in Earth Science* 6. DOI: 10.3389/feart.2018.00235.

Wood, K., Y. Verbelen, S. Kaluvan, E. Liu, T. B. Scott, T. Richardson, and M. Watson (2018). ""Dragon Eggs" - drone deployed autonomous volcanic sensing networks". *AGU Fall Meeting Abstracts*. Vol. 2018. AGU, V23D–0113.

Wood, K., A. Albadra, L. Berthoud, A. Calway, M. Watson, H. Thomas, T. Richardson, E. Liu, and G. Chigna (2019). "Determining the three-dimensional structure of a volcanic plume using Unoccupied Aerial System (UAS) imagery". *Journal of Volcanology and Geothermal Research*, p. 106731. DOI: 10.1016/j.jvolgeores.2019.106731.

Xi, X., M. S. Johnson, S. Jeong, M. Fladeland, D. Pieri, J. A. Diaz, and G. L. Bland (2016). "Constraining the sulfur dioxide degassing flux from Turrialba volcano, Costa Rica using unmanned aerial system measurements". *Journal of Volcanology and Geothermal Research* 325, pp. 110–118. DOI: 10.1016/j.jvolgeores.2016.06.023.

Yeo, D., E. Shrestha, D. A. Paley, and E. M. Atkins (2015). "An Empirical Model of Rotorcrafy UAV Downwash for Disturbance Localization and Avoidance". *AIAA Atmospheric Flight Mechanics Conference*. American Institute of Aeronautics and Astronautics. DOI: 10.2514/6.2015-1685.

Zahorec, P., J. Papčo, P. Vajda, F. Greco, M. Cantarero, and D. Carbone (2018). "Refined prediction of vertical gradient of gravity at Etna volcano gravity network (Italy)". *Contributions to Geophysics and Geodesy* 48.4, pp. 299–317. DOI: 10.2478/congeo-2018-0014.

Zakšek, K., M. R. James, M. Hort, T. Nogueira, and K. Schilling (2018). "Using picosatellites for 4-D imaging of volcanic clouds: Proof of concept using ISS photography of the 2009 Sarychev Peak eruption". *Remote Sensing of Environment* 210, pp. 519–530. DOI: 10.1016/j.rse.2018.02.061.

Zhang, C. and J. M. Kovacs (2012). "The application of small unmanned aerial systems for precision agriculture: a review". *Precision Agriculture* 13.6, pp. 693–712. DOI: 10.1007/s11119-012-9274-5.

Zimmer, M., T. R. Walter, C. Kujawa, A. Gaete, and L. Franco-Marin (2017). "Thermal and gas dynamic investigations at Lastarria volcano, Northern Chile. The influence of precipitation and atmospheric pressure on the fumarole temperature and the gas velocity". *Journal of Volcanology and Geothermal Research* 346, pp. 134–140. DOI: 10.1016/j.jvolgeores.2017.03.013.

Zorn, E. U., N. Le Corvec, N. R. Varley, J. T. Salzer, T. R. Walter, C. Navarro-Ochoa, D. M. Vargas-Bracamontes, S. T. Thiele, and R. Arámbula Mendoza (2019). "Load Stress Controls on Directional Lava Dome Growth at Volcán de Colima, Mexico". *Frontiers in Earth Science* 7. DOI: 10.3389/feart.2019.00084.